2012

Design, Construction, and Characterization of a Large Scale Steel Structural System for Real Time Hybrid Testing

Ryan Ahn
Lehigh University

Design, Construction, and Characterization of a Large Scale Steel Structural System for Real Time Hybrid Testing

By

Ryan Ahn

A Thesis
Presented to the Graduate and Research Committee
of Lehigh University
in Candidacy for the Degree of
Master of Science
in
Structural Engineering
Lehigh University

August, 2012

This thesis is accepted and approved in partial fulfillment for the requirements of the Master of Science.

_____
Date

_____
Dr. James M. Ricles
Thesis Advisor

_____
Dr. Richard Sause
Thesis Advisor

_____
Dr. Sibel Pamukcu
Department Chair
Department of Civil and
Environmental Engineering

Acknowledgements

The research presented herein is based on work supported by the National Science Foundation under Award Numbers CMS-1011534 and CMS-0420974, within the George E. Brown, Jr. Network for Earthquake Engineering Simulation Research (NEESR) program. Support for the experiments was also provided through NSF Award No. CMS-0402490 NEES Consortium Operation. Additional funding for this research was provided by the Pennsylvania Infrastructure Technology Alliance (PITA), which is funded by a grant from the Pennsylvania Department of Community and Economic Development (PA DCED).

The research was conducted at the NEES Real-Time Multi-Directional (RTMD) Earthquake Simulation Facility located in the Advanced Technology for Large Structural Systems (ATLSS) Engineering Research Center at Lehigh University. The facility is affiliated with the Lehigh University Department of Civil and Environmental Engineering, Dr. Sibel Pamukcu, Department Chair.

I would like to thank Dr. James M. Ricles and Dr. Richard Sause, thesis advisors, for their guidance and for the opportunity to work on this project. Thank you to my fellow student researchers especially Dr. Yunbyeong Chae, Research Scientist and Akbar Mahvashmohammadi and Baiping Dong, Ph.D. candidates, for their help in understanding dampers. Thank you to the entire ATLSS staff, especially current lab

foreman Darrick Fritchman and former lab foreman John Hoffner for their guidance in the sometimes complicated process of design and constructing a large scale test setup and Thomas Marullo and Gary Novak for assisting me in running experiments. I would also like to recognize the following ATLSS staff members for their help, including Joe Griffiths, Russ Longenbach, Jeff Sampson, Adam Kline, Roger Moyer, and Todd Anthony.

Finally, a special thanks to my family for their support and guidance in all my endeavors. Without them, this would not have been possible.

Contents

Tables

Figures

Abstract

Large scale structures with dampers are being studied as part of ongoing research related to the use of dampers to limit seismically induced damage. Large scale frame testing is being conducted at Lehigh University in collaboration with Purdue University, the University of Illinois, City College of New York, the University of Connecticut, and the Lord Corporation under an NSF-funded NEESR research project. A test bed consisting of a 0.6-scale moment resisting frame (MRF) and a 0.6-scale damped brace frame (DBF) will be used in testing different types of dampers.

A simplified design procedure is used to design the test frame. This procedure uses strength considerations to design a lateral load resisting frame, then allows an engineer to add damping devices to ensure the frame does not exceed other performance objectives, in this case drift limits. The fabrication and erection of this test frame were conducted at the NSF NEES RTMD Earthquake Simulation Facility at the ATLSS Center at Lehigh University in Bethlehem, PA.

This thesis focuses on the experimental setup of the two 0.6-scale test frames. The DBF test frame was characterized to determine its as-built structural characteristics and to ensure the experimental setup functioned properly. A static stiffness matrix was developed to compare with computer models of the structure, for use in hybrid testing and in developing semi-active control laws. This was achieved using static testing and a flexibility approach. Full-bridge load cells installed on the members of the DBF were used to obtain the internal member forces for the beams, columns, and diagonal braces. An assessment of the results indicated the distribution of member forces in the DBF is as

expected and that the level of friction in the test setup (between the DBF and bracing frame) is low and well within the acceptable range.

Chapter 1.
Introduction

1.1 Overview

Dampers have been used for many years to improve the seismic response of buildings. They accomplish this task by adding supplemental damping to a structural system to reduce the drift and inelastic deformation demands of the primary lateral load resisting system and by reducing the acceleration and velocity demands of non-structural components. Current research is trying to improve the design process by integrating the design of the supplemental damping system with the design of the structural system to produce an efficient and effective design. To accomplish this goal, a simplified design procedure for buildings with passive damping devices has been developed that is practical, probabilistic and performance-based. The procedure is based on designing the system for the code design base shear (i.e., strength) and using dampers to meet performance objectives for the design (e.g., drift control; or members remaining elastic.)

With the goal of producing a simplified design procedure, several steps need to be completed. They include validating the simplified design procedure using large-scale real-time hybrid testing. To accomplish this task a prototype steel structure with a supplemental damping system was designed using the simplified design procedure. A 0.6-scale test structure consisting of a damped braced frame (DBF) to house the dampers and a moment resisting frame (MRF) to provide strength is designed and constructed.

This research is being conducted within the National Science Foundation (NSF) George E. Brown, Jr. Network for Earthquake Engineering Simulation Research (NEESR) program. It is a joint project between researchers at Lehigh University, Purdue University, the University of Illinois, City College of New York, the University of Connecticut, and the Lord Corporation. Experiments of the test structure described herein take place at the Real-Time Multi-Directional (RTMD) Earthquake Simulation Facility at the Advanced Technology for Large Structural Systems (ATLSS) Center at Lehigh University.

1.2 Objective

The objective of this thesis is to document the details and characterization tests of a 0.6-scale 3-story steel test structure. This thesis describes detailed planning and construction of the test structure, the experimental setup, and measuring of the test structure static characteristics. It serves as a reference for the test program in which the test structure will be tested.

1.3 Scope of thesis

The work covered in this thesis is a follows. Chapter 2 presents background information of the use of dampers in building structural systems, the simplified design procedure, and the prototype structure. Chapter 3 discusses the layout and design of the 0.6-scale test structure, including the design details. Chapter 4 discusses the fabrication and experimental setup for the test structure. Also covered are the design of the loading system, reaction points, lateral bracing and other components of the test setup. Chapter 5 covers the instrumentation needed to measure deformations, reactions and internal

member forces in the test structure. Also covered is the assessment of other members forces and test frame reactions using measured responses and statics. Chapter 6 discusses the characterization of the DBF using static and sinusoidal testing. It includes the assessment of frictional forces in the test setup and the development of the frame's static stiffness matrix. Chapter 7 provides a summary and conclusions of the thesis and recommendations for future work.

Chapter 2.
Background

2.1 General

This chapter serves to provide background on the overall research project. It begins by discussing various types of supplemental damping devices for seismic hazard mitigation. It then discusses a simplified design procedure for designing structures with supplemental damping systems and concludes by describing the prototype structure that will be used for the NEESR studies at Lehigh.

2.2 Supplemental damping systems

Supplemental damping systems can be used to reduce the response of a structure subjected to seismic forces, and thus enhance the structure's performance. Supplemental damping systems accomplish this by supplementing the inherent damping in the structure. Damping devices can be passive, active, or semi-active devices. Their classification is based on how the damping properties of the device are controlled.

Passive damping devices are one in which the damper does not have the ability to change its properties. Passive dampers are widely used in the structural engineering community due to their simplicity and relative stability. Passive damping devices dissipate energy using a variety of methods including component yielding, friction, phase transformation in metals or deformation of visco-elastic solids or fluids (Soong and Spencer 2002).

In semi-active and active controlled damping devices their responses are monitored by a computer. The computer has a control law that modifies the characteristics of the damper to allow it to provide the appropriate level of damping that would better control the response of the structural system.

The test program discussed in this thesis considered two types of passive dampers (elastomeric dampers and viscous fluid dampers) and one type of semi-active damping device (magneto-rheological (MR) dampers). The elastomeric dampers use an elastomeric material compressed inside a steel tube section that provides damping through shear deformation of the elastomer and friction. One of the goals of a portion of the overall research project is to develop a new generation of these low cost dampers (Mahvashmohammadi, 2013). Figure 2.1 and Figure 2.2 show a single damper and the placement of a group of dampers in the test structure, respectively.

Viscous fluid dampers use a viscous fluid to produce a damping force. The viscous dampers used in this study were manufactured by Taylor Devices and can develop a maximum nominal damper force of 130 kips. Figure 2.3 is a schematic of a similar viscous damper manufactured by the Taylor Devices that is similar to the one used in this study and Figure 2.4 shows the placement of the viscous dampers in the test structure.

MR dampers have iron-carbon particles suspended in a fluid, where the particles are aligned using a magnetic field. Aligning the particles changes the viscosity of the fluid. This fluid passes through orifices near the circumference of the damper piston head, where a change in viscosity increases the damper force. The MR dampers used in this study are manufactured by the Lord Corporation and have a maximum nominal damper

force of 70 kips. Figure 2.5 is a schematic of an MR damper that is similar to the one used in this study. Figure 2.6 shows the placement of the MR dampers in the test structure.

2.3 Simplified design procedure

A simplified design procedure (SDP) for designing with supplemental passive damping devices has been developed by Lee et al. (2005). It differs from typical methods of designing structural systems with dampers, where instead of using numerical optimization algorithms to locate and size supplemental dampers for an existing structure the SDP uses practical analysis and a design procedure to integrate the design of the supplemental dampers into the structural design. The procedure involves designing the structural system for the code design strength and then uses dampers to meet performance objectives for the design (e.g., drift control or members remaining elastic.)

In the SDP a trial MRF of lateral stiffness K_o is selected. Then a range of values for the design parameters α (which represents the ratio of diagonal bracing lateral stiffness to MRF lateral story stiffness) and β (which represents the ratio of damper stiffness to MRF lateral story stiffness)is selected for the selected values of α and β a first-modal period for the structure and damping reduction factor, B, are determined, enabling the seismic coefficient for the design base shear to be established. An equivalent lateral force analysis is then performed. The design having the smallest α and β values that satisfies the design performance objectives is chosen. Based on the value for β, the dampers are then designed. This process can then be iterated to improve the MRF design. Figure 2.7 shows a flow chart of the SDP developed by Lee et al. using visco-elastic (VE) dampers.

2.4 Prototype structure

In order to evaluate the SDP a prototype structure was designed by Dong (2013) using the procedure. The prototype structure is assumed to be located in Southern California, with a Seismic Group of I, a Site Class of D, and a Seismic Category of D. It was designed using the 2006 IBC Code. The structure is three stories tall with a basement. It has a symmetrical floor plan consisting of 6 bays by 6 bays, with each being 25ft in width. Figure 2.8 shows the floor plan of the prototype structure, where moment resisting frames (MRF) and the damped braced frames (DBFs) are labeled. Because of the symmetrical layout of the building only one quarter of the building will be considered in the creation of the test structure. The seismic tributary area of the floor plan for the test structure is indicated in Figure 2.8. In the experimental study ground motions in only one direction are considered (e.g, North-South), therefore only one MRF and one DBF are considered for the test structure.

Assuming a rigid floor diaphragm (i.e. a composite slab) the DBF and MRF in the north-south direction are assumed to have the same drift in the test structure, are therefore aligned side by side in the test structure. Figure 2.9 shows an elevation of the test structure. The lean-on column represents the gravity load system within the tributary area. The seismic weight and mass of ¼ of the building floor plan is applied on a lean-on column at each floor level.

In developing performance objectives the seismic hazard levels defined by FEMA (2003) for the Maximum Considered Earthquake (MCE) and Design Basis Earthquake (DBE) are used. The MCE is defined as an earthquake having a 2% probably of occurrence in 50

years. The DBE is an earthquake with 2/3rds the intensity of the MCE with approximately a 10% probability of occurrence in 50 years. The performance objectives for the design of the prototype structure are as follows: (1) 1.5% maximum drift under DBE; (2) the DBF remains elastic under the DBE; and (3) 2.5% maximum drift under MCE. These performance objectives were incorporated into the design of the MRF and DBF using the SDP, see Figure 2.10 and Figure 2.11.

Further details of the specific design of the prototype structure appear in Dong (2013).

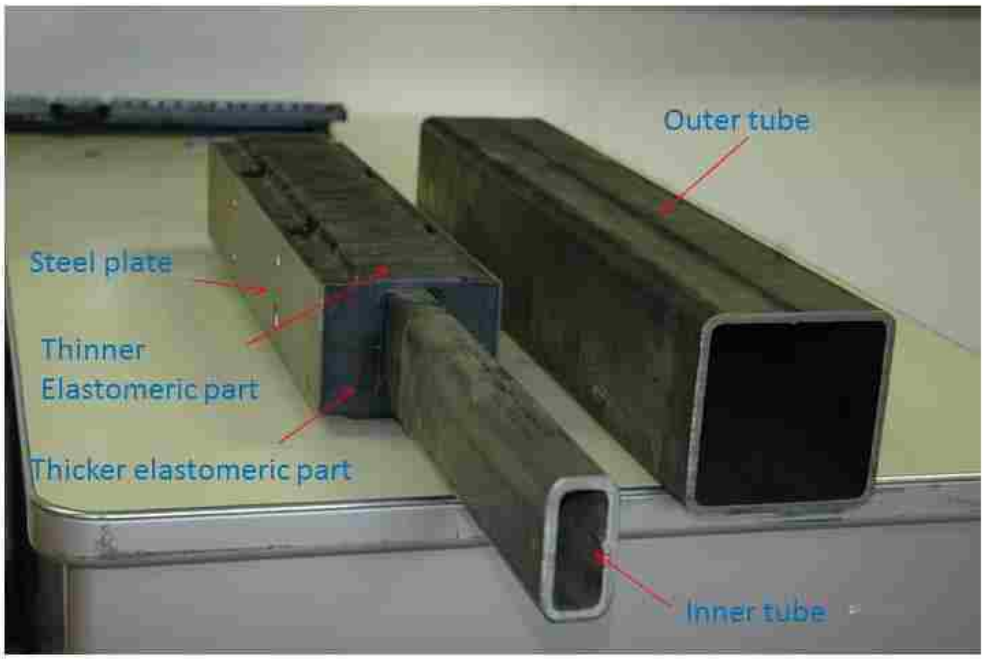

Figure 2.1 Elastomeric Damper Components (Mahvashmohammadi, 2013)

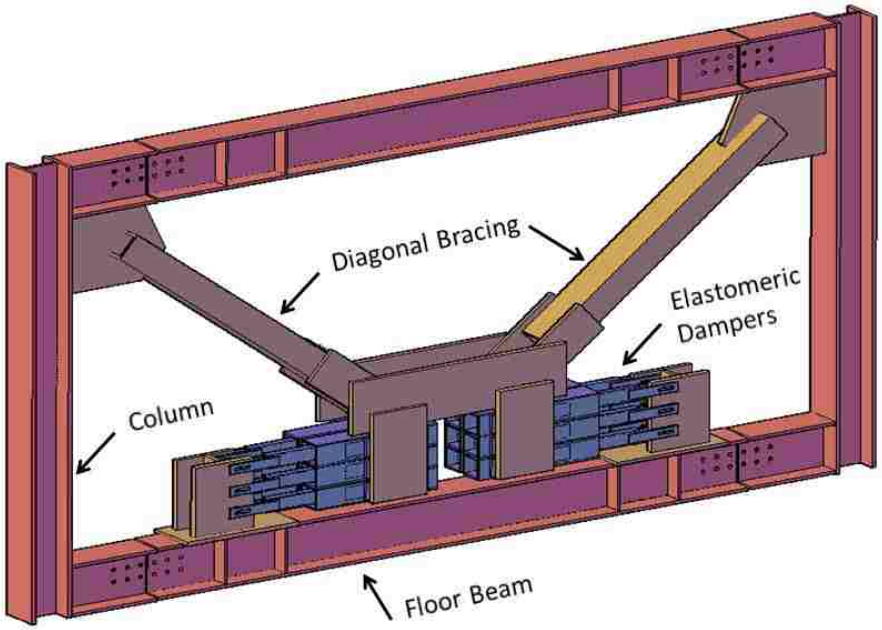

Figure 2.2 Elastomeric Damper Placement in DBF (Mahvashmohammadi, 2013)

Figure 2.3 Viscous Damper Manufactured by Taylor Devices (Dong 2013)

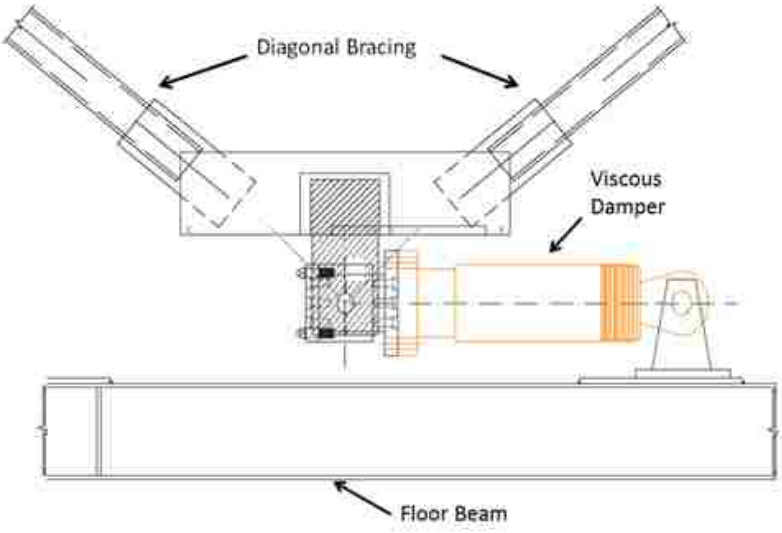

Figure 2.4 Viscous Damper Placement in DBF (Dong, 2013)

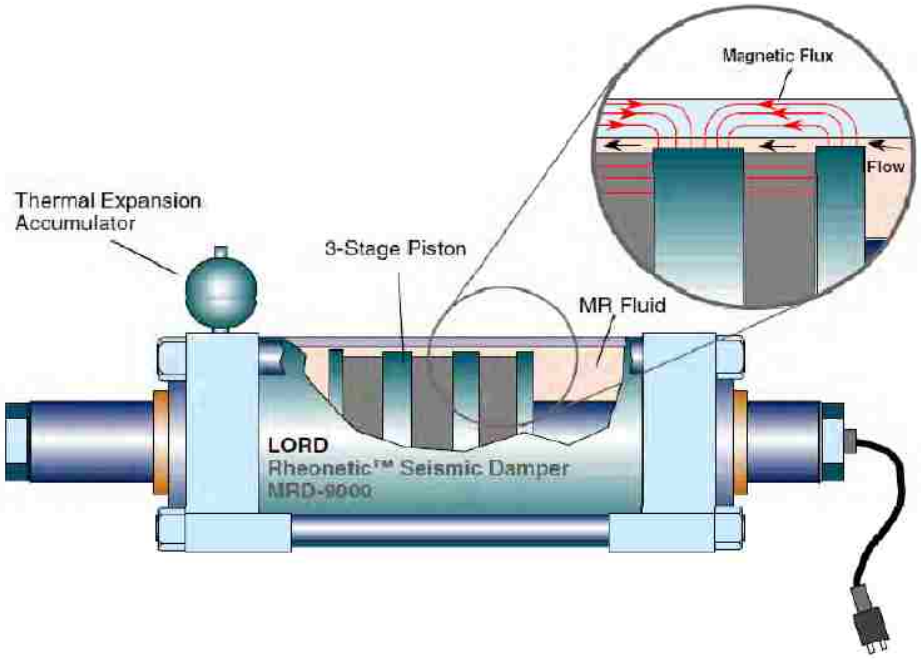

Figure 2.5 Schematic of the 1st Generation Large-Scale MR Damper Manufactured by Lord Corporation (Yang 2001)

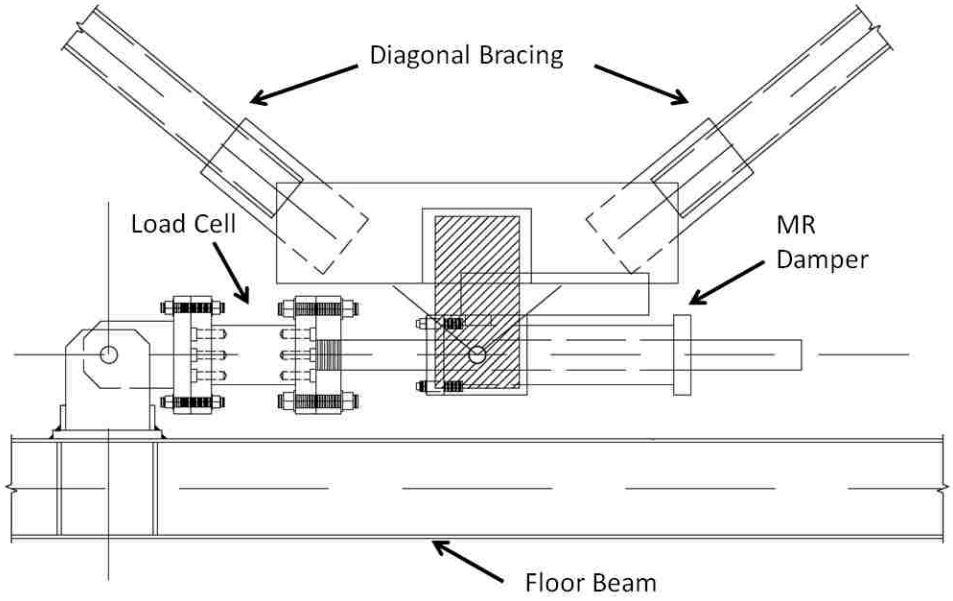

Figure 2.6 MR Damper Placement in DBF (Dong, 2013)

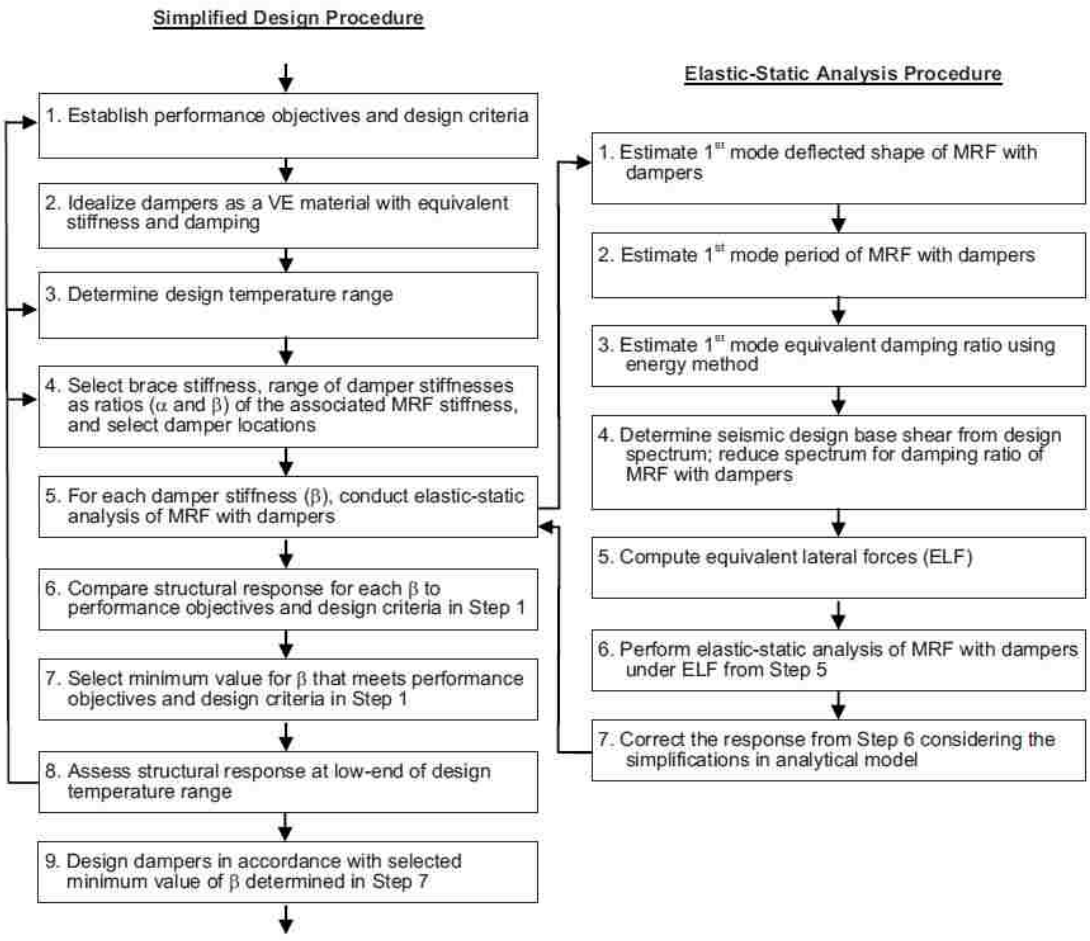

Figure 2.7 Simplified Design Procedure and Elastic-Static Analysis Procedure (Lee et al 2009)

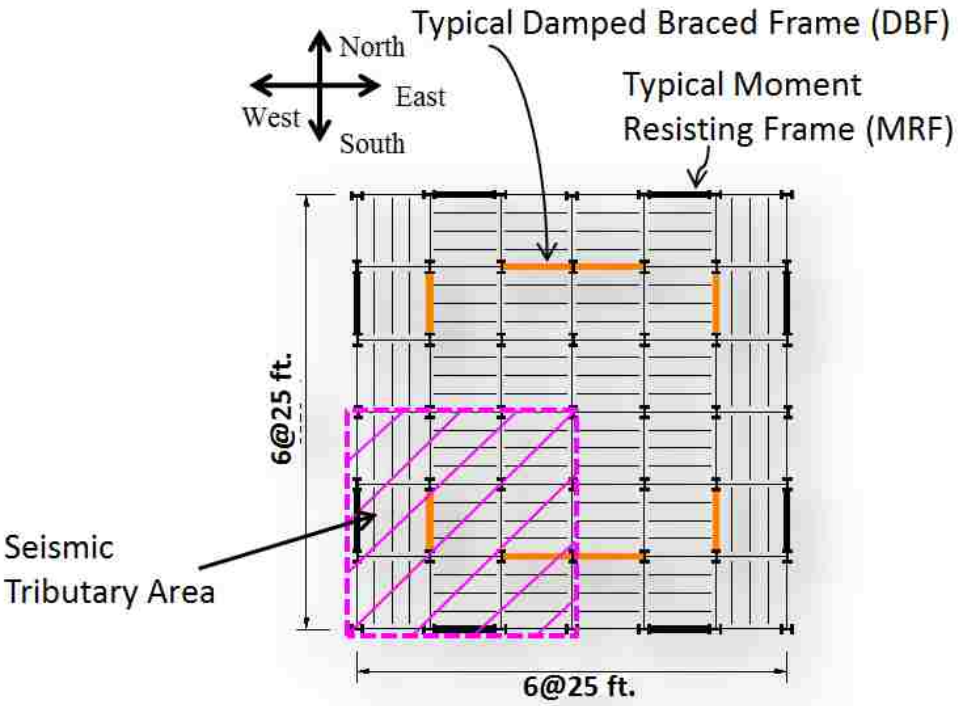

Figure 2.8 Plan View of Prototype Structure with Tributary Seismic Area Marked (Dong, 2013)

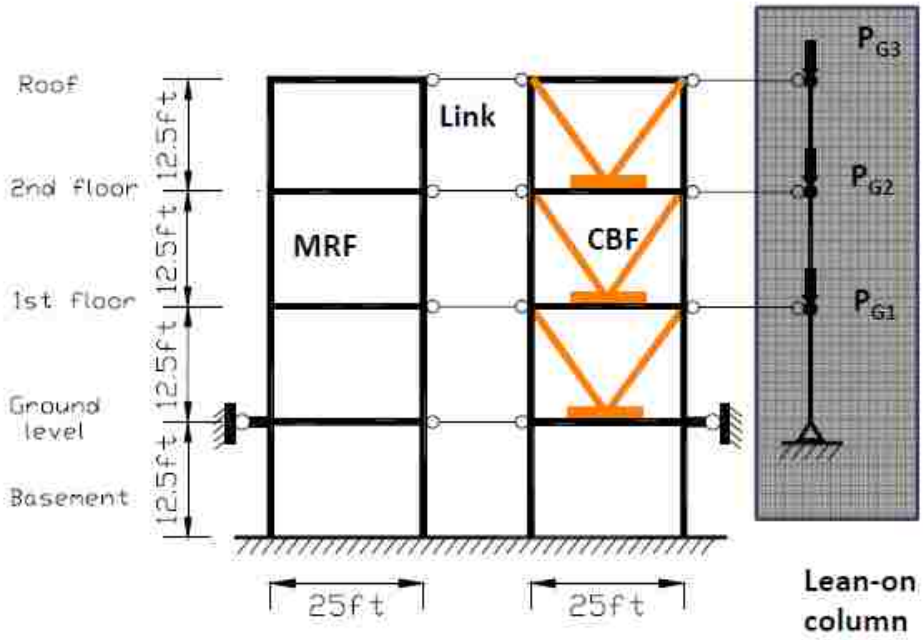

Figure 2.9 Elevation of Full Scale Prototype for Developing Test Structure (Dong, 2013)

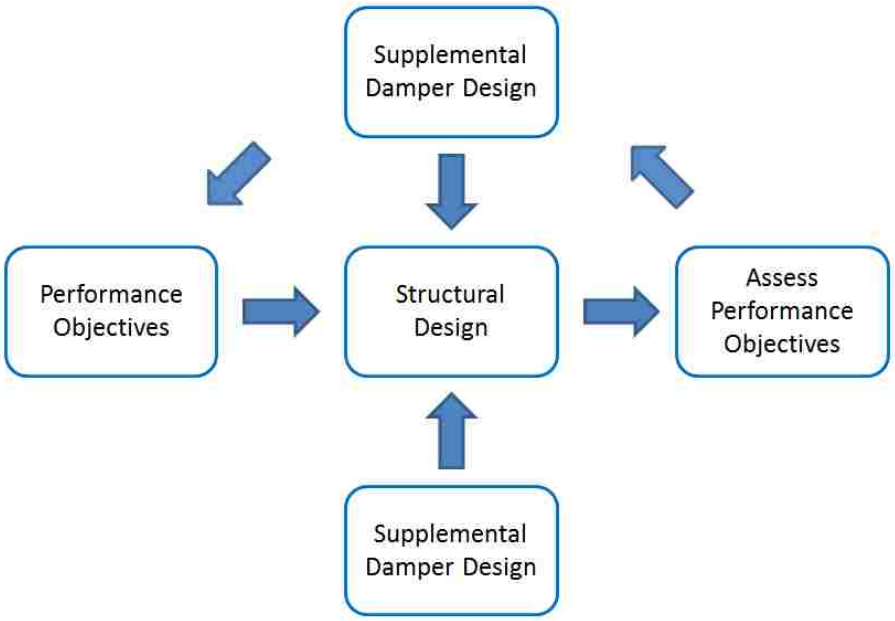

Figure 2.10 MRF Design Flow Chart (Dong, 2013)

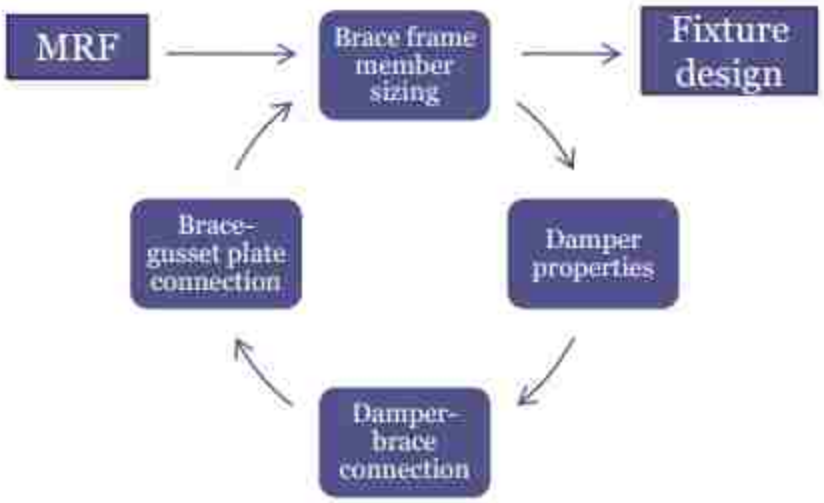

Figure 2.11 DBF Design Flow Chart (Dong, 2013)

Chapter 3.
Design of Test Structure

3.1 General

A scale model of the prototype structure had to be developed in order to allow for testing in the ATLSS laboratory. Based on space restrictions, a 0.6-scale model was chosen. To design this scaled model the bay widths and floor heights where scaled to 0.6 their original sizes. In order to allow the SDP to be used the lateral applied forces were scaled. (Dong, 2013) These scaled forces were then used to determine member sizes via the SDP. Figure 3.1 shows the scaled configuration of the frame, which will tested in the lab.

Using the SDP the MRF was designed first using 100 percent of the scaled design base shear. A summary of scaled lateral forces as well as distributed gravity loads used by Dong for the design of the MRF test structure are listed in Table 3.1 The MRFs beams and columns were designed for strength, where drift limits and other performance objectives are not considered at this point. In order to protect the beam-to-column welds the MRF was designed with reduced beam section (RBS) connections. These will be described in detail later.

After the MRF was designed, the damped braced frame (DBF) was designed based on the performance objectives that: 1) the system remain elastic under the DBE; and 2) the system develop no more than 1.5% story drift during the MCE. Because several different damper types are going to be used during the test program, the maximum expected

damper force for each type of damper had to be considered. The force from the elastomeric dampers controlled the design.

All structural steel sections used for the two frames is A992 Grade 50 steel. All plates used in the construction are A572 Grade 50 steel.

3.2 MRF design and layout

The moment frame of the test structure that was constructed for laboratory testing was a one bay three story MRF with RBS connections. The beams and columns used in both the prototype MRF and the scaled test specimen MRF are listed in Table 3.1. This scaled MRF will be used for numerous earthquake tests before it needs to be replaced. After the beams are damaged to the degree where they need to be replaced, they will be removed and replaced, but the columns will be reused for the next series of tests. With this in mind RBS connections were chosen. They will act as fuses and help protect the column from sustaining significant damage during a test, because they will yield before the column yields. These fuses will ensure that the connection satisfies a weak beam-strong column configuration. Additionally they will help protect the beam-to-column connection from damage which could result in low cycle fatigue. The selected RBS dimensions are shown in Table 3.3. Figure 3.2 shows an elevation of the layout of the MRF that was chosen.

3.2.1 **Beam-to-column connections**

The moment frame used for laboratory testing had two major objectives. The first objective was to function as much as possible as a traditional MRF and second was to be relatively easy to replace after sustaining damage. It was with these two goals in mind two different beam-to-column connection designs were considered. The first was a bolted

end plate connection. The second was a standard moment connection with fully welded flanges and a welded web.

The bolted end plate connection was considered because it could be easily replaced after the beam sustained damage during testing. It featured a beam with reduced beam sections cut into it and an endplate attached to either end of the beam with full penetration welds. These welds would be to detailed to satisfy the 2005 AISC Seismic Provisions (AISC 2005b). To connect the end plate to the column several bolts would be used. These bolts were sized to avoid overcoming their pre-compression force when the beam was subjected to combined axial tension force and moment. Once the beam had sustained damage the connections would be unbolted and replaced with another beam with end plates that had been prefabricated.

There were several drawbacks of the bolted end plate configuration. One was that it would be more costly than a traditional fully welded connection due to the costs associated with fabricating the end plates and the bolts. Another drawback was the difficulty in finding a bolt configuration that would satisfy the anticipated level of force in the beam without overcoming the pre-compression force in the bolts. This is important because any gap opening in the connection could affect the test results. Due to the width of the column flanges, only a limited number of bolts could be used in the connection. This number of bolts did not allow for a connection that would satisfy the requirement to not overcome the pre-compression force with either A325 of A490 bolts. The final drawback of this proposed connection type was that the bolted end plate is not a prequalified connection for seismic applications, as defined under the 2005 AISC Seismic Provisions (AISC 2005b).

Due to the limitations of the endplate design it was therefore decided that a traditional fully welded connection would be used. In designing this connection it was important to consider the purpose of the connection. Steel MRFs were developed in the 1960s and are designed to be ductile during seismic shaking. The design of these connections typically featured full penetration welds used to connect the beam flanges to the column and a shear tab that bolted to the beam web. However during the Northridge Earthquake of January 17, 1994 many buildings featuring this design suffered brittle fractures of their beam-to-column connections. In an effort to avoid this problem in future earthquakes, several studies of traditional moment frames were conducted. These included the SAC (2000) studies that subjected numerous moment connections to cyclic loading. It was determined that four primary factors led to the failures: 1) weld toughness; 2) weld access hole geometry; 3) inadequate panel zone strength; and 4) inadequately restrained beam webs. These factors were incorporated into the FEMA 350 (FEMA 2000) recommendations and later adopted in AISC 341-05 Seismic Provisions for Structural Steel Buildings (AISC 2005b) and AISC 358-05 Prequalified Connections for Special and Intermediate Steel Moment Frames for Seismic Applications (AISC 2006). All three of these documents were used to detail the connections for the MRF.

3.3 MRF details

The following describes the details of the MRF test structure and why they were chosen.

3.3.1 **Weld Access Holes**

Special consideration was given to the weld access hole geometry because studies have indicated that weld access hole geometry has a significant effect on the ductility of MRFs

(Ricles et al. 2004). These studies resulted in a specification for a modified weld access hole, which is included in the AISC seismic specification (AISC 2005b). Figure 3.3 shows a schematic of the modified access hole that appears in the specification. The exact weld access hole geometry used for the MRF beam-to-column connections is provided in Figure 3.4 through Figure 3.6.

3.3.2 **Panel Zone Design**

Special care was taken to not only follow but to exceed recommendations for panel zone strength in the MRF, because the frame will be used for numerous tests. Reinforcement consisted of continuity plates at all floor levels and doubler plates at the 1st, 2nd and ground floors.

3.3.2.1 Continuity Plates

Under the AISC 358-05 (AISC 2006) continuity plates are required for all SMRFs not meeting a very limited set of exceptions, which this frame did not meet. The provision allows for a one-sided connection like the one designed for this moment frame to have a continuity plate with a thickness that is at least one-half the thickness of the beam flange, but requires a two sided connection to have a continuity plate at least the full thickness of the beam flange. In an effort to minimize panel zone damage as much as possible in order to reuse the columns in future testing, a plate roughly as thick as the beam flange was chosen for each floor. Table 3.4 summarizes the plate size chosen as well as the beam flange size. All plates were A572 Grade 50 steel.

The design of each continuity plate was the same regardless of floor, because besides thickness the geometry depended on the column. Care was taken to fit the plates in such a

manner as to avoid welding in the columns k-region. Figure 3.7 shows the layout of the continuity plates. Each continuity plate was attached to the column web with a two sided ¼ inch fillet weld and to the column flange by a groove weld. Both welds used an E70-T1electrode. Details showing the placement of the continuity plates and welds can be found in Figure 3.8 through Figure 3.10.

The original design of the ground floor continuity plates would interfere with the bolts that attached the ground link to the frame, and therefore the continuity plate design had to be modified to accommodate the bolts. The easiest solution was move the continuity plates below the beam flange and add a second set and equal distance above the beam flange. The same thickness of plate was used for simplicity. A drawing of this configuration is shown in Figure 3.11; Figure 3.12 shows the final configuration with the ground link attached.

3.3.3 **Doubler Plates**

AISC 341-05 (AISC 2005b) requires panel zones to be able to resist the shear force created by the maximum expected beam moment developed at the column face. To check that this minimum thickness was sufficient, the shear demand associated with the maximum expected beam moment at the face of the column was compared to the panel zone shear capacity. The shear capacity was calculated using the following equation, which is based on the AISC Seismic Provision (AISC 2005b) and includes only the contribution of the column web and doubler plates to the panel zone shear capacity:

$$V_{pz} = 0.55 * F_y d_z (t_{cw} + 2t_{doubler}) \quad (3\text{-}1)$$

where:

V_{pz} = shear resistance of panel zone, kips.

F_y= the yield stress of the panel zone components, ksi

d_z= panel zone depth between continuity plates, inch

t_{cw} = thickness of column web, inch

$t_{doubler}$ = thickness of each doubler plate, inch

Only the third floor beam was able to achieve this requirement without additional strengthening. A pair of doubler plates was sized for the 1st, 2nd and ground floors that would allow this requirement to be met. In order to minimize shear buckling in the panel zone doubler plates during inelastic deformations the AISC Seismic Provisions (ASIC 2005b) require the panel zone to meet the following minimum thickness requirement:

$$t \geq (d_z + w_z)/90 \quad (3\text{-}2)$$

where:

t = thickness of column web or doubler plates or column web and doubler plates if plug welds are used, inch

w_z= panel zone width between column flanges, inch

Again the 3rd floor panel zone met this criterion. The doubler plates installed at the other floors however required plug welds in order to meet this requirement. In addition to the plug welds a half inch slot weld was used to attach the doubler plate to the column flange. Special consideration was taken to limit the size of the weld in the column k region. At

the top and bottom of the doubler plate a fillet weld was used. All welds were made using an E70T-1 electrode. Doubler plates were sized to continue about 5 inches above and below the beam. The final doubler plate sizes, along with column web thicknesses are summarized in Table 3.5 and drawings of beam-to-column connection details at each floor are show in Figure 3.8 through Figure 3.10.

3.3.4 **Weld criteria**

Weld criteria for the MRF welds was adapted from that used by Zhang (2005). All welds were specified to conform to the AWS 5.20-95 Specification and Section 4.2 of AWS D1.1/D1.1M:2005 (AWS 2005), and were performed using the flux core arc welding procedure. An E70T-1 electrode was used for all “shop” welds, and an E7018 electrode was used for the flange and web full penetration welds. All welds used to fabricate the frames had a minimum Charpy V-Notch toughness of 20 ft-lbf at -20°F and 40 ft-lbf at 70°F by AWS classification test methods. Further details about the welding of these connections are presented in Chapter 4.

3.4 DBF design and layout

The Damper Braced Frame (DBF) test structure was designed by Dong to be used as a test bed for testing various dampers (Dong 2013). It was designed to remain elastic during all testing to allow it to be used numerous times. The DBF is a three story one bay structure with an inverted chevron bracing configuration. The columns are W8x67 sections, the beams are all W12x40 sections and the braces are HSS8x6x3/8 sections. An overall layout of the frame is shown in Figure 3.13.

The frames beams are not continuous but have a T-section connection located 2ft from the centerline of the column. The purpose of the connection is to allow for a pinned connection that would limit the moment developed within the gusset plate region. In order to avoid slipping in the T-section connection a set of tapered pins were used in addition to bolts. This connection was designed to transfer only shear and axial force in the beam and thus act like a pin. Figure 3.14 shows a schematic of this connection. Further details of this connection including design forces are available in Dong (2013). Also shown in Figure 3.14 are details of the upper gusset plate and beam-to-column connection.

The DBF was detailed by Dong and further details can be found in his dissertation (Dong, 2013).

Table 3.1 - MRF Test Structure Design Loads

Floor	0.6-scale Test Frame
1st Floor Lateral	89 kips
2nd Floor Lateral	62 kips
3rd Floor Lateral	44.6 kips
Distributed Dead Load	0.17 klf
Distributed Live Load	0.13 klf

Table 3.2 - MRF Member Sizes

Member	Prototype MRF	0.6-scale Test Structure
Columns	W14X176	W8X67
Ground Floor Beam	W30X124	W18x46
1st Floor Beam	W30X124	W18x46
2nd Floor Beam	W21X122	W14x38
3rd Floor Beam	W16x50	W10x17

Table 3.3 – 0.6 Scale Test Structure RBS Dimensions

Location	a (in)	b (in)	c (in)
1st Floor Beam	4.5	13	1.4375
2nd Floor Beam	4.5	12	1.375
3rd Floor Beam	4.5	8.5	0.875

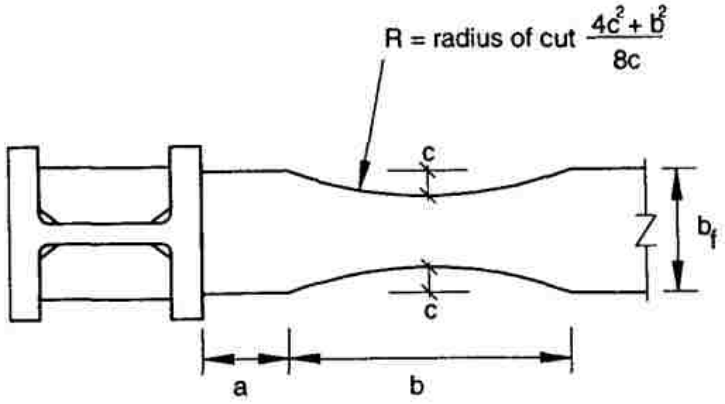

Table 3.4 – 0.6 Scale Test Structure Continuity Plate Sizes

Floor	Continuity Plate Thickness (in)	Beam Flange Thickness (in)	Steel Type
Ground	0.625	0.605	A572 Gr50
1st	0.625	0.605	A572 Gr50
2nd	0.500	0.515	A572 Gr50
3rd	0.313	0.330	A572 Gr50

Table 3.5 - 0.6 Scale Test Structure Doubler Plate Sizes

Floor	Doubler Plate Depth Above Beam (in)	Plate Thickness (in)	Web Thickness (in)	Steel Type
Ground	5	0.375	0.605	A572 Gr50
1st	5	0.375	0.605	A572 Gr50
2nd	5	0.3125	0.515	A572 Gr50
3rd	-	-	0.330	A572 Gr50

Table 3.6 - DBF Member Sizes

Member	Prototype DBF	0.6-scale Test Structure
Columns	W14X176	W8X67
Ground Floor Beam	W	W12x40
Beams	W	W12x40
Braces	HSS	HSS8x6x3/8
Tees	-	WT5x15

Table 3.7 – 0.6 Scale Test Structure DBF Components

Component	Gusset Plate Thickness (in)	Steel Type
Upper Gusset	0.375	A572 Gr50
Lower Gusset	0.5	A572 Gr50

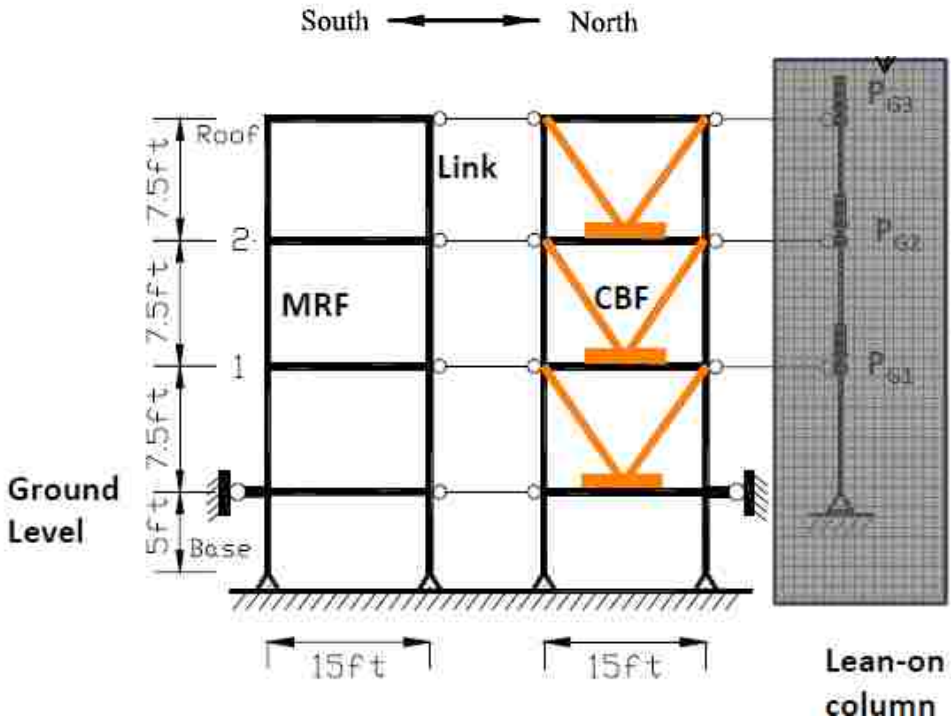

Figure 3.1 Elevation of 0.6-Scale Test Structure (Dong, 2013)

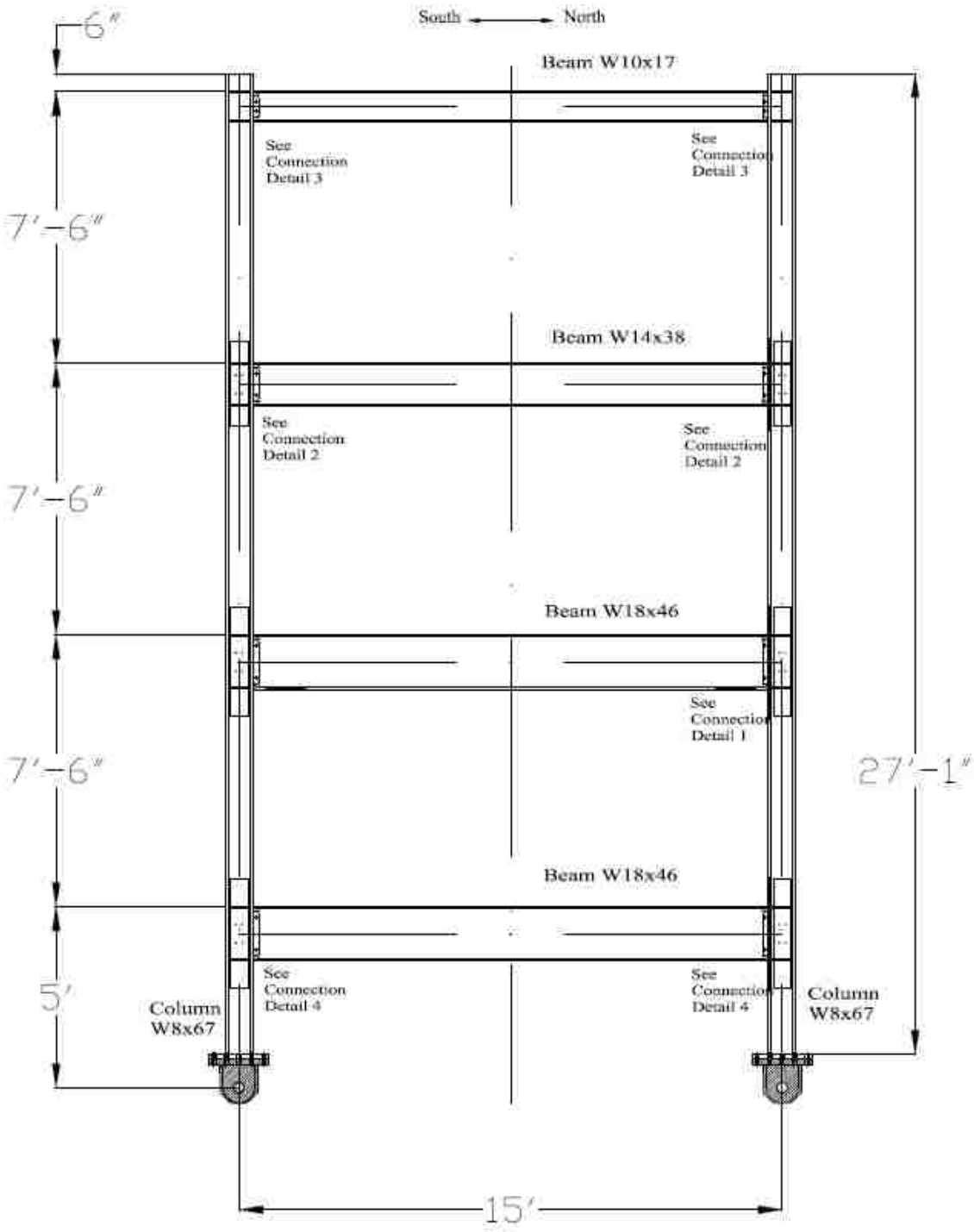

Figure 3.2 – Elevation of MRF Test Frame

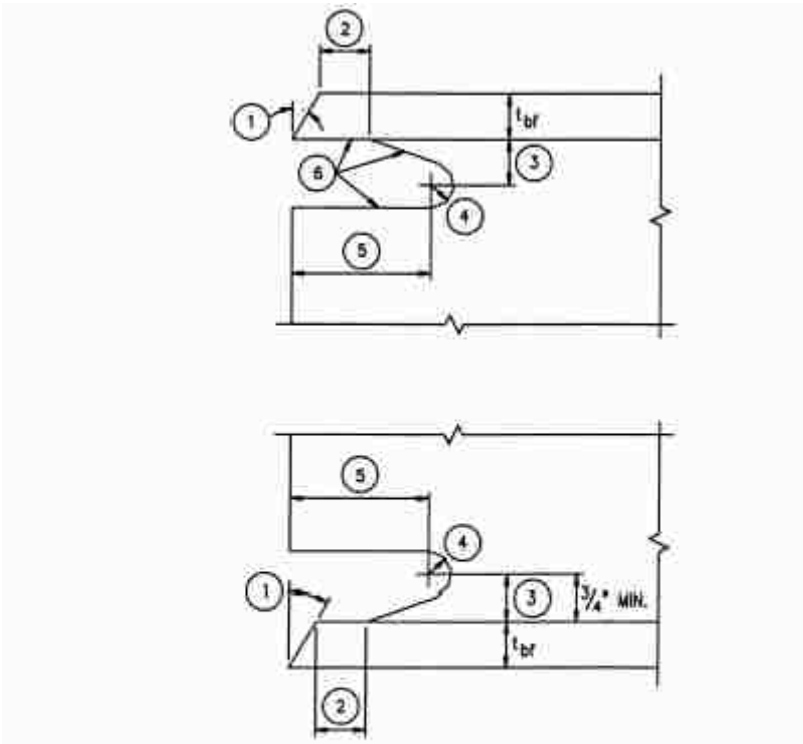

Notes: 1. Bevel as required by AWS D1.1 for selected groove weld procedure.
2. Larger of t_{bf} or $^1/_2$ in. (13 mm) (plus $^1/_2$ t_{bf}, or minus $^1/_4$ t_{bf})
3. $^3/_4$ t_{bf} to t_{bf}, $^3/_4$ in. (19 mm) minimum ($\pm\,^1/_4$ in.) ($\pm$ 6 mm)
4. $^3/_8$ in. (10 mm) minimum radius (plus not limited, minus 0)
5. 3 t_{bf} ($\pm\,^1/_2$ in.) ($\pm$13 mm)

Figure 3.3- Modified Weld Access Hole Details (AISC 2005)

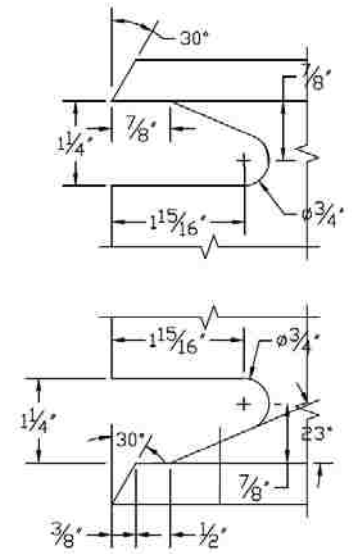

Figure 3.4 - 1st Floor Weld Access Hole Details

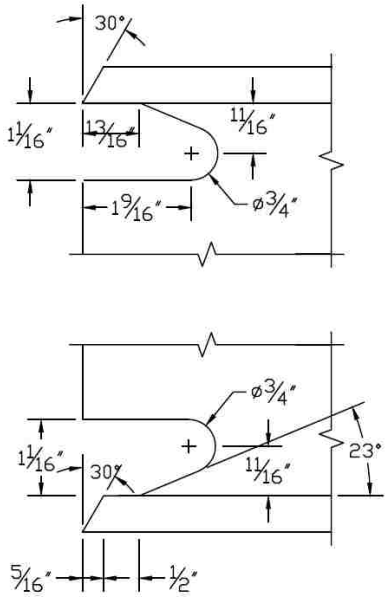

Figure 3.5 - 2nd Floor Weld Access Hole Details

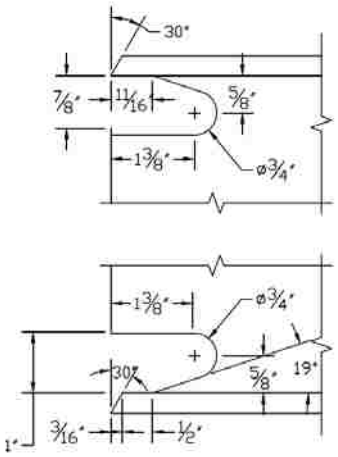

Figure 3.6- 3rd Floor Weld Access Hole Details

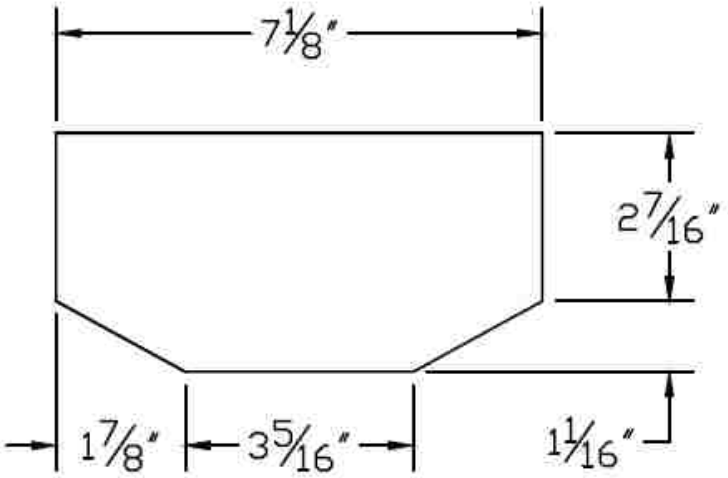

Figure 3.7 - Continuity Plate Details

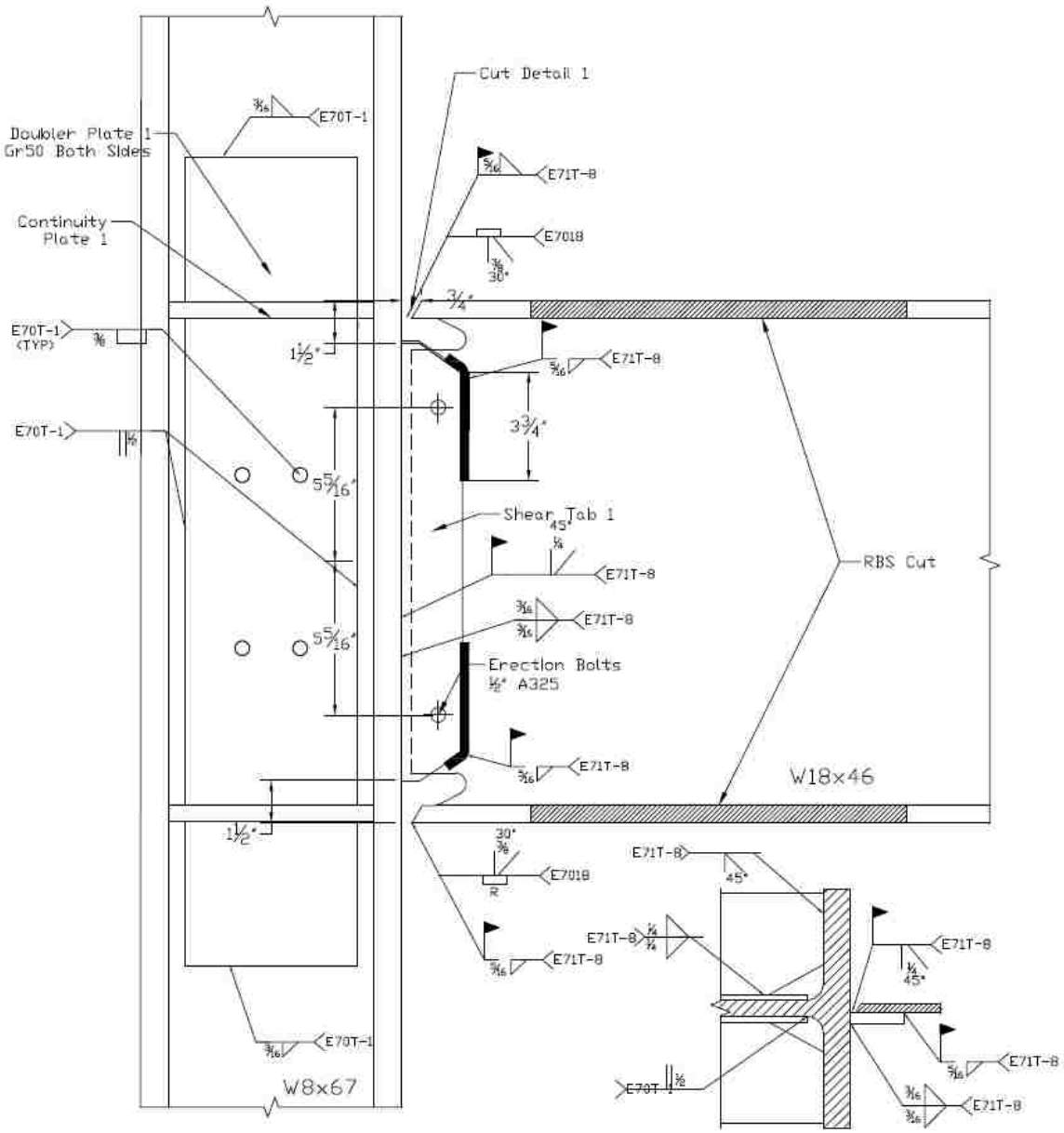

Figure 3.8 – MRF 1st Floor Beam-to-Column Connection Details

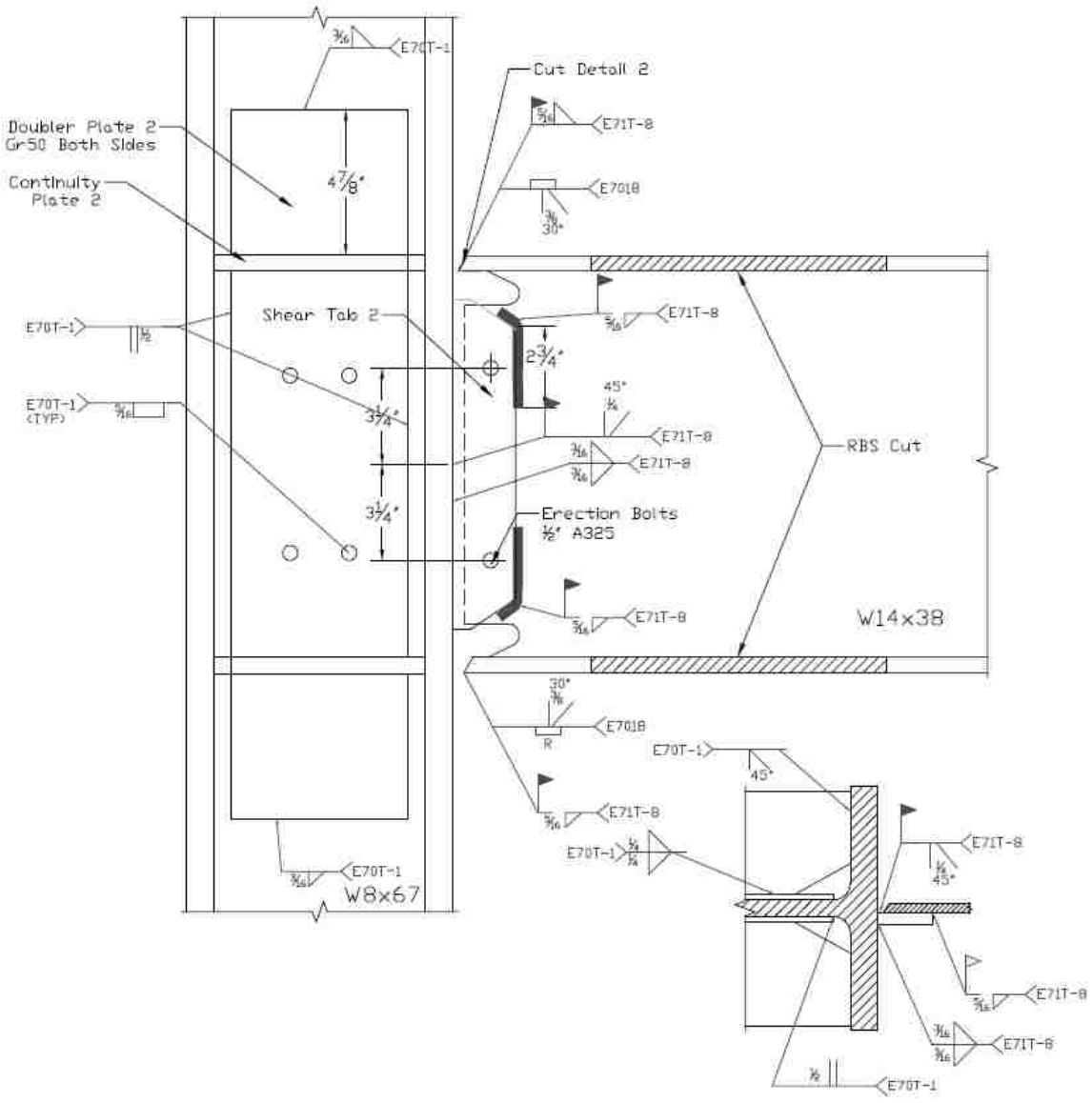

Figure 3.9 – MRF 2nd Floor Beam-to-Column Connection Details

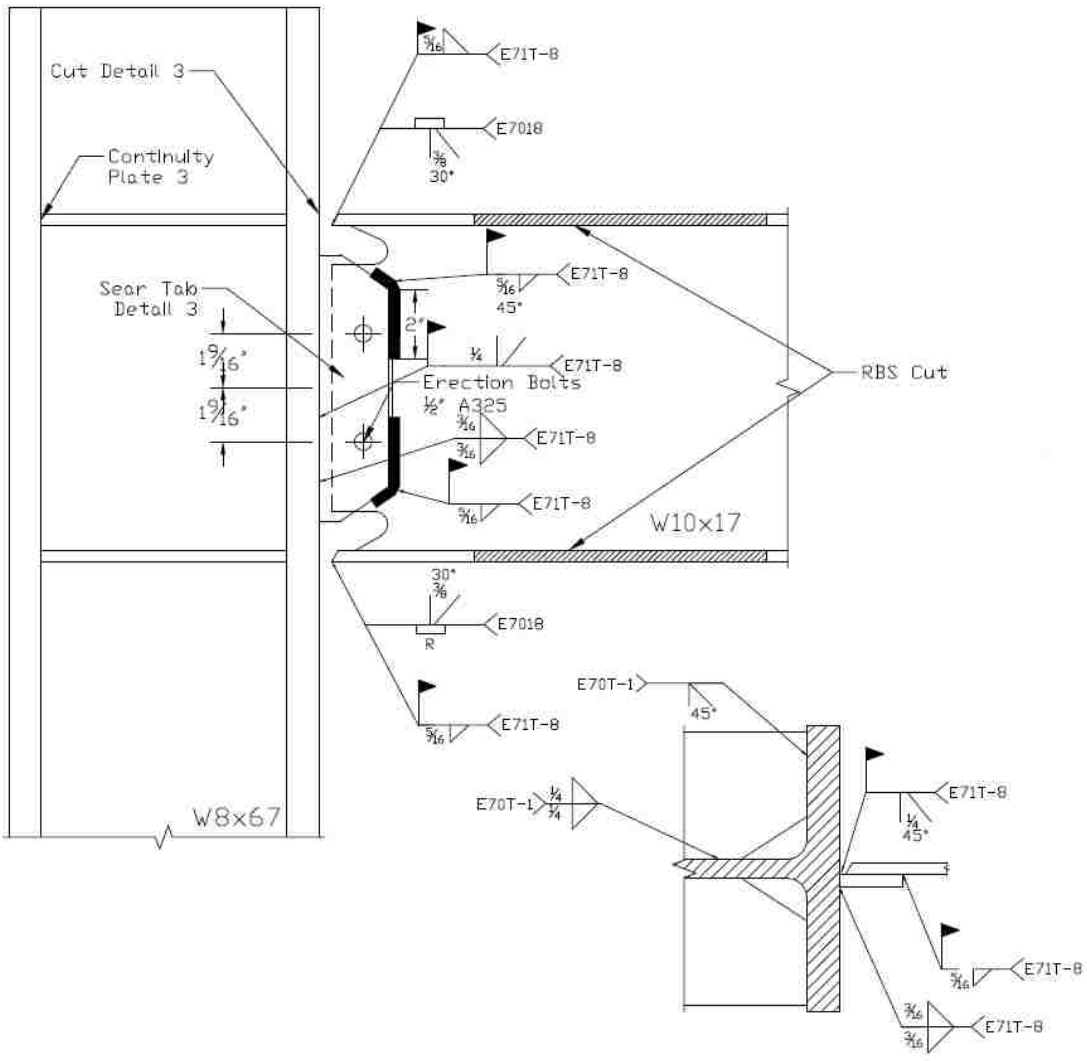

Figure 3.10- MRF 3rd Floor Beam-to-Column Connection Details

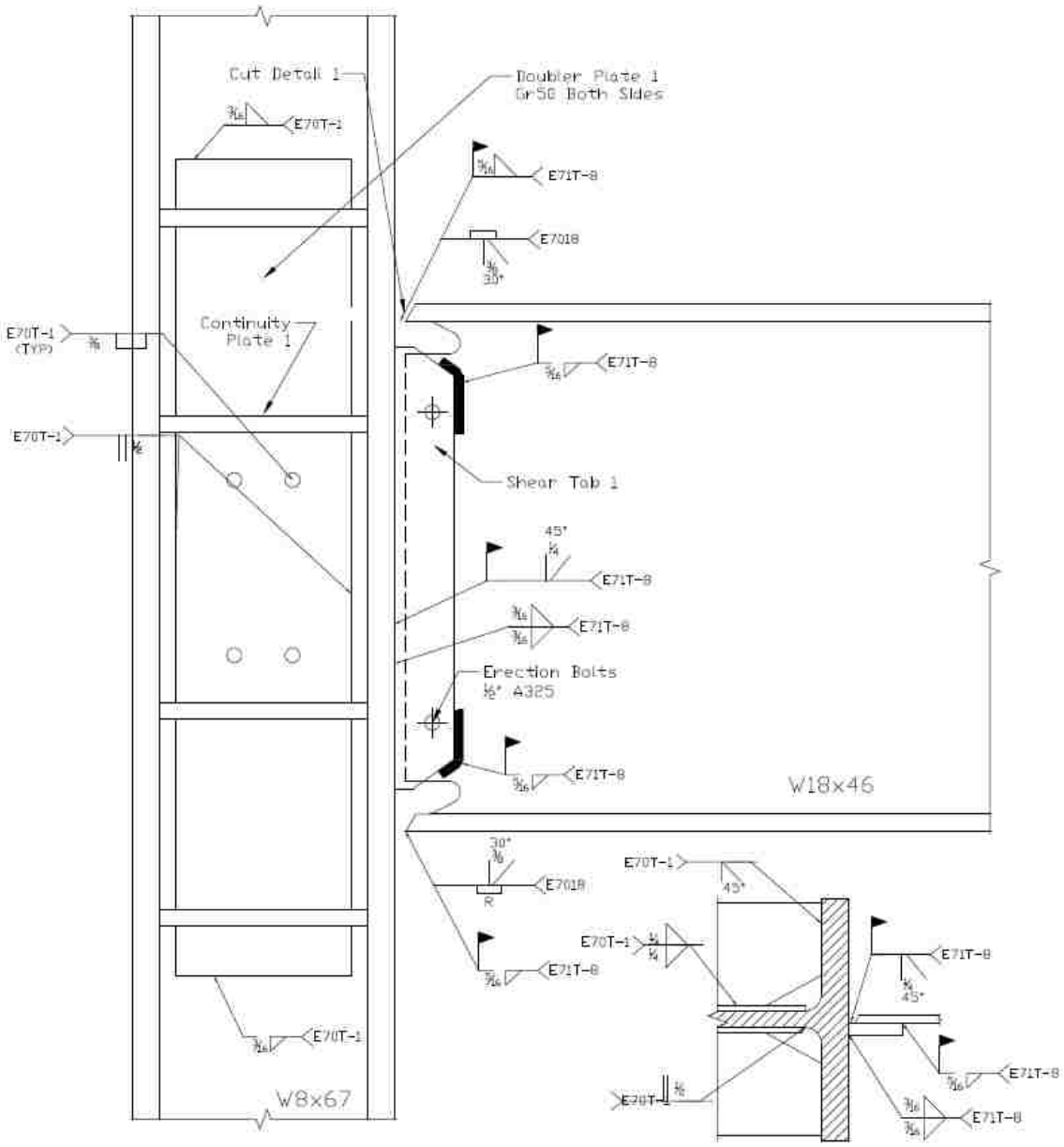

Figure 3.11 - MRF Ground Floor Beam-to-Column Connection Details

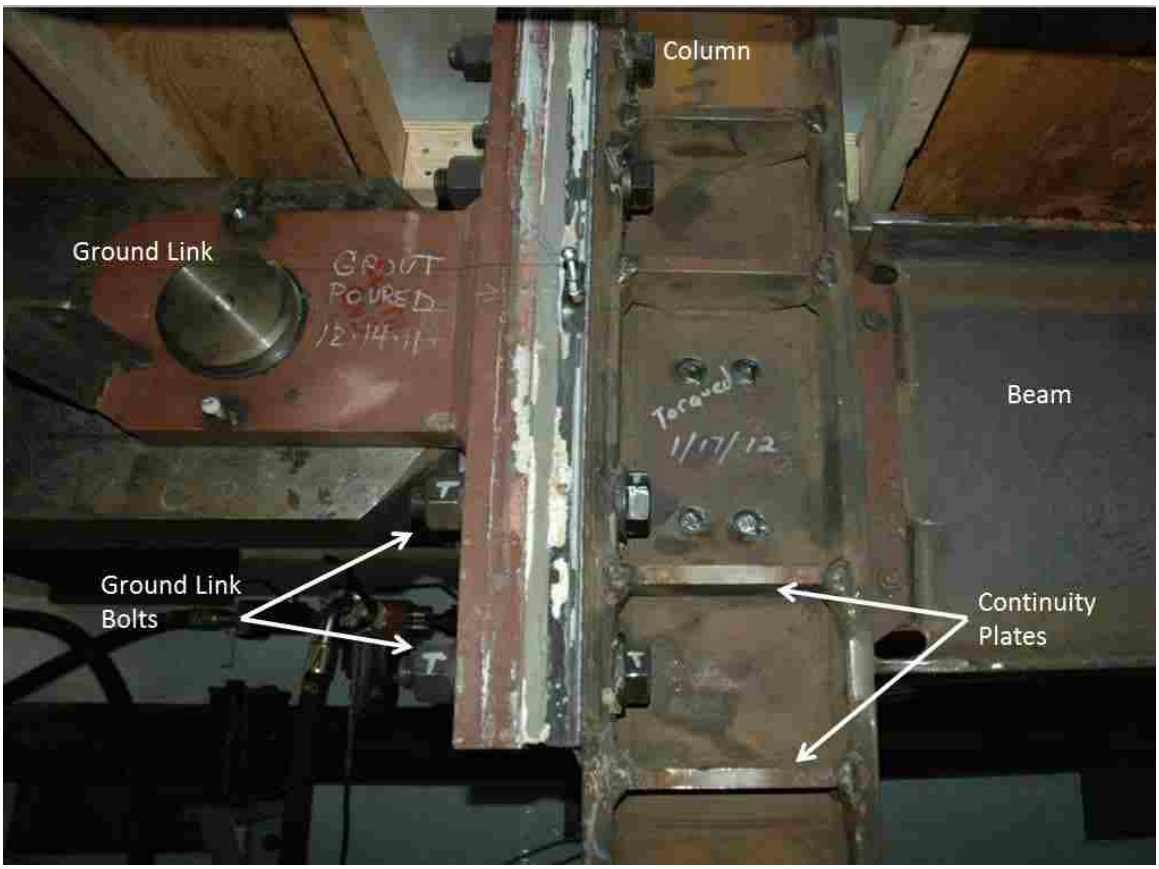

Figure 3.12 - MRF ground floor beam-to-column connection

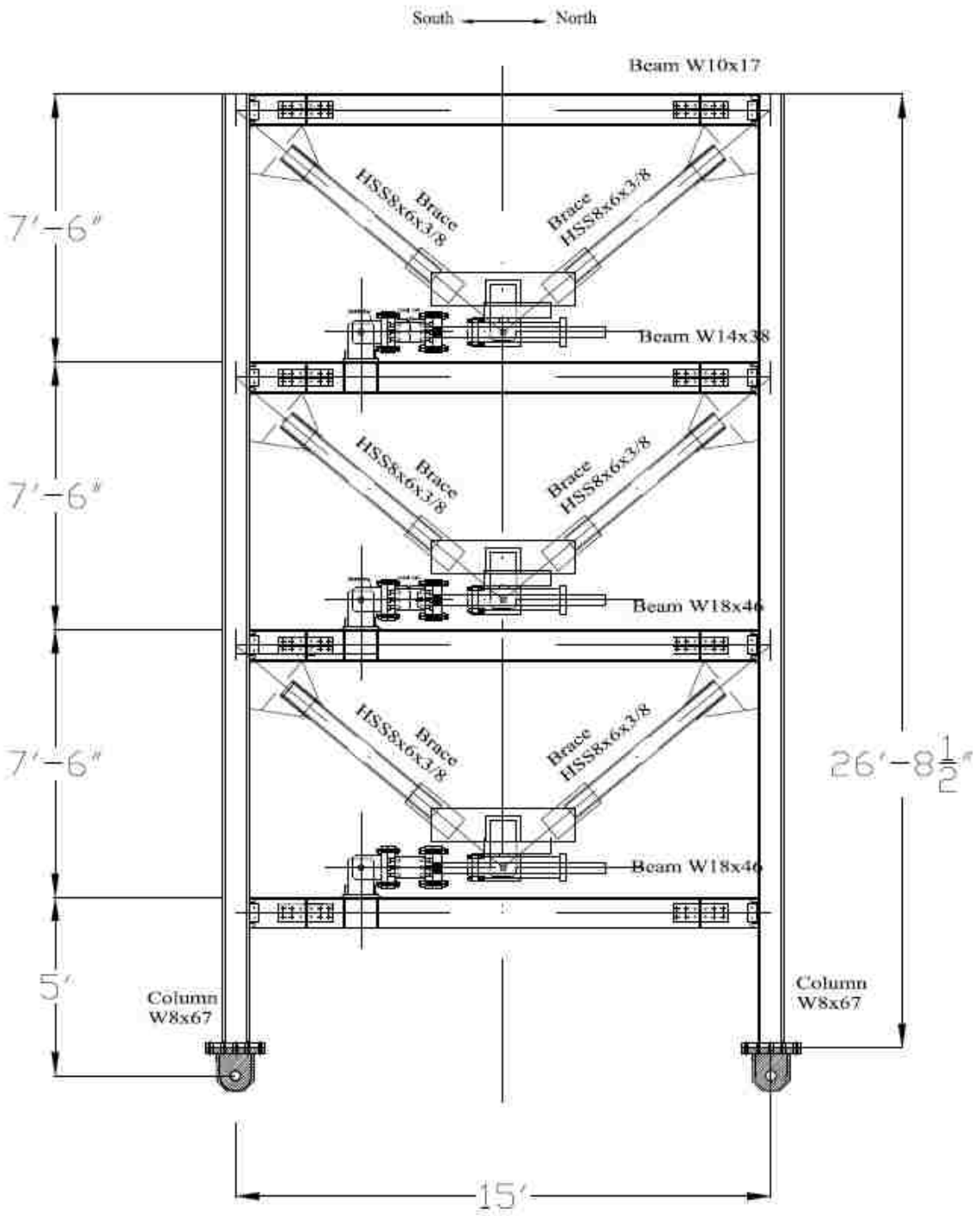

Figure 3.13 – Overall elevation of DBF

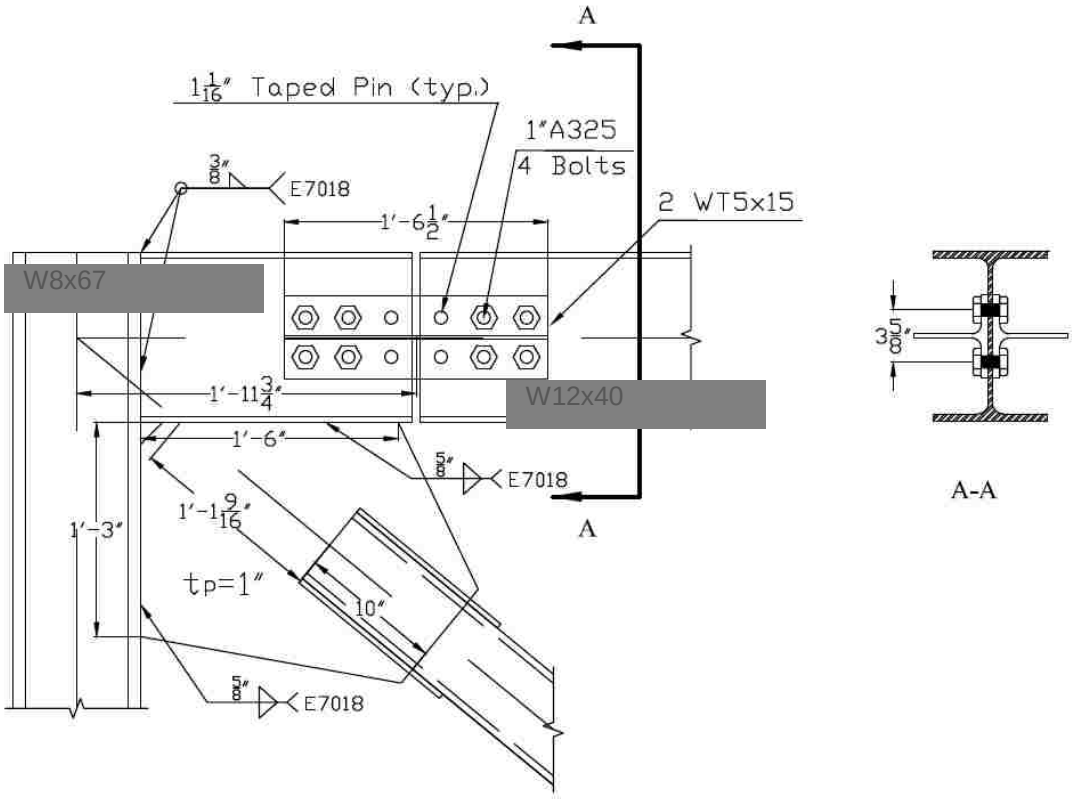

Figure 3.14 – Roof Level DBF Beam-to-Column and T-Section Connection Details

Chapter 4.
Experimental Setup

4.1 General

This section describes the fabrication and erection of the DBF and MRF of the test structure. It also describes the experimental test setup for the test structure. The test setup consists on the components shown in Figure 4.1 through Figure 4.5. These components include the MRF and DBF, 3 actuators, an external bracing frame to provide out of plane bracing while allowing in plane movement, a set of loading beams at each floor to apply lateral forces from the actuators, a pair of ground links and a bay link. Details of the loading system, out-of-plane bracing of the structure and ground links are provided in this chapter.

The DBF frame was constructed and installed prior to the MRF frame being constructed. This allowed the DBF to be tested independently. Modifications made to the original test setup to allow the MRF to be tested are noted in this chapter.

4.2 Fabrication and erection

Both frames were constructed at the ATLSS Center.

4.2.1 Measured section properties

The member sections and components were measured when they arrived from the mill. This information was needed for use in instrumentation calibration. The measured and nominal section properties are listed in Table 4.1 and Table 4.2.

4.2.2 **DBF fabrication**

The DBF was fabricated in the horizontal position as shown in Figure 4.6. It was then moved to the test setup to be tested. Figure 4.7 shows the DBF in the bracing frame. After it was placed in the bracing frame the ground links were attached to the columns. The loading beam support shelves were then attached to the columns. The loading beam system was then installed and posttensioned to 500 kips. The loading beam to frame connection was installed at this time. External bracing was then added to brace the beams.

Due to the initial availability of only one actuator, a single actuator was installed for a brief period of testing, and then the other two actuators were attached. More details of the fabrication and erection can be found in Dong (2013).

4.2.3 **MRF fabrication**

The MRF was fabricated in several phases. The first phase of frame construction consisted of cutting the beams to the appropriate length. Once this was completed the beams were laid out and the reduced beam sections cut. This was done with a template to ensure that each beam was cut to the same precision. Once the section was laid out the RBS section was cut using a torch. After cutting, the profile was then ground to a surface roughness of 250 μinch using various grinding tools, finishing with a pencil grinder. The RBS was inspected to ensure that the proper dimensions had been reached and the proper maximum roughness had been achieved. Figure 4.8 shows the completed 2nd floor reduced beam section prior to assembly.

The next phase involved prepping the ends of the beams to allow the full penetration welds to the column to be made. This prep work included beveling both the web and the flange of each beam, drilling erection bolt holes and fabricating the weld access holes. The weld access hole profiles specified in Figure 3.4 through Figure 3.6 were used. The beam webs were beveled to 45º and the flanges were tapered to 30º. Figure 4.9 shows the completed 2nd floor beam end detail.

The columns also needed to be prepped. The first part of prepping the columns involved installing doubler plates. While welding the plates to the column flange care was taken to avoid buildup of weld in the k region of the column as this would lead to cracking. After doubler plates were installed continuity plates were installed on the beams. Finally, shear tabs were installed at each floor to attach the beams to the column. These shear tabs served two purposes. First they aided in the erection and alignment of the frame. And secondly they served as permanent backing bars for the beam web-to-column full penetration weld. Doubler plates were also installed at this time. The welds connecting the doubler plates to the column were all made using an E70-T1 electrode. Figure 4.10 shows the second floor column with all plates welded into place.

For efficiency, the MRF was bolted together using ½ inch erection bolts placed through the shear tabs in the horizontal plane. Bolting it horizontally assured that the frame was both square and plumb. Figures Figure 4.11 and Figure 4.12 show the frame being assembled in this manner. The column base plates were tacked into position at this time. Also while in this position backing bars and runoff tabs were installed on the flanges to allow the beam flange full penetration weld to be completed later. Two welds between the beam web and the shear tab, reinforcing each shear tab was also placed at this time.

To weld the beam webs the frame was tipped on its side as shown in Figure 4.13. This was done to allow easy access to the welds. It was felt that it was not necessary to replicate the typical field condition (vertical) for these welds because they were less likely to fail then the beam flange welds. Figures 4.14 and 4.15 show the 3rd floor web before and after welding.

The frame was then positioned vertically to complete the flange welds. This was done in an effort to simulate field conditions. These welds carry the most force and are the most likely to fail so it was important that they were done as close to field conditions as possible. Figure 4.16 shows the frame in the configuration that the flange welds were completed. The beam flange welds were made using multiple passes to fill the groove. While the frame was in this vertical configuration the base plates were welded to the columns. Figure 4.17 and Figure 4.18 show the ground floor beam top flange and 2nd floor bottom flange prior to welding and Figure 4.19 and Figure 4.20 show the same flanges after welding, prior to the removal of the runoff tabs. Figure 4.21 shows a flange after the removal of the runoff tabs.

After welding was complete the full penetration welds were tested using the ultrasonic testing method. The welds were certified using the static loading criteria of AWS D.1.1-2010 Article 6 Part F. One weld failed inspection, and was subsequently repaired and reinspected. It subsequently passed. A copy of the ultrasonic testing report is available in the Appendix.

After all welding was completed the backing bars and run off tabs on the lower flange of all beams were removed and the weld was backgouged to bare metal. A reinforcing weld

was then applied. The run off tab from the top flange was removed but the backing bar was left in place. The welds were then profiled. Figure 4.21 shows a representative weld profile. The web welds were left as they were and were not profiled.

Shelves to support the loading beams were attached then attached to the columns. Details of these shelves are discussed in section 4.3.2. After the frame had been completely welded all strain gauges and full bridges were installed, prior to the test frame being placed in the bracing frame. Small holes were drilled into the top of the columns in order to attach rigging to lift the frame. This was done to avoid yielding the 3rd story beam. The frame was lifted into the bracing frame and attached to the base crevices. With the test specimen in place the loading beam extensions described in section 4.3.2 were put in place and the ground link and bay link were installed. Finally lateral bracing was installed to support the test specimen.

4.3 Loading system

The test structure was loaded at each floor level by one hydraulic actuator. The actuators have a stroke of ±500 mm (±19.7 inch). The first floor actuator (model 200-100-1700) has a capacity of 2300 kN (517 kips) while the second and third floor actuators (model 200-100-1250) have a capacity of 1700 kN (382 kips). A summary of the hydraulic characteristics of the actuators can be found in

Table 4.3. Figure 4.22 shows the dimensions of the actuators.

4.3.1 **DBF loading system**

The actuators were attached to the DBF frame using a set of loading beams. Each set of loading beams consisted of a pair of HSS 12X12X3/8 beams with two 1.5 inch Dywidag® rods threaded through each beam. The rods were connected to a mounting plate on the actuator on the north end and to a steel I-section on the south end. This configuration is shown in Figure 4.23 through Figure 4.26. The whole system was then posttensioned to 500kips to ensure that it would not develop any decompression during testing. The loading beams were supported on shelves, which were also used to laterally brace the columns as shown in Figure 4.27.

To attach the loading beams to the DBF a load attachment was designed. This attachment needed to serve two purposes: 1) it had to allow force transfer force from the loading beams to the DBF without slipping; 2) it had to be detachable in order allow characterization testing of the MRF of the test structure. To achieve these goals a series of bolted and welded plates was developed. Designs for this connection can be seen in Figure 4.29 and Figure 4.28. Note that the lower plate has tapped holes while the upper plate has smooth holes. This prevents the connection from slipping and still allows it to be detached for future MRF characterization, thus accomplishing both goals of the connection. This connection was designed for 200 kips of axial force in each tube.

4.3.2 **MRF loading system**

Due the fact that characterization testing of the MRF and DBF was to be conducted in two phases, the initial loading beam configuration had to be modified to allow the MRF to be loaded. This involved adding an additional 19’-2” to the loading beams. In order for this to happen the loading beam end piece at the south end of the DBF was removed from the original loading beam configuration and moved to the south side of the MRF. A 19’-

2” long section of loading beam was added and the Dywidag® rods were lengthened using couplers. The beams were spliced using the series of welds and lap plates shown in Figure 4.30. The splice was designed to carry 300 kips in each beam for a total of 600kips, which exceeds the capacity of the actuator. The final configuration for loading both frames is shown in Figure 4.31.

The four Dywidag® rods were each tensioned to 125 kips to posttension the beam and actuator attachment assembly together with 500kips of force thus ensuring that during testing no decompression would occur.

In order to support the beams a pair of shelves was attached to each column. The beams then rested on these shelves. These shelves were similar to the shelves on the DBF, but it was important to make the shelves on the MRF detachable so that once the frame sustained damage it could be lifted up to repair the beams. Figure 4.32 shows the layout of this system of shelves.

4.4 Bracing of test structure

The test specimen will be tested in the north-south direction and thus needed to be braced in the east-west plane, henceforth referred to as out-of-plane.

4.4.1 **Bracing frame**

A pair of bracing frames were used to brace the MRF and DBF of the test structure in the out-of-plane direction. These frames were designed for a previous test conducted by Herrera (2005) and were subsequently modified by Gonner (2009). An elevation of the

bracing frames is shown in Figure 4.33. The test structure is braced off of the loading beam system, which is in turn braced by the bracing frame.

In order to allow placement and removal a previously tested frame the south most two columns (columns 1 and 2 of Figure 4.33) of the east bracing frame were cut 1 foot above the lowest beam. In order to test the MRF this had to be repaired. A bolted connection was designed that would allow this section of the bracing frame to be removed to allow test frames to be easily installed and removed. Figure 4.34 through Figure 4.37 shows details of this connection. The connection was design to carry the full axial load and bending moment of the column.

4.4.2 **Loading beam bracing**

To brace the loading beams an adjustable plate system was used. This plate system had a sheet of Teflon® PTFE mounted to each plate where it contacted the loading beam. The beam also had a sheet of Teflon® PTFE mounted to it. These sheets reduced the friction between the plate and the beam. Figure 4.38 shows this bracing system. The plates were able to be adjusted in order to reduce the friction while still allowing the beam to be braced.

4.4.3 **DBF lateral bracing**

At each quarter point of the beams of the DBF lateral bracing is provided by the loading beams and a series of plates. Figure 4.39 shows the locations of these lateral braces and Figure 4.40 shows the details for the individual braces used to brace the beams. The columns were braced at each floor level using the detail shown in Figure 4.27. This detail also served to support the loading beams.

4.4.4 **MRF lateral bracing**

The MRF was laterally braced in a manner similar to that of the DBF. A lateral bracing layout was developed that would allow the MRF beams to conform to AISC seismic requirements for lateral bracing of SMRF (AISC 2005b). This included a requirement to have a supplemental lateral brace at a distance equal to one-half the depth of the beam away from the RBS. The locations where bracing are provided are shown in Figure 4.41. The third floor required an additional brace to meet the required minimum unbraced length due to the smaller beam size at the roof level. Figure 4.42 shows the design of the 1st floor MRF lateral bracing. Similar bracing details were used for the other floors.

4.5 External reactions

In order to transfer applied forces out of the structure and into the reaction floor of the laboratory two different types of fixtures were used. The first is a column base reaction fixture. This reaction fixture was attached to the base of each column and served to remove the axial and shear forces developed in the frame due to overturning moment. The second type of fixture was a pair of “ground links”. The ground links functioned to remove the rest of the base shear force at the ground level of the test structure.

4.5.1 **Ground links**

The test structure had two “ground links” to remove lateral forces near the base. Each consisted of a clevis and load cell which were attached to the column at the ground floor as shown in Figure 4.43. The force was then transferred into a W14x257 spreader beam, which then transferred the force into a pair of braces constructed of back to back angles. The spreader beam and brace configuration is shown in Figure 4.44. The ground link was

originally designed by Herrera (2005) and was later modified by Dong (2013). Details of this modification appear in Dong (2013).

Prior to the MRF being installed, the ground link load cell and clevis were installed on the south column of the DBF. A W14x455 column section was installed between the spreader beam and the ground link load cell, and functioned as a transfer beam. This extension was then removed to allow that MRF to be installed and the load cell and clevis portions of the link were moved to the south end of the MRF. The final configuration is shown in Figure 4.1.

4.5.2 **Bay link**

To connect the two frames and complete the ground link system a “bay link” needed to be designed. This section would be subjected to both axial force and end rotation. In order to reduce the moment associated with this rotation, the moment of inertia of the section was reduced by orienting a wide flange section on its weak bending axis and then trimming the flanges. The flanges were only trimmed near the ends to maintain the axial stiffness of the member near midspan. Figure 4.45 shows the design of the bay link. The end plates were designed to match the existing hole pattern provided for the ground link. This member was designed to carry 200 kips of compressive or tensile force and an end rotation of up to 0.03 radians.

4.6 Rigid Links

During initial DBF characterization, the frame needed to be tested without dampers to assess the properties of the test setup. In order for the DBF to be stable a set of “rigid links” had to be put into the frame in place of the dampers. Each link consisted of a HSS

pipe section welded to two end plates. These end plates were then bolted into existing damper clevis attachment. This configuration is shown in Figure 4.46 and Figure 4.47.

Table 4.1 - Average measured DBF WF section dimensions and computed section properties (figure adapted from Lewis 2004)

Section	Location	d (in)	t_w (in)	t_f (in)	b_f (in)	A (in^2)	I_x (in^4)	Z_x (in^3)
W12x40	Ground Floor	11.88	0.31	0.50	8.00	11.33	291	54.4
	Nominal	11.90	0.30	0.52	8.01	11.70	307	57.0
W12x40	1st Floor	11.88	0.31	0.50	8.00	11.33	291	54.4
	Nominal	11.90	0.30	0.52	8.01	11.70	307	57.0
W12x40	2nd Floor	11.88	0.31	0.50	8.00	11.33	291	54.4
	Nominal	11.90	0.30	0.52	8.01	11.70	307	57.0
W12x40	3rd Floor	11.88	0.31	0.50	8.00	11.33	291	54.4
	Nominal	11.90	0.30	0.52	8.01	11.70	307	57.0
W8x67	South Column	8.89	0.59	0.90	8.16	18.90	253	66.2
	Nominal	9.00	0.57	0.94	8.28	19.70	272	70.1
W8x67	North Column	8.91	0.59	0.90	8.19	18.88	254	66.3
	Nominal	9.00	0.57	0.94	8.28	19.70	272	70.1

Note: A = cross sectional area
I_X = moment of inertia about X-X axis
Z_X = plastic section modulus about X-X axis
Calculated values exclude fillet region.
Nominal values taken from AISC (2005a).

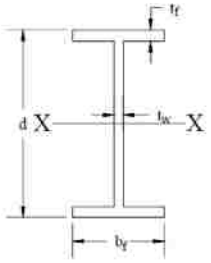

Table 4.2 - Average measured MRF member dimensions and computed section properties (figure adapted from Lewis 2004)

Section	Location	d (in)	t_w (in)	t_f (in)	b_f (in)	A (in^2)	I_x (in^4)	Z_x (in^3)
W18x46	Ground Floor	18.03	0.37	0.57	6.00	13.13	671	86.3
	Nominal	18.10	0.36	0.61	6.06	13.50	712	90.7
W18x46	1st Floor	18.03	0.36	0.56	6.00	12.81	658	84.4
	Nominal	18.10	0.36	0.61	6.06	13.50	712	90.7
W14x38	2nd Floor	14.19	0.35	0.47	6.88	11.19	375	60.2
	Nominal	14.10	0.31	0.52	6.77	11.20	385	61.5
W10x17	3rd Floor	10.19	0.26	0.32	3.98	5.06	81	18.6
	Nominal	10.10	0.24	0.33	4.01	4.99	82	18.7
W8x67	South Column	8.89	0.59	0.90	8.16	18.90	253	66.2
	Nominal	9.00	0.57	0.94	8.28	19.70	272	70.1
W8x67	North Column	8.91	0.59	0.90	8.19	18.88	254	66.3
	Nominal	9.00	0.57	0.94	8.28	19.70	272	70.1

Note: A = cross sectional area
I_X = moment of inertia about X-X axis
Z_X = plastic section modulus about X-X axis
Calculated values exclude fillet region.
Nominal values taken from AISC (2005a).

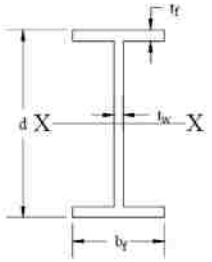

Table 4.3 - Hydraulic actuator specifications (RTMD 2012)

Actuator Type	200-100-1700	200-1000-1250
Quantity	1	2
Load Regulation Accuracy	0.2% FS (but no higher than 0.23KN)	0.2% FS (but no higher than 0.17KN)
Load Tracking Dynamic Bandwidth	> 10Hz	> 10Hz
Displacement Regulation Accuracy (Static)	0.2% FS (but no higher than 0.1mm)	0.2% FS (but no higher than 0.1mm)
Displacement Tracking Dynamic Bandwidth	> 10Hz	> 10Hz
Load Capacity	2300KN @ 20.7MPa	1700KN @ 20.7MPa
Speed Capacity	0.84m/s (33in/s)	1.14m/s(45in/s)
Piston Diameter	424mm	378mm
Piston Rod Diameter	200mm	200mm
Stroke	500 mm	500 mm
Total Chamber Volume	114 liters	84 liters
Chamber Internal Leakage	0.15 liters/min/bar	0.15 liters/min/bar
Chamber External Leakage	0.01 liters/min/bar	0.01 liters/min/bar
Moving Part Mass (Piston & Rod Assembly)	950Kg (approximately)	900Kg (approximately)
Actuator Weight	6100Kg	6120Kg
Actuator Dimension	5.36m —1.25m — 1.35m (length —width —height)	5.36m —1.25m — 1.35m (length —width —height)

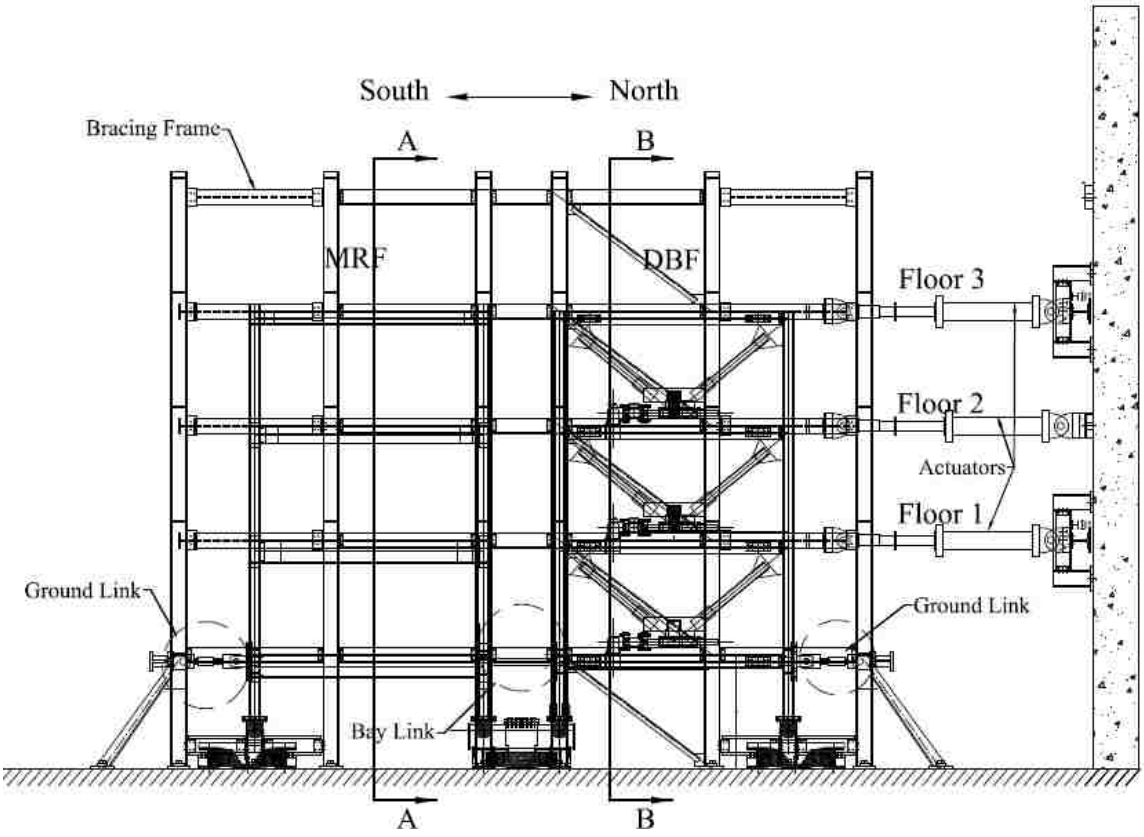

Figure 4.1 – Elevation of bracing frame with DBF and MRF installed

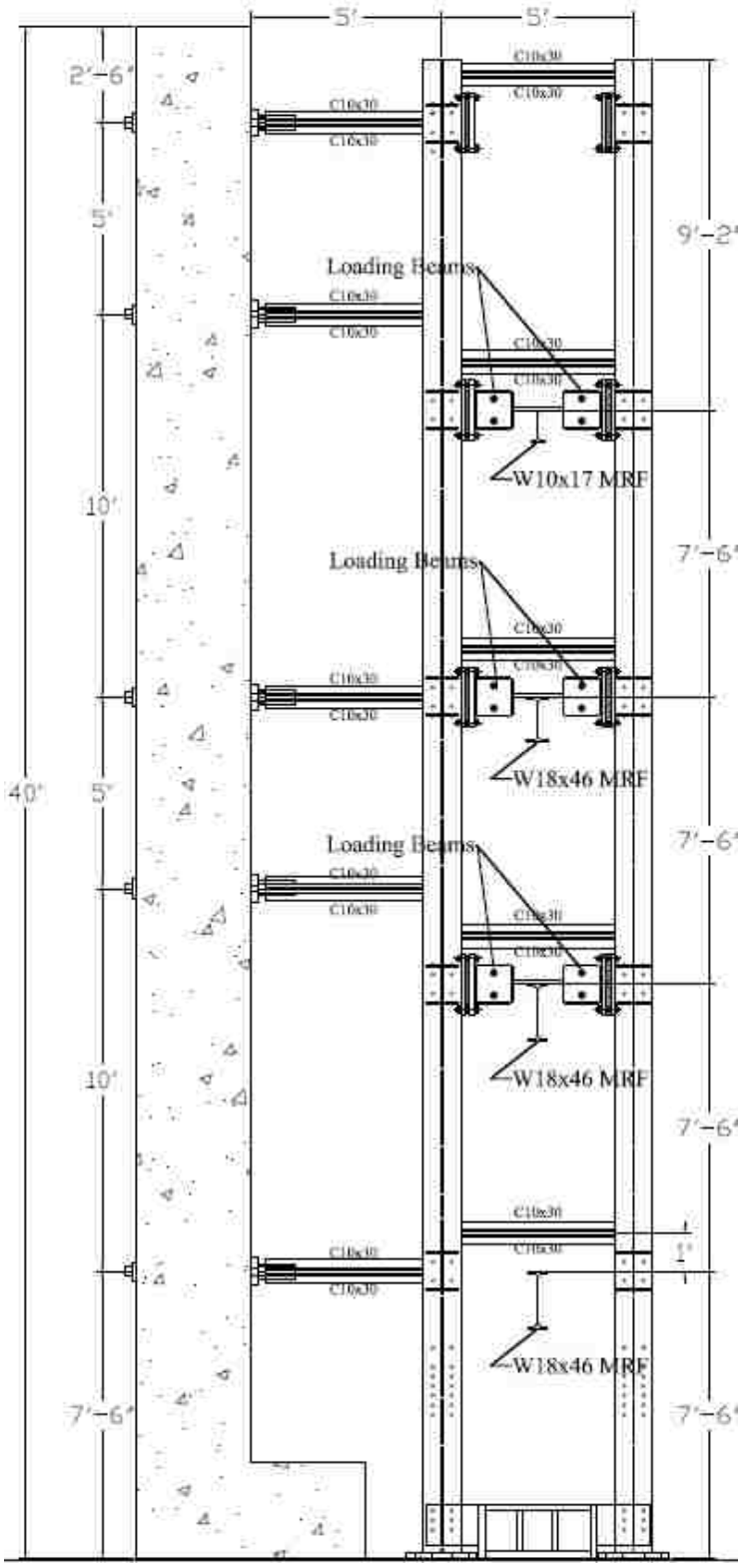

Figure 4.2 – Section A-A of Figure 4.1

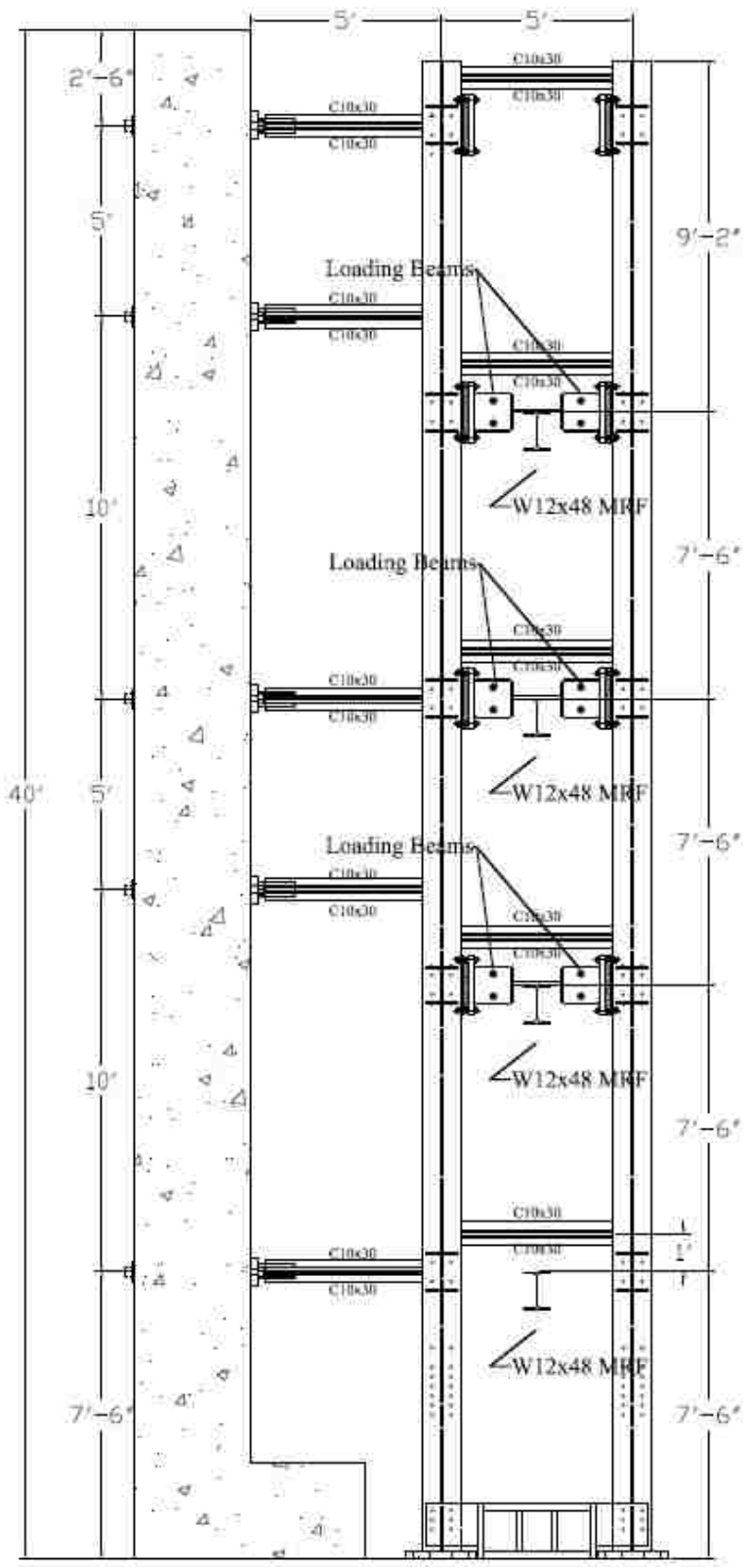

Figure 4.3 – Section B-B of Figure 4.1 (Note DBF Braces Not Shown)

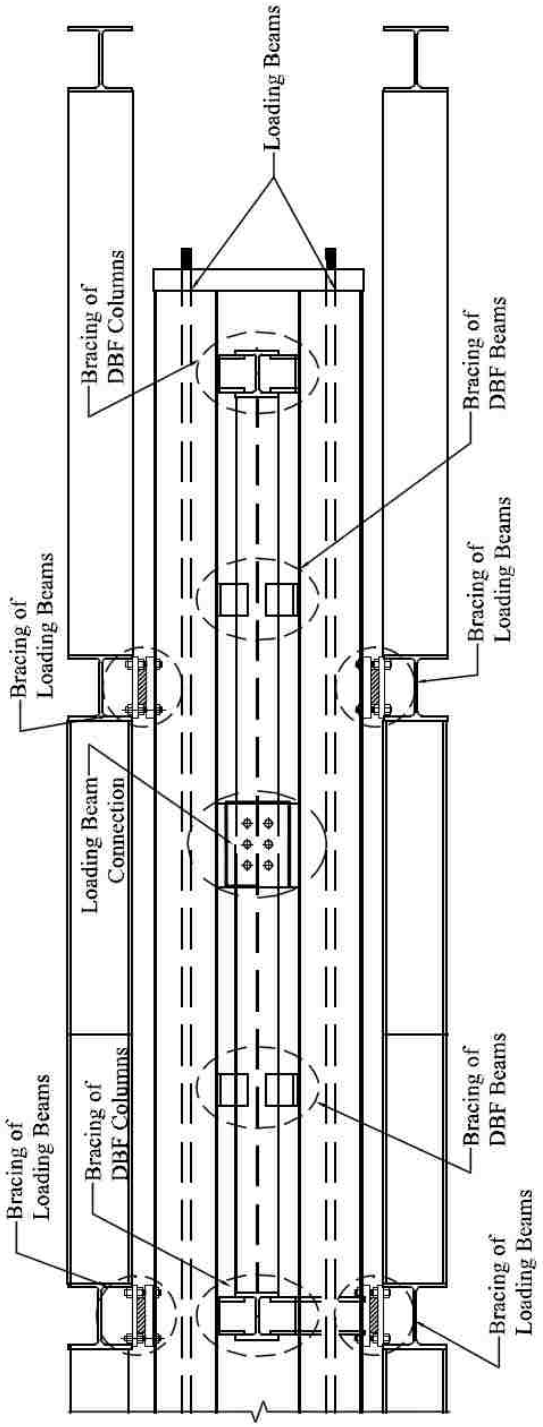

Figure 4.4 – Plan View of DBF Test Setup

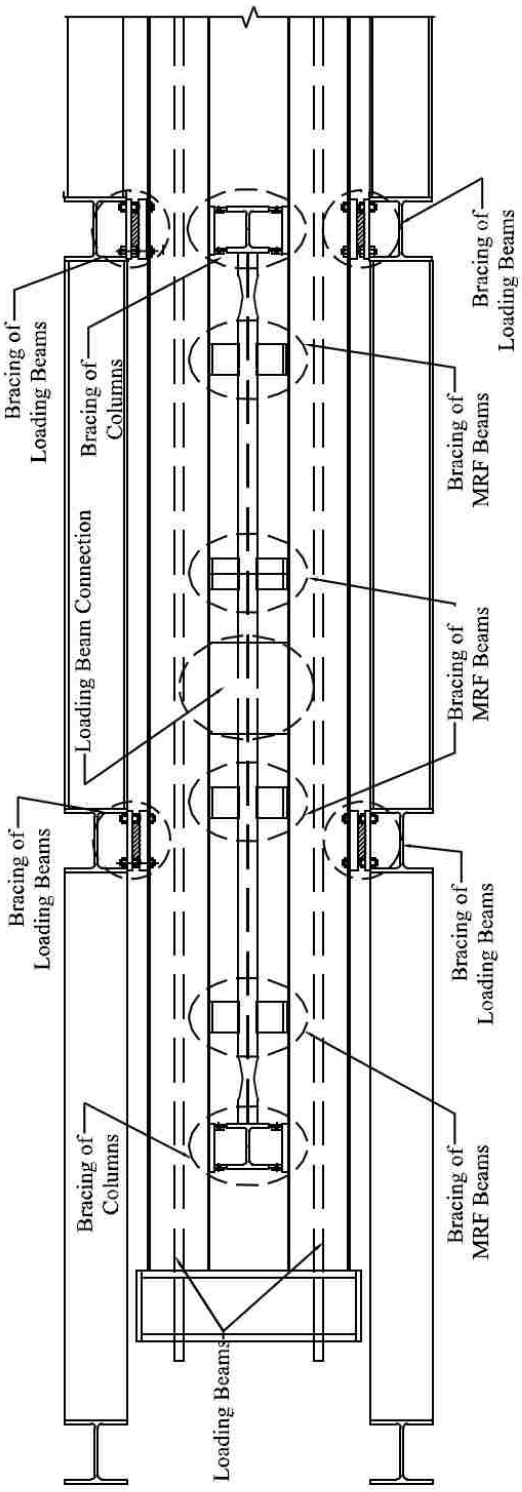

Figure 4.5 – Plan View of MRF Test Setup

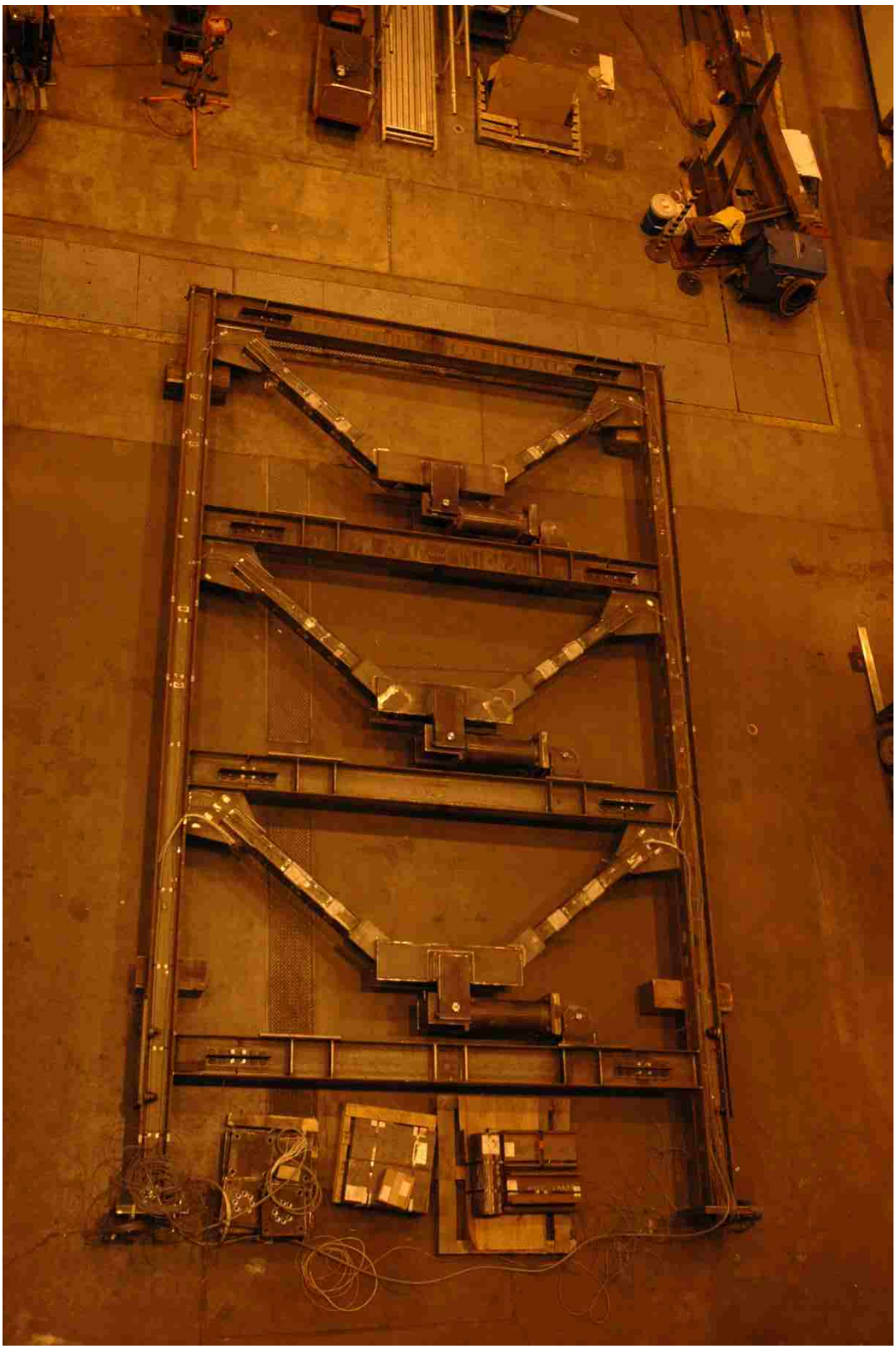

Figure 4.6- DBF assembly

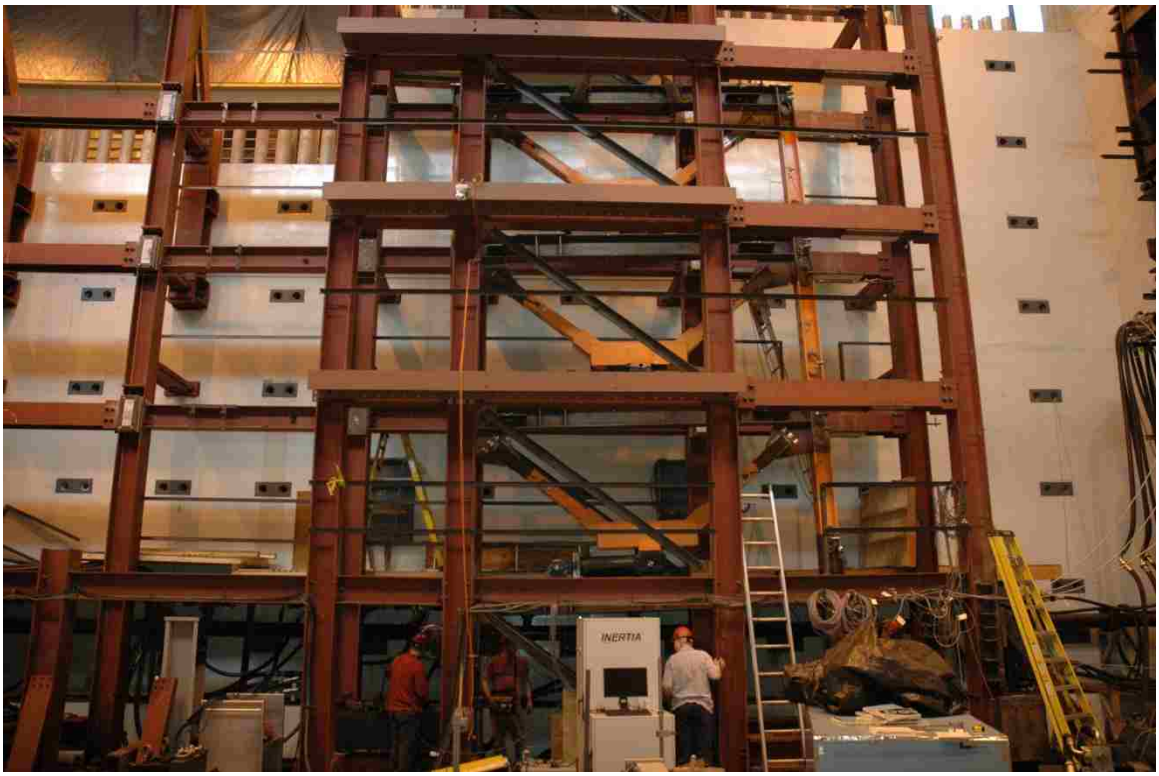

Figure 4.7- DBF in bracing frame

Figure 4.8 – Top view of 2nd Floor Beam RBS cut

Figure 4.9 – Side View of 2nd Floor Beam End Details

Figure 4.10 – MRF 2nd Floor Column with Doubler and Continuity Plates Attached

Figure 4.11 – MRF Being Assembled

Figure 4.12 – MRF Laid Out on Lab Floor

Figure 4.13 – MRF Orientation for Web Weld

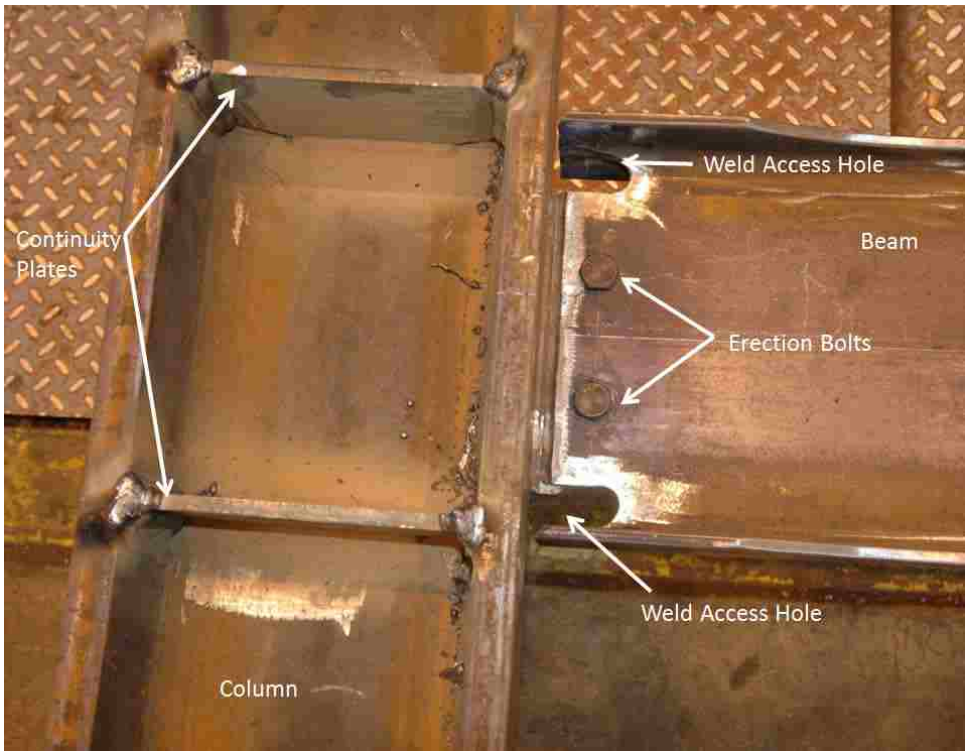

Figure 4.14- 3r[d] Floor web before welding

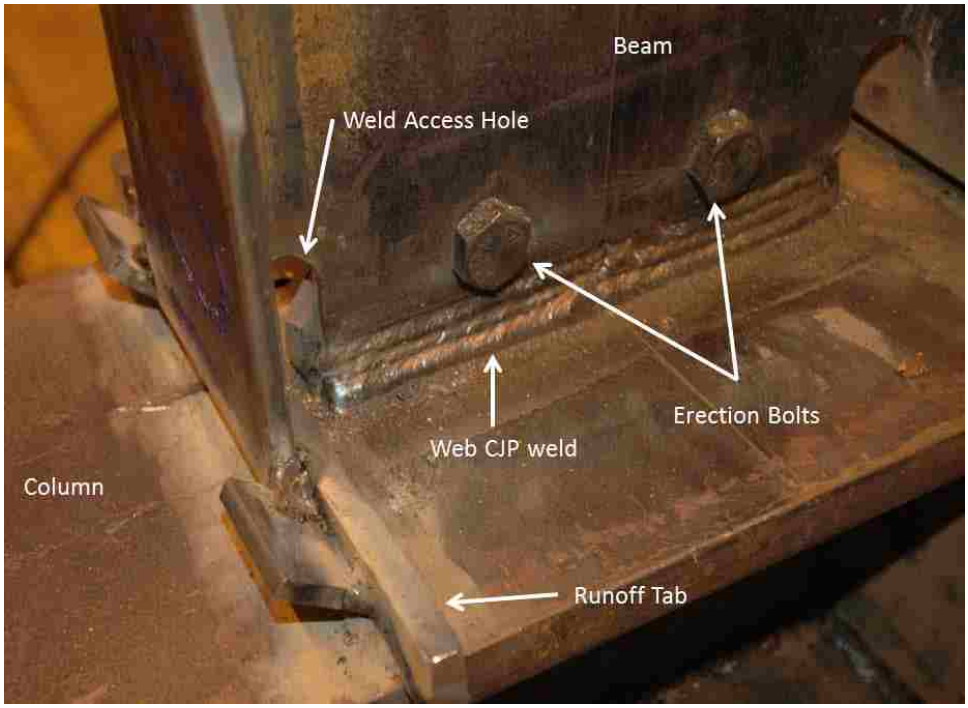

Figure 4.15- 3[rd] Floor web after welding

Figure 4.16- MRF Orientation for Beam Flange Welds

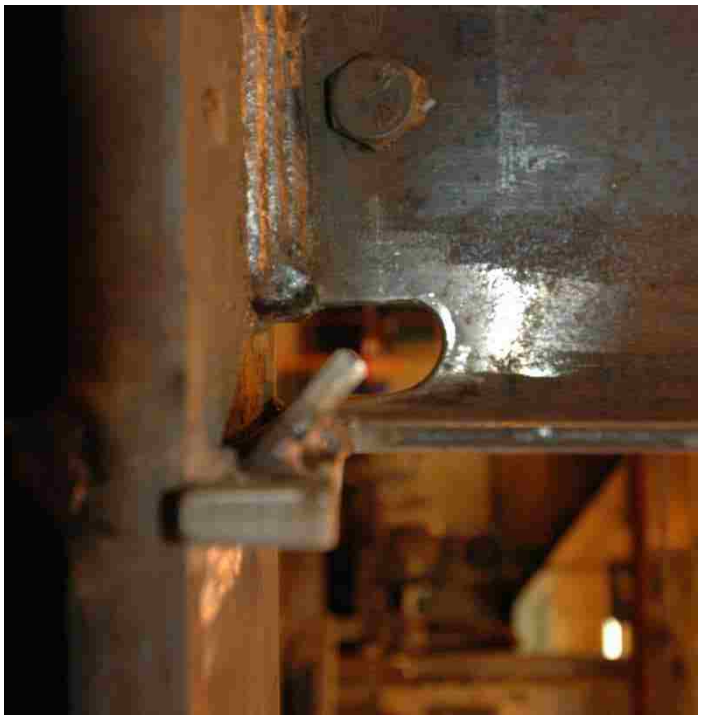

Figure 4.17- 2nd Floor Beam Bottom Flange with Run Off Tabs in Place Prior to Welding

Figure 4.18- Ground Floor Beam Bottom Flange with Runoff Tabs in Place Prior to Welding

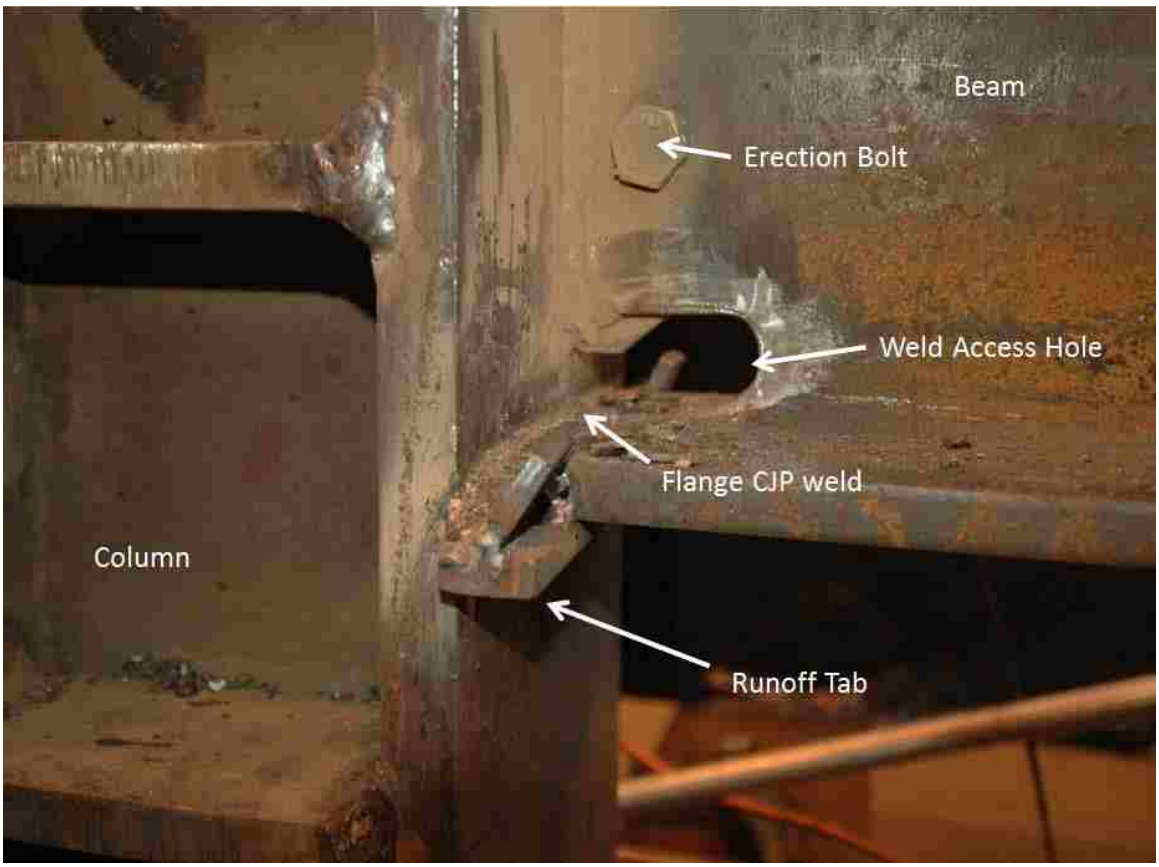

Figure 4.19- Ground Floor Bottom Flange with Run Off Tabs, Post Welding

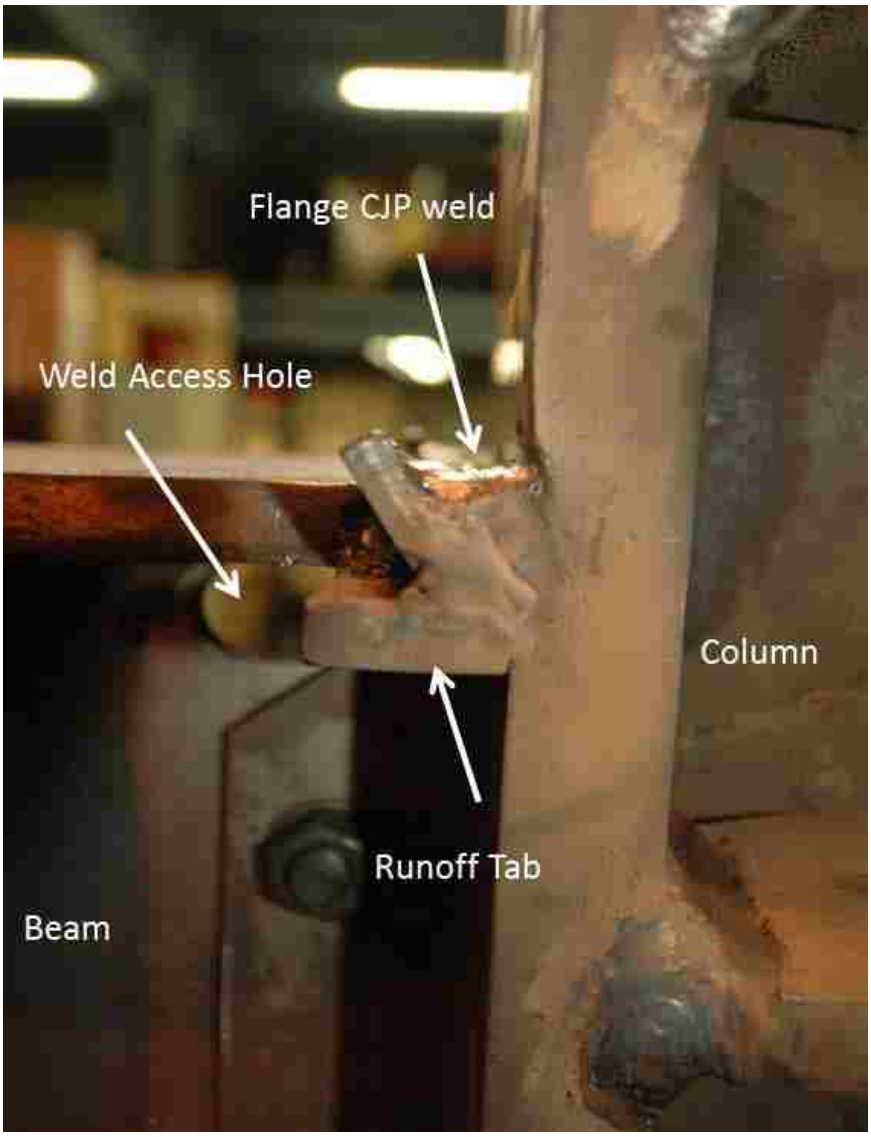

Figure 4.20- Ground Floor Top Flange with Run Off Tabs, Post Welding

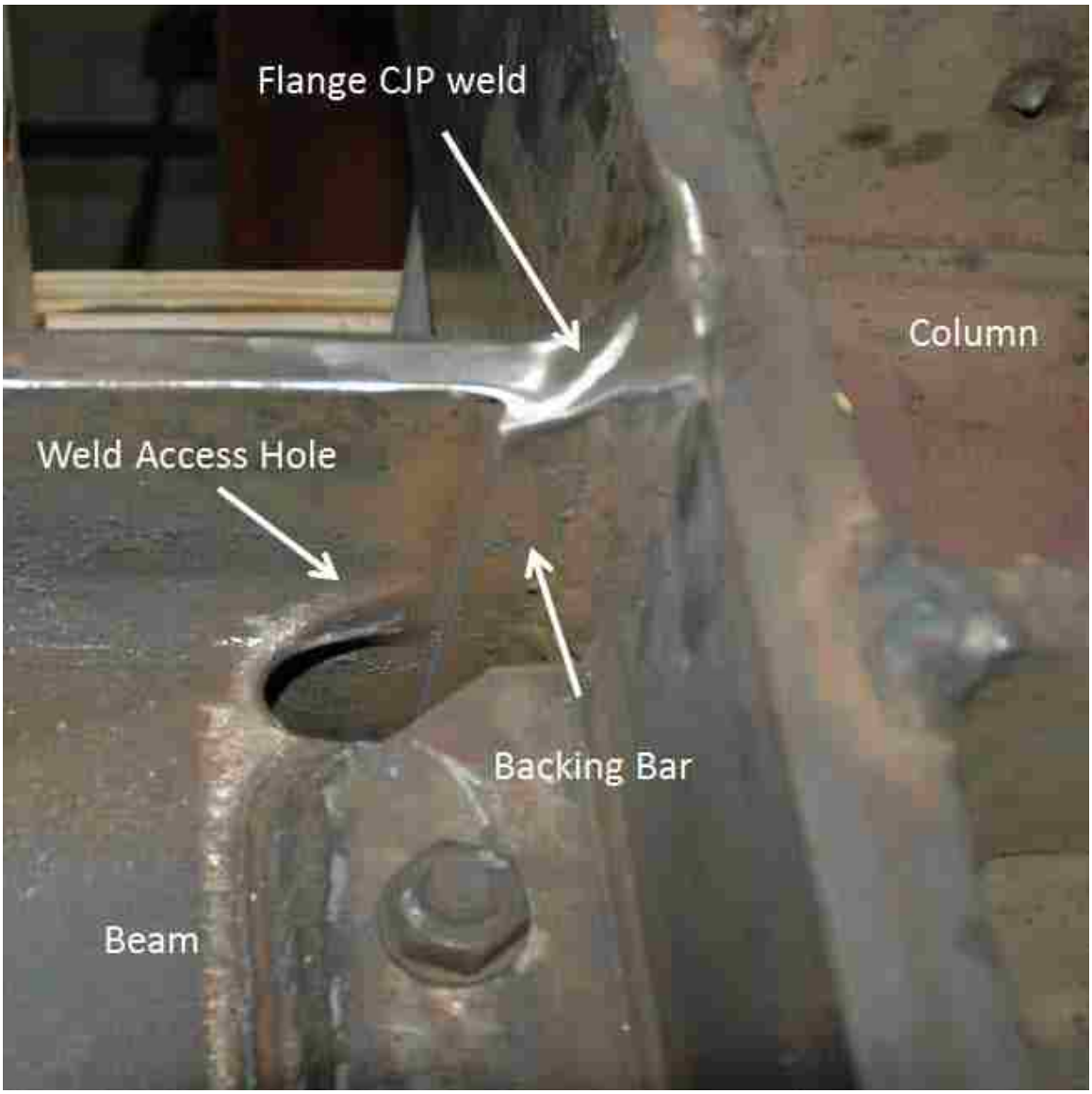

Figure 4.21- Ground Floor Top Flange with Run Off Tabs Removed and Weld Ground

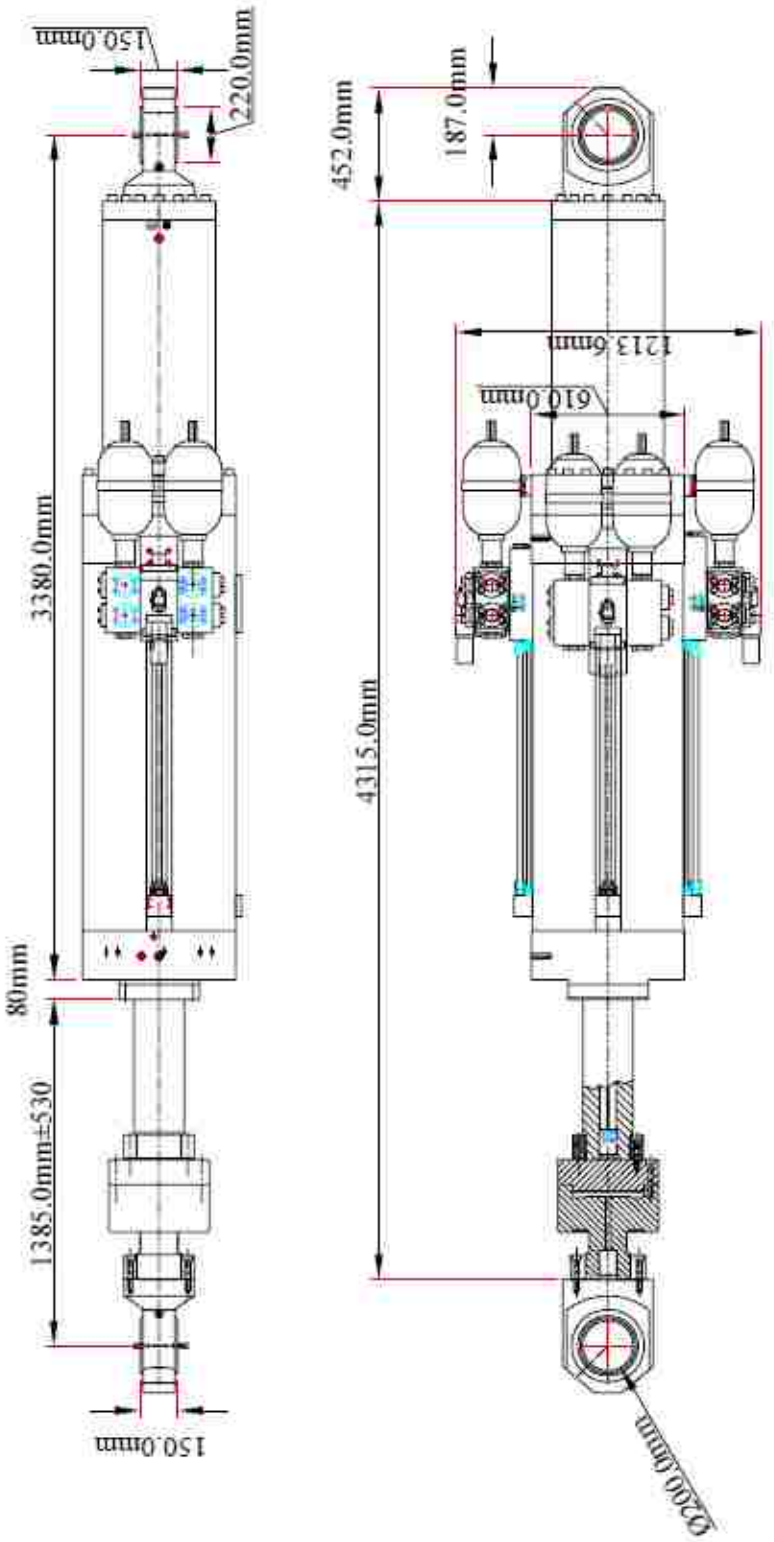

Figure 4.22 – Actuator Dimensions (Servotest, 2003)

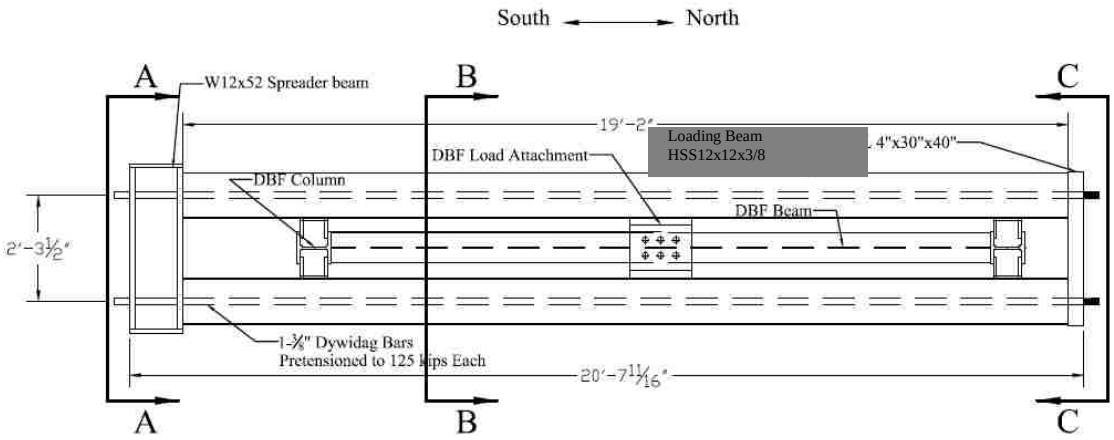

Figure 4.23 – Top View of Loading Beam Configuration for DBF Testing

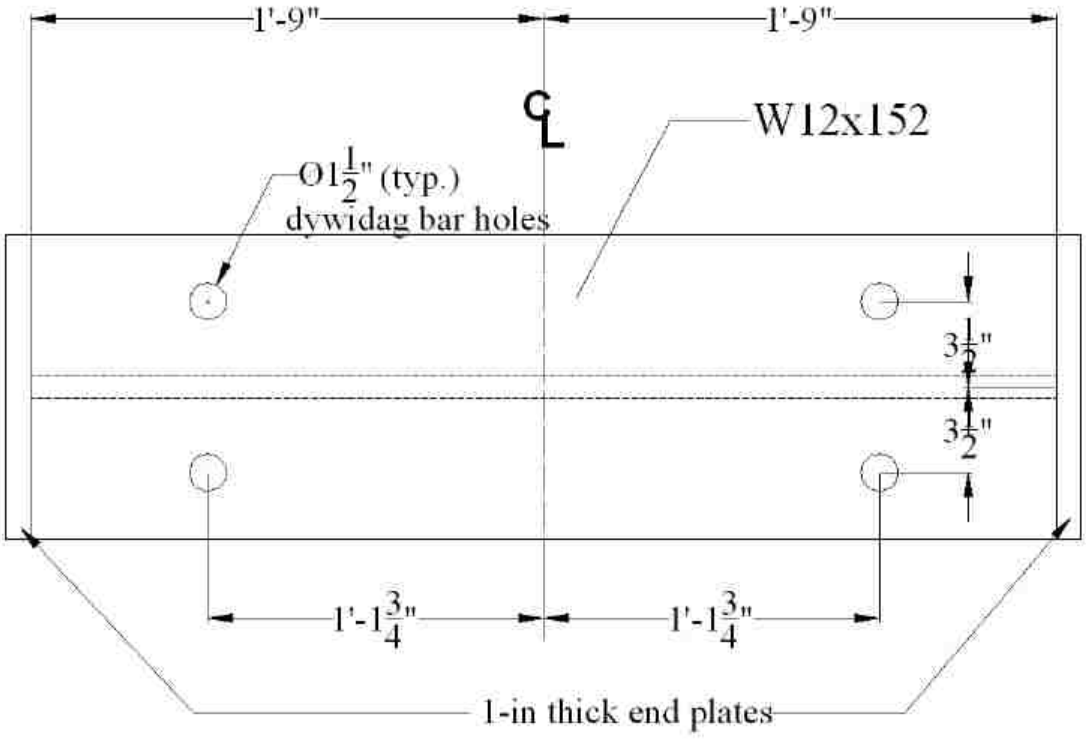

Figure 4.24 – Section A-A of Figure 4.23 (Gonner 2009)

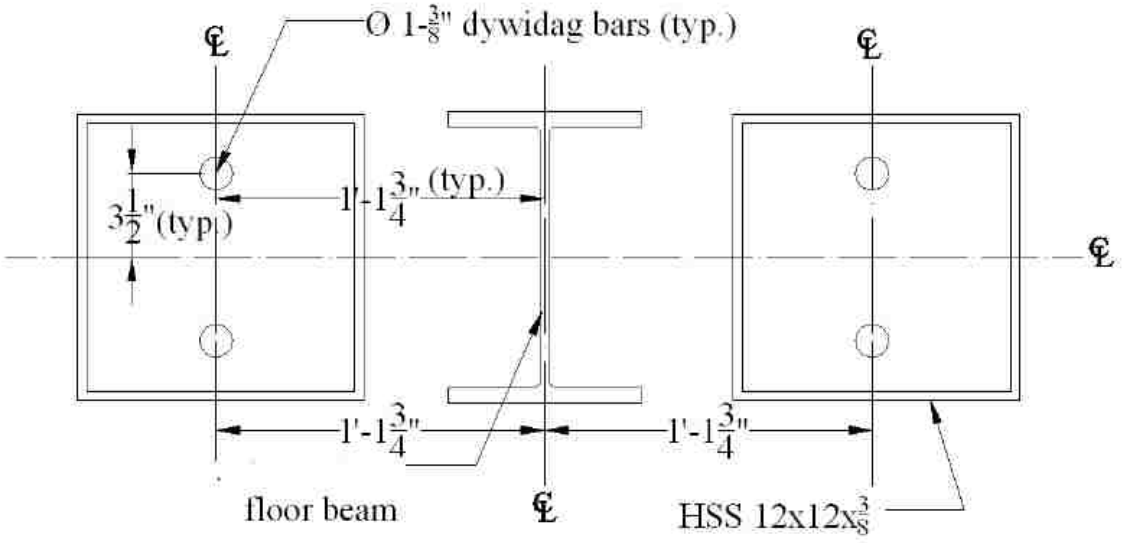

Figure 4.25 – Section B-B of Figure 4.23 (Gonner 2009)

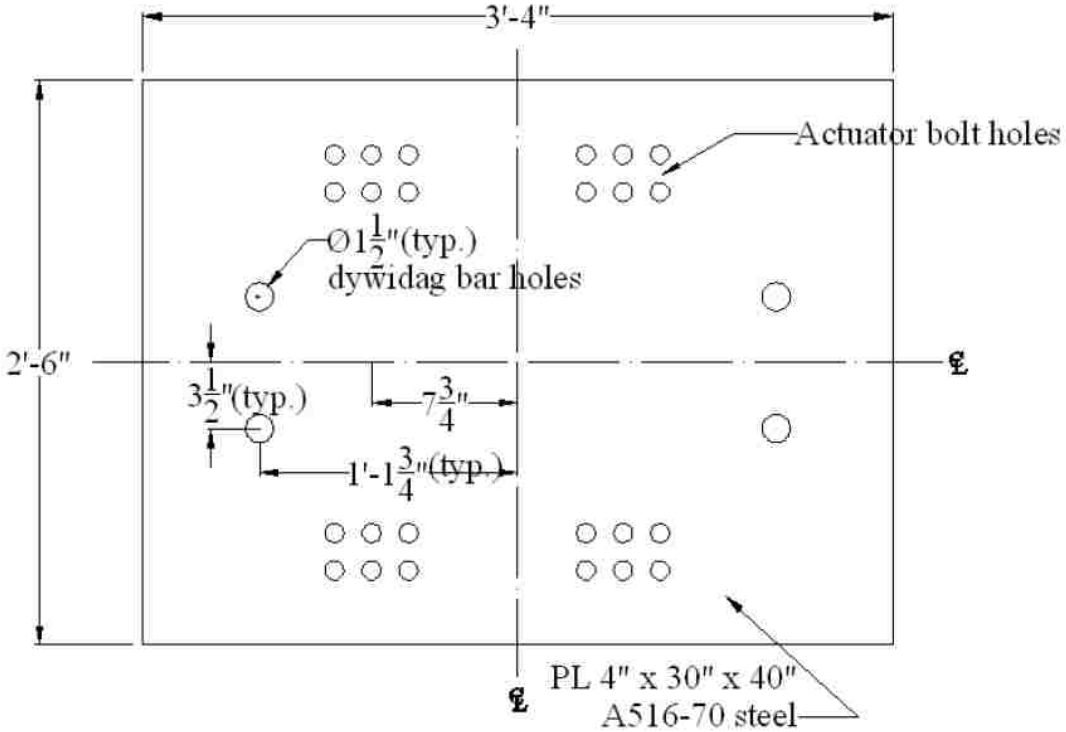

Figure 4.26 – Section C-C of Figure 4.23 (Gonner 2009)

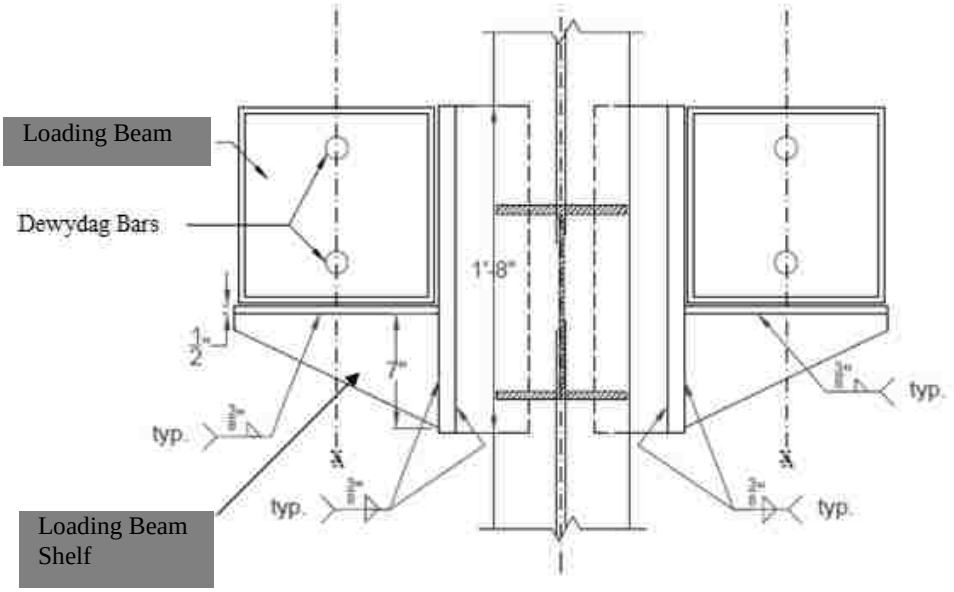

Figure 4.27- DBF Column Bracing and Loading Beam Shelves (Dong 2013)

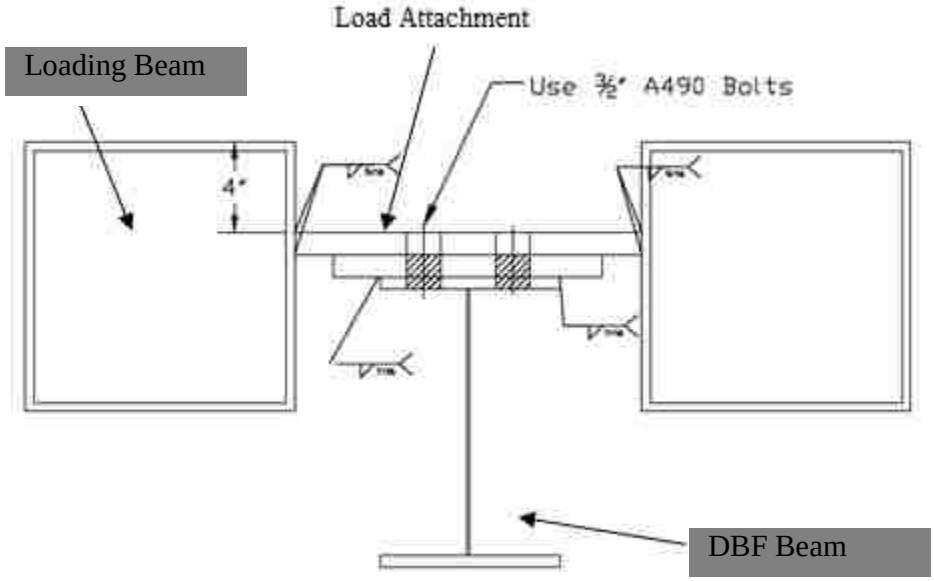

Figure 4.28 – N-S elevation of DBF Load Attachment

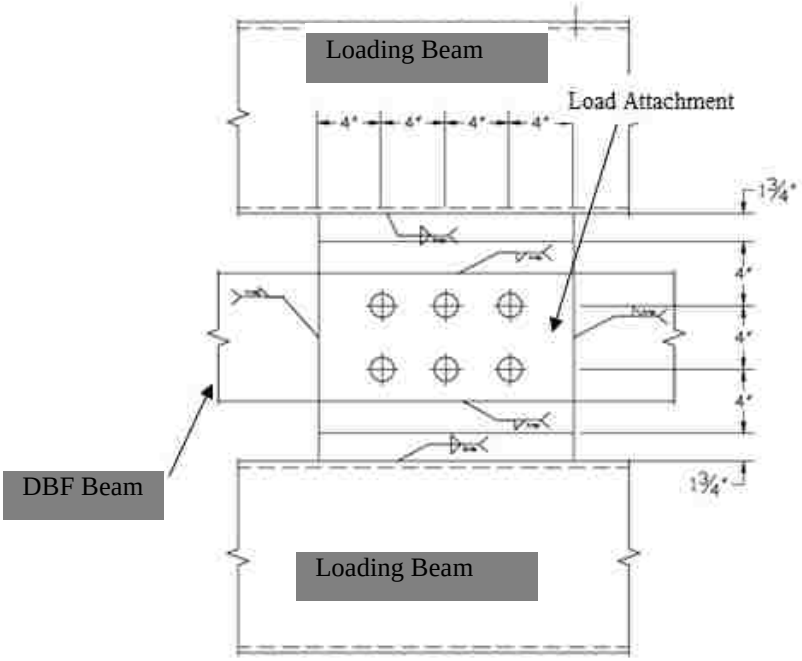

Figure 4.29 – Plan View of DBF Load Attachment

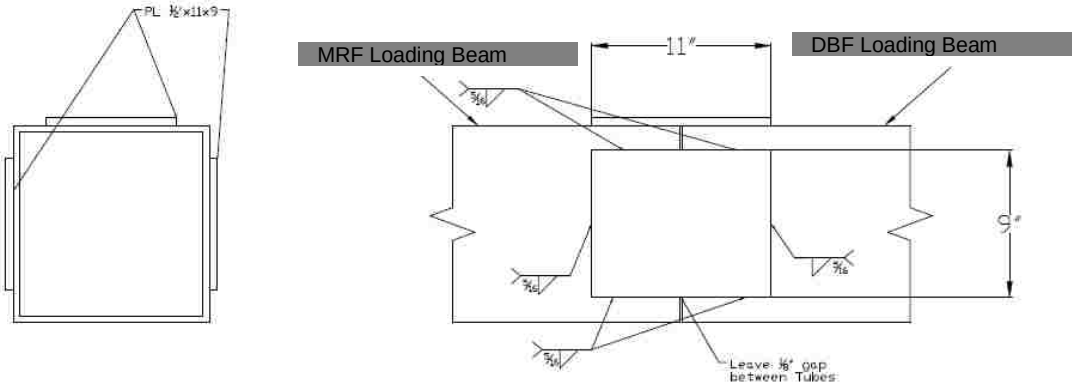

Figure 4.30- Loading Beam Splice

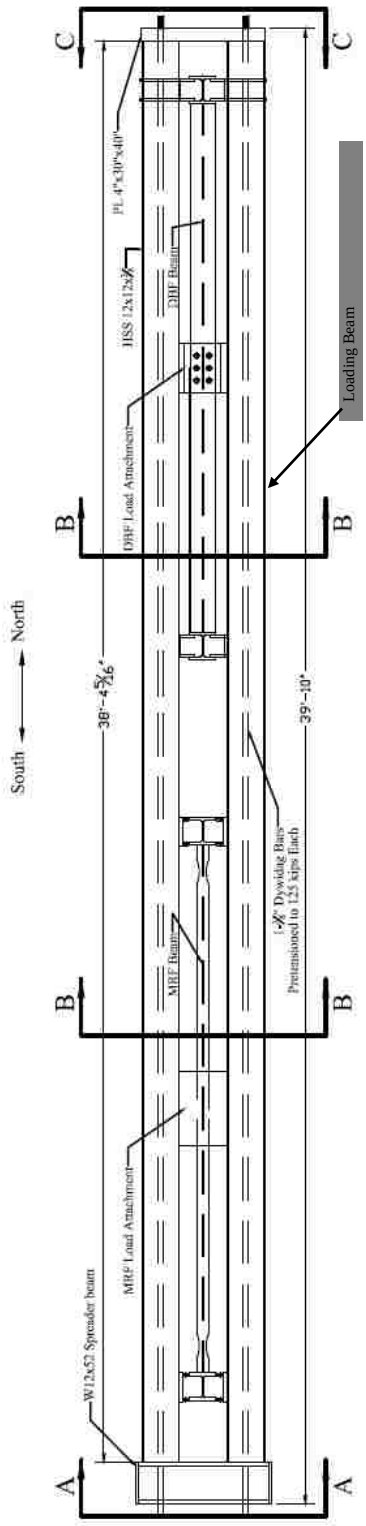

Figure 4.31 – Top View of Loading Beam Configuration for MRF Testing

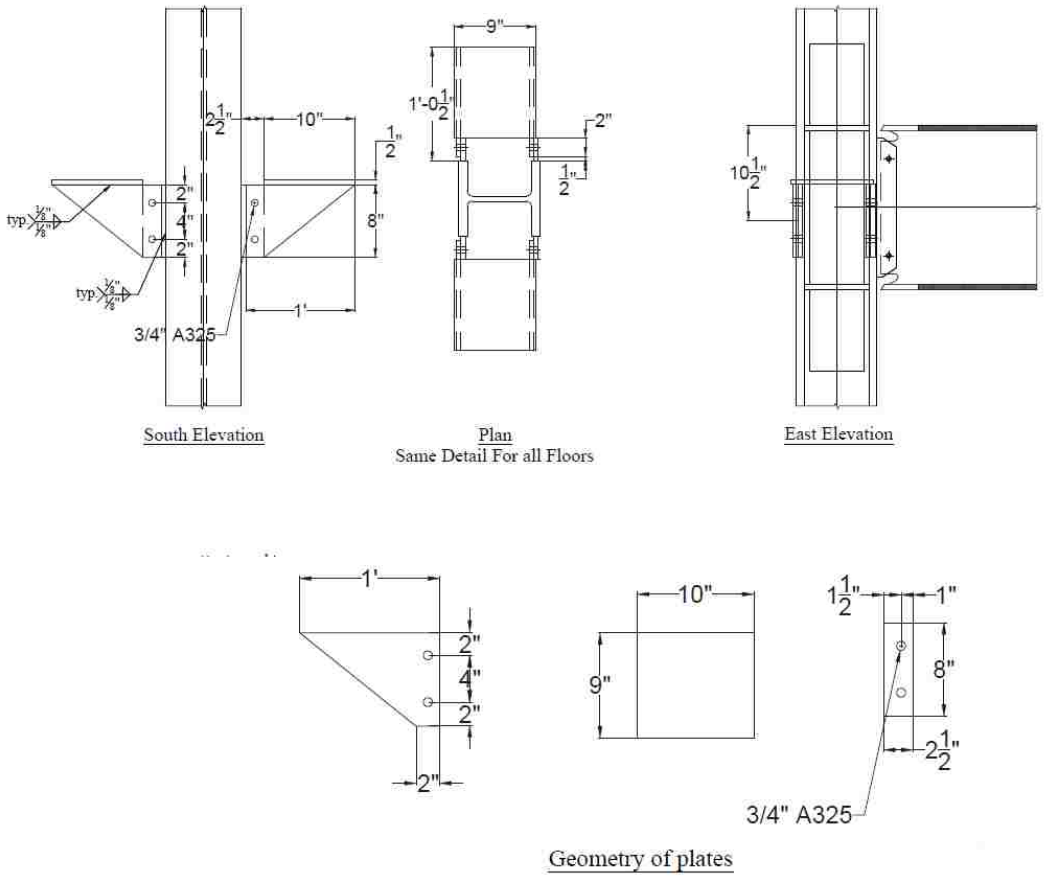

Figure 4.32 – MRF Loading Beam Shelf

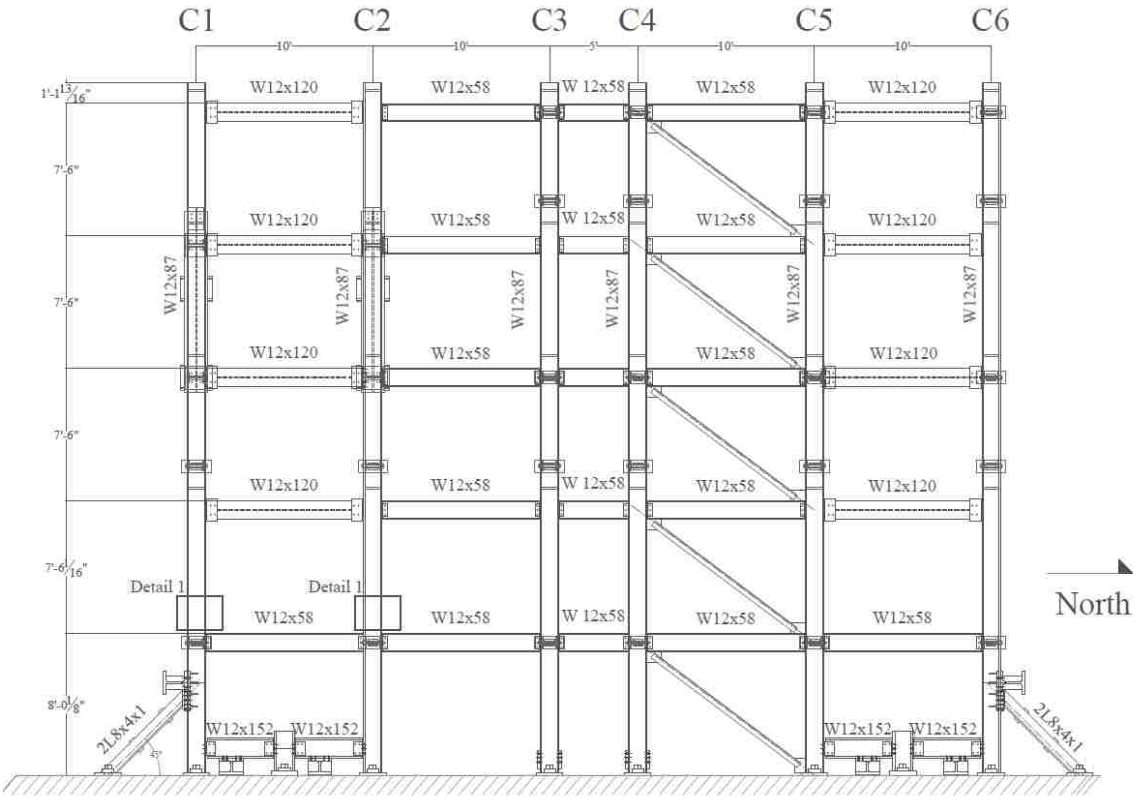

Figure 4.33 – Elevation of Bracing Frame (Herrera 2005)

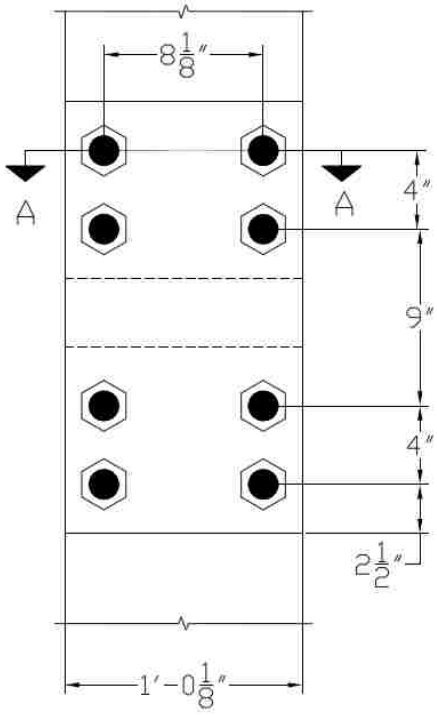

Figure 4.34- Bracing Frame Column Repair (Detail 1 of Figure 4.33) East Elevation

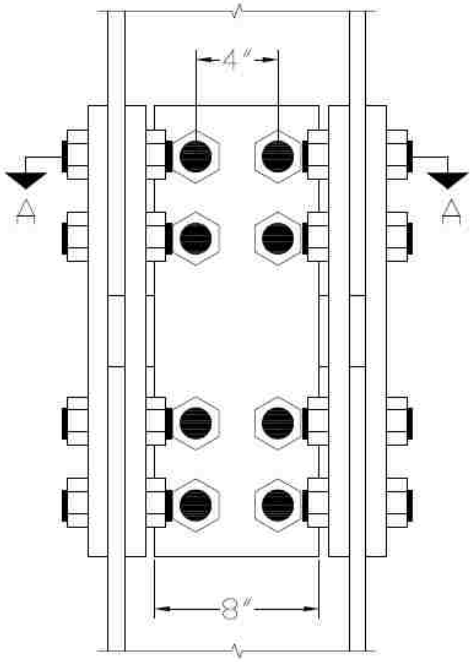

Figure 4.35- Bracing Frame Repair (Detail 1 of Figure 4.33) South Elevation

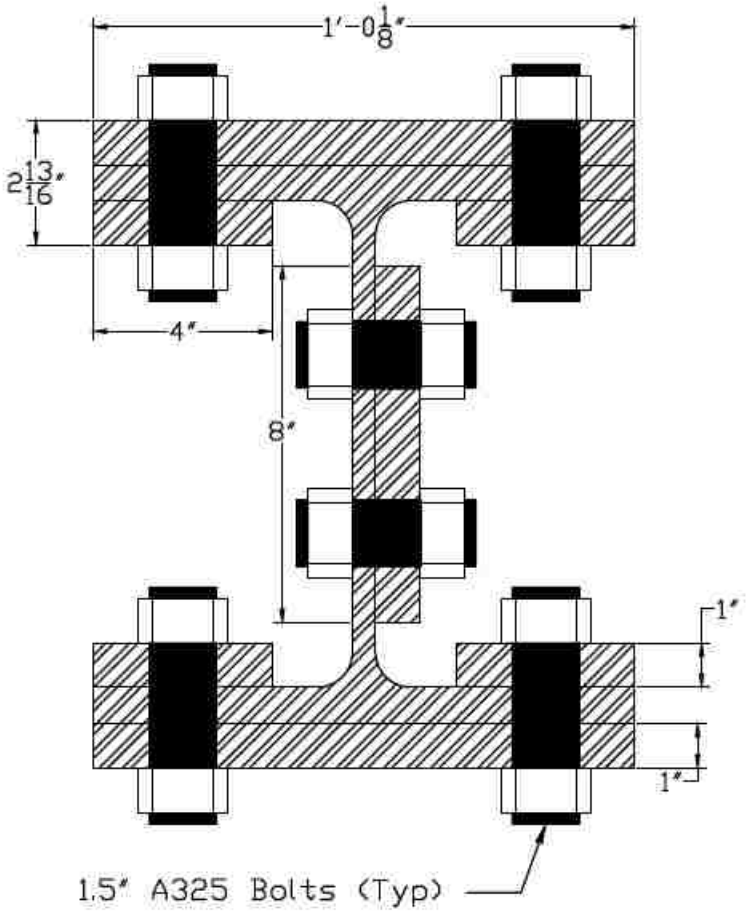

Figure 4.36- Bracing Frame Repair (Cross Section A-A of Figure 4.34, Bracing Frame Beams Not Shown For Clarity)

Figure 4.37- Photograph of bracing frame repair

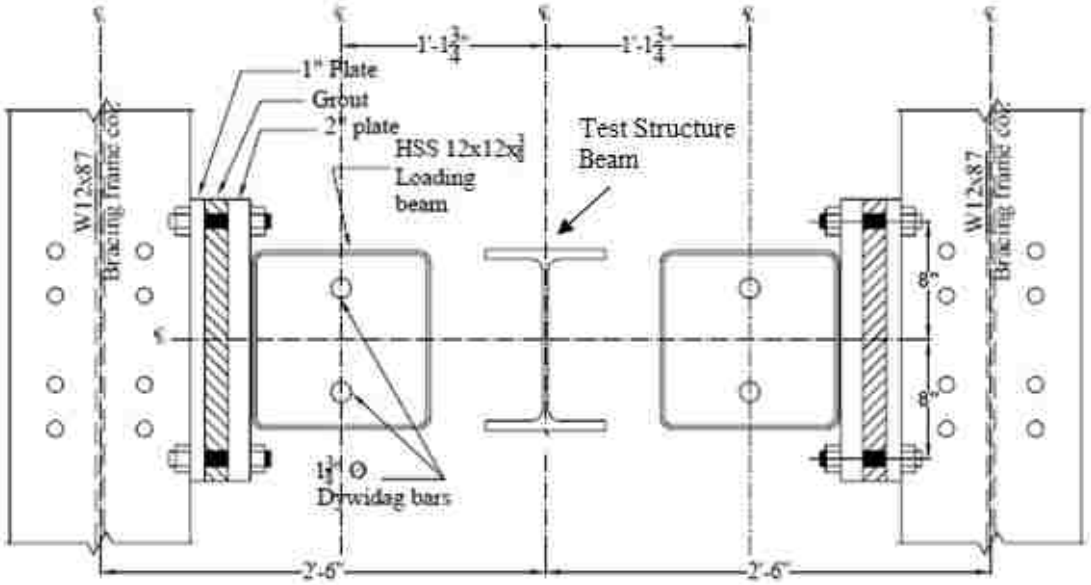

Figure 4.38- Bracing of Loading Beam by Bracing Frame (Gonner 2009)

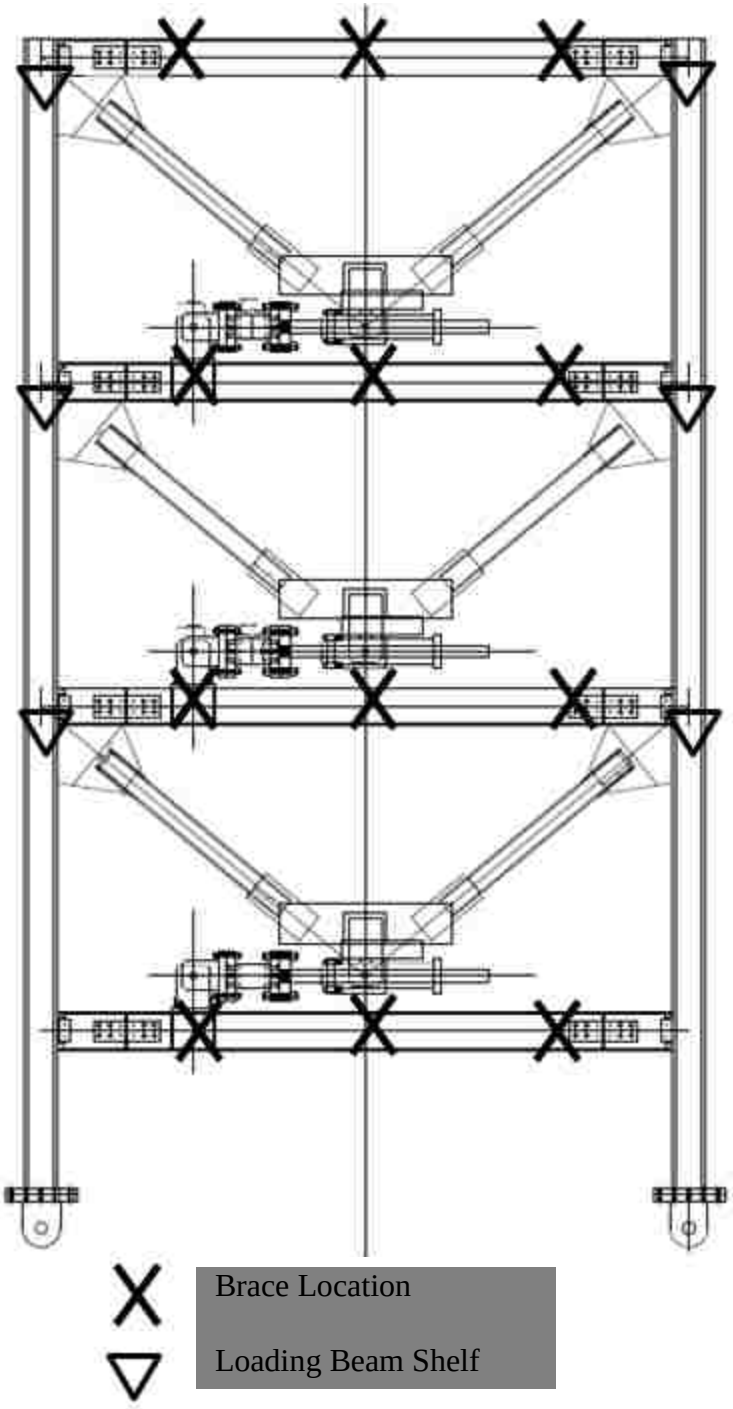

Figure 4.39 – Locations of DBF lateral bracing and loading beam shelves

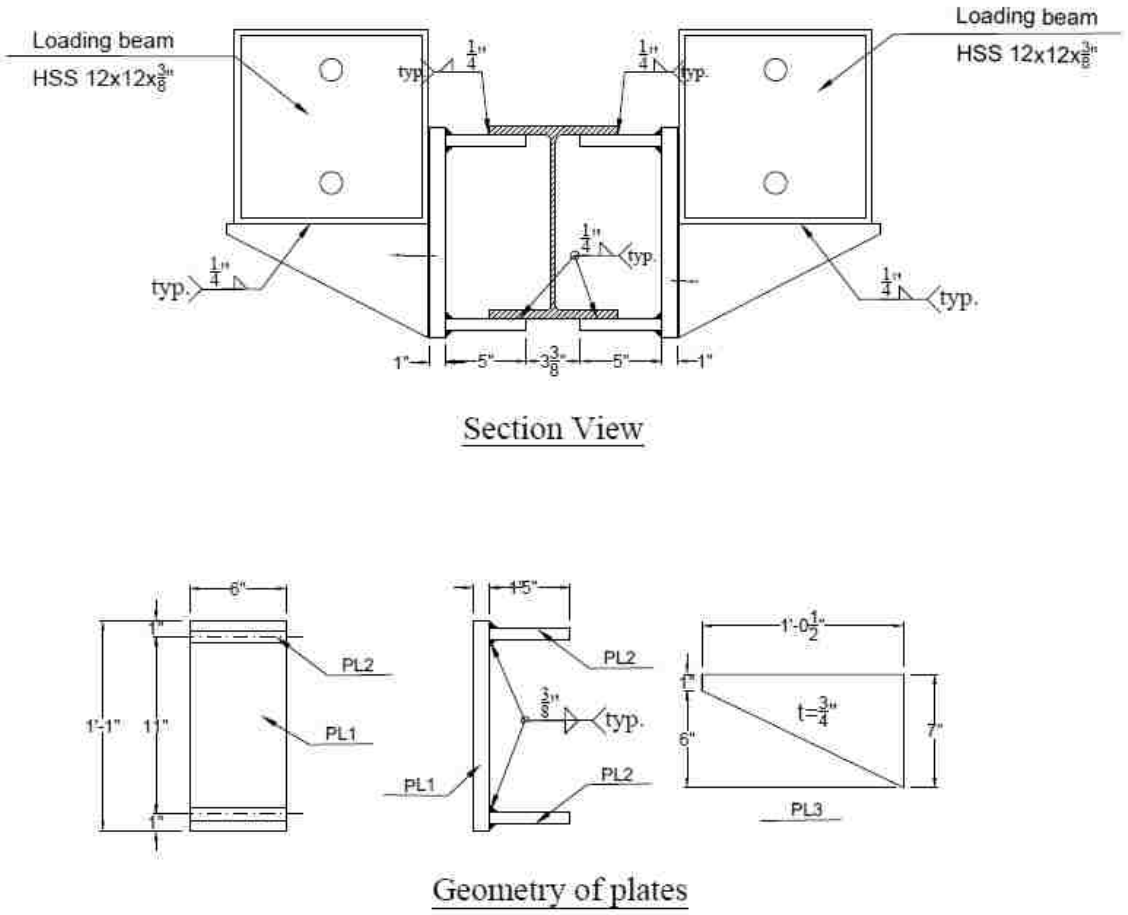

Figure 4.40 – Typical DBF lateral bracing

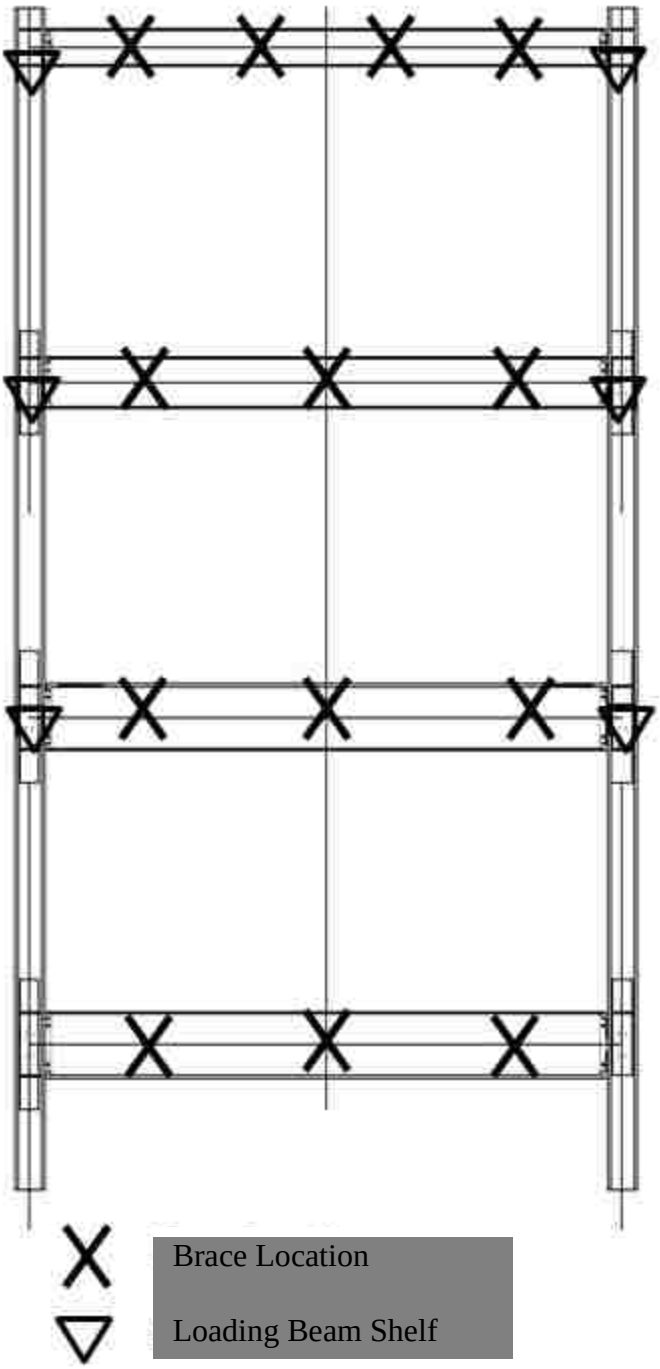

Figure 4.41- MRF Out-of-Plane Bracing and Loading Beam Shelves

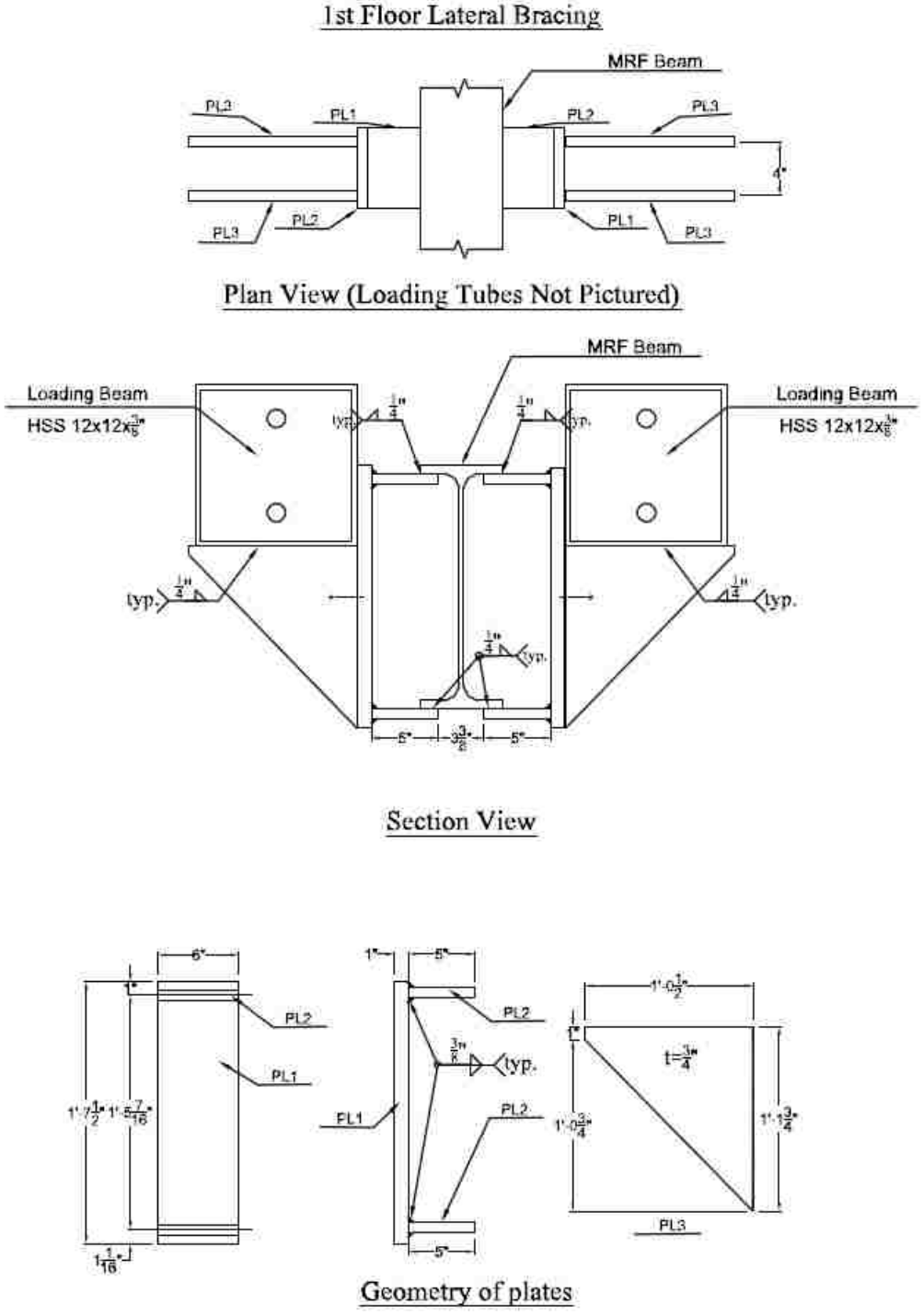

Figure 4.42- MRF 1st Floor Beam Lateral Bracing Detail

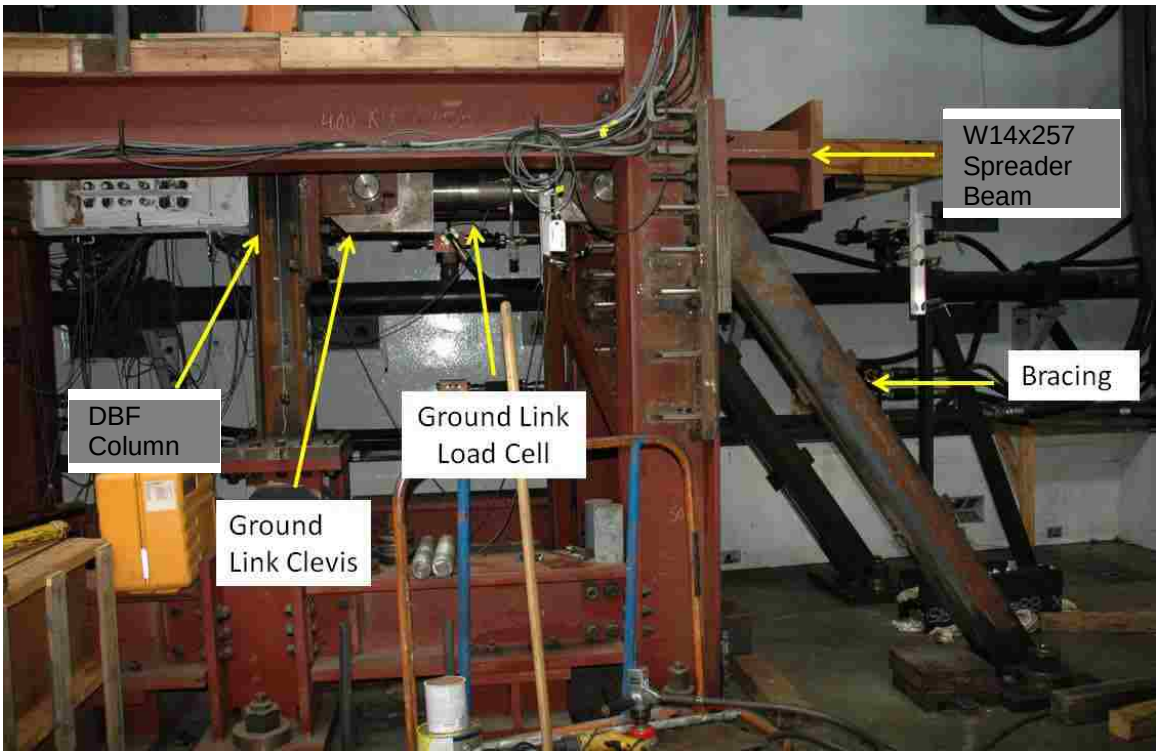

Figure 4.43- Ground Link

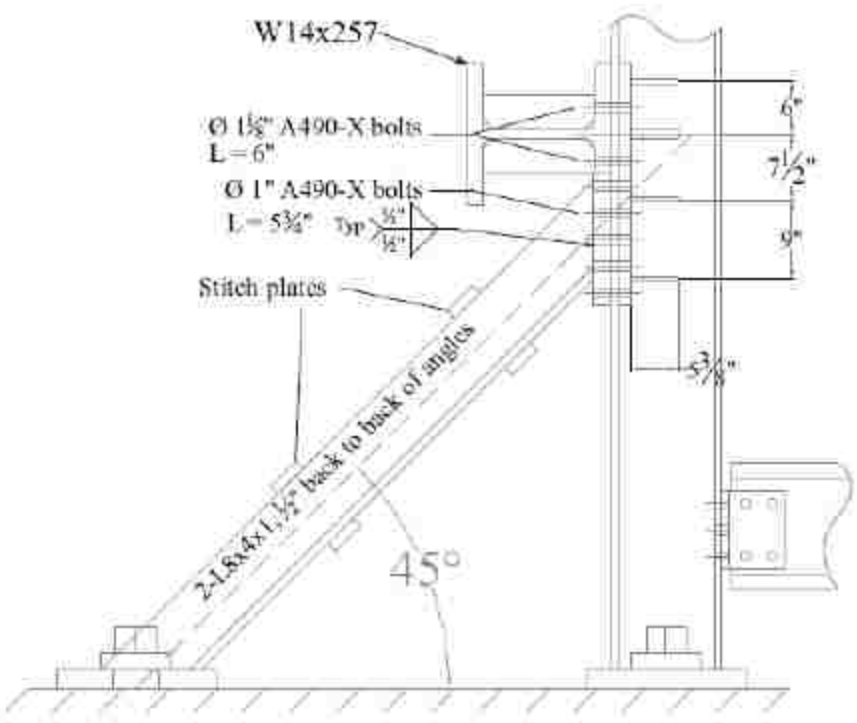

Figure 4.44- Typical Ground Link Reaction Spreader Beam and Braces (Herrera 2005)

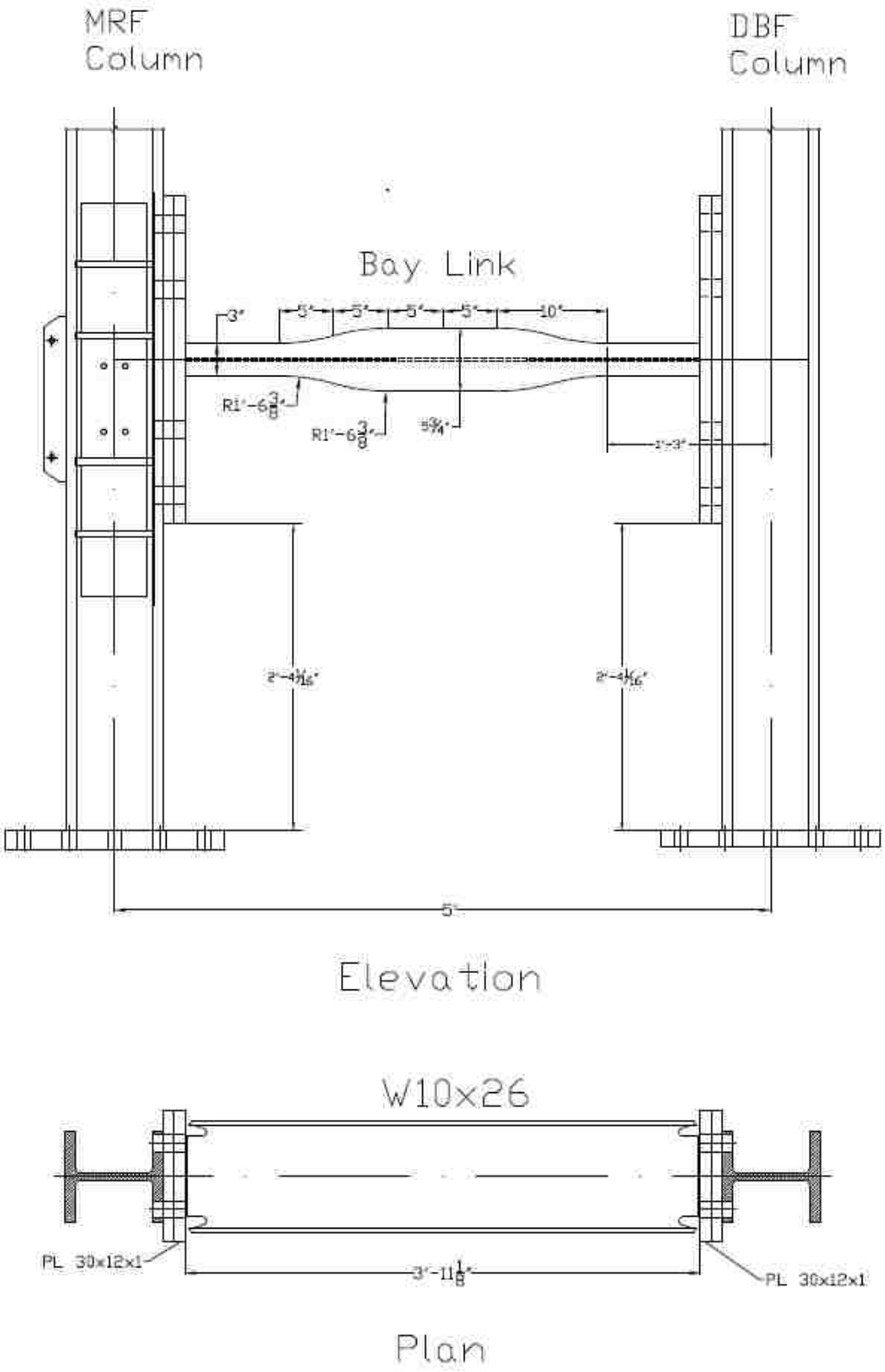

Figure 4.45- Bay Link Detail

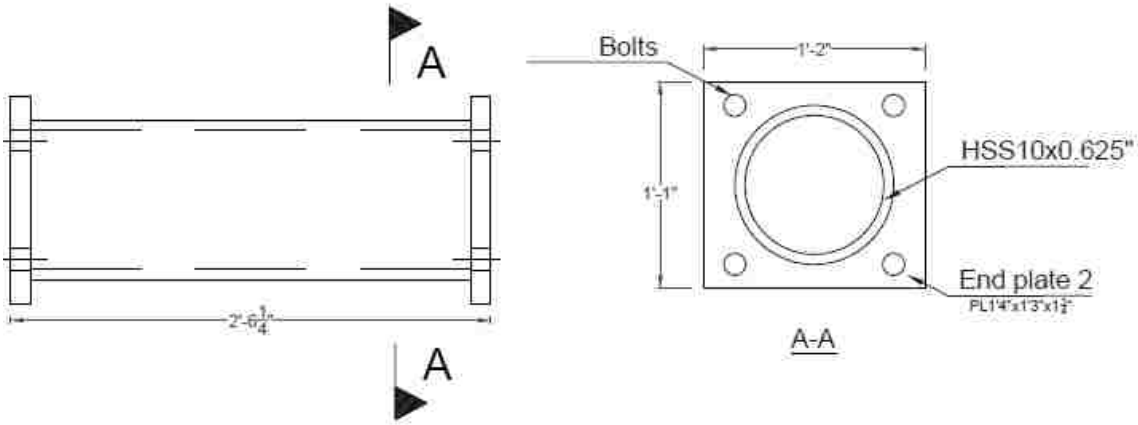

Figure 4.46 Rigid Links (Dong, 2013)

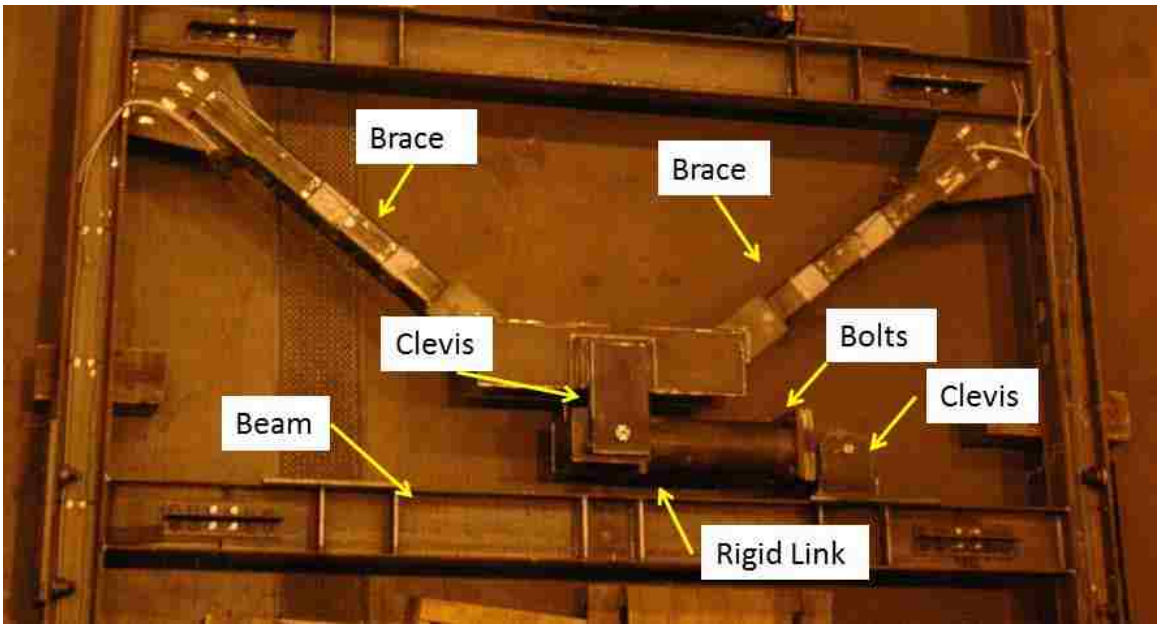

Figure 4.47- DBF assembly

Chapter 5.
Instrumentation

5.1 General

This chapter describes the instrumentation installed in the test setup to collect the data used to evaluate the test structure and testing fixtures. It begins by summarizing the type and locations of the instrumentation. The determination of member internal forces from measured data is also discussed. The final portion of this chapter discusses the calibration of the bay link instrumentation and determination of the axial stiffness of the bay link.

5.2 Description of Instruments

Various types of instruments were used to collect data on the MRF and DBF including internal full bridge load cells (referred to herein as *full-bridges*) to measure structural member moment and axial forces; linear variable differential transducers (LVDT), linear potentiometers, and temposonics to measure displacements; load pins and load cells to measure reaction forces; thermo couples used to measure temperature; accelerometers to measure accelerations; and strain gauges to measure strain in the members. Included in this section are diagrams of the most common instrumentation configurations. In the following subsections each instrument type is described as well as its placement in the MRF and DBF.

5.2.1 **Internal full bridge load cells**

The general full bridge internal load cell layout for each frame consisted of a full bridge to measure axial force at the mid-height of each story; in addition a pair of full bridges was also located on each column, one above and one below the axial force full bridge, to measure moment at these locations. A similar configuration was used on the braces of the DBF. Since the moment diagram varies linearly in each member the moment diagram could be determined from the two moment full bridges. An additional axial force full bridge was located on the section of column below the ground beam to measure the vertical reaction force at the base of each frame.

Each full bridge consists of 4 single strain gauges wired as a Wheatstone bridge as to measure either axial strain or bending strain. This strain is then converted to a force or moment measurement, using calibration factors (the X factors given in Table 5.1). These factors are based on the theoretical relationship between the full bridge strain output and either axial force or bending moment. Details are discussed later.

Figure 5.1 shows the locations of the 38 sets of full bridges on the DBF. There are 14 full bridges installed on the DBF to measure axial force, where the strain gauges for each are wired in the configuration shown in Figure 5.2. Additionally, there are 24 moment full bridges that are wired in the configuration shown in Figure 5.3. All full bridges used on the DBF were of 350 ohm resistance. This resistance was selected based on the availability of 350 ohm data acquisition cards. They also used an excitation voltage of 10V.

Figure 5.4 shows the location of the 20 full bridges on the MRF. Eight of the full bridges were wired to measure axial force, while the remaining 12 were wired to measure

moment. Specific bridge locations on the columns were chosen where the member remained elastic. This was done to ensure they would continue to function throughout testing. All MRF full bridges were created using four 120 ohm strain gauges. 120 ohm gauges were chosen for the MRF instead of 350 ohm gauges due to data acquisition limitations. The MRF full bridges were excited at 6V instead of the customary 10V due to current limitations of the data acquisition cards.

It is important to know the force applied to each frame. During initial static and dynamic testing of the DBF this was accomplished using only the reading from the actuator load cell. However once the MRF was installed a measure of the force in the loading beams between each of the two frames was needed. This measurement was obtained using full bridges on the loading beams that were configured to measure only axial force. A total of six full bridges were used, with one installed on each loading beam. The gauge was placed on the portion of loading beam between the two frames. In selecting an exact location, care was taken to avoid a location that would contact either the MRF or DBF columns during any test in which the frames were not connected to the loading beams. This was done in order to ensure that the gauges did not get damaged during testing.

A full bridge strain gauge was installed at the center of the bay link in order to determine axial force in the link. The location of this full bridge is indicated in Figure 5.5.

All full bridges for the DBF and MRF used the sign convention shown in Figure 5.6 through Figure 5.8.

5.2.2 **Full bridge calibration**

With the exception of the full bridge on the bay link it was not possible to calibrate the full bridges, due to the cost and difficulty associated with calibrating them. Therefore a calibration based on theory was used to relate the voltage output of the bridge to the axial force or moment in the member. The theoretical calibration coefficient needed for converting voltage to axial force for the wiring configuration in Figure 5.2 is (Dally 1991):

$$X_A = \frac{2EA}{S_g V_{in}(1+\nu)} \tag{5-1}$$

where

X_A= axial full bridge calibration factor without gain, kips/volt

E= Young's modulus (29000ksi for steel), ksi

A= area of member, inch^2

S_g = gauge factor of gauges in circuit

V_{in} = excitation voltage of the bridge, Volts

ν = Poisson's ratio (0.28 for steel)

Dally also showed that the theoretical calibration coefficient needed for converting voltage to bending moment for the wiring configuration in Figure 5.3 is:

$$X_m = \frac{2EI_x}{dS_g V_{in}} \tag{5-2}$$

where:

X_m= moment full bridge calibration factor without gain, kip-in/volt

E= Young's modulus (29000ksi for steel), ksi

I_x= Area of member, in^4

d = depth of the member, in

S_g = gauge factor of gauges in circuit

V_{in} = excitation voltage of the strain gauge, V

Lewis (2004) showed in his research that these coefficients can be used to accurately translate the voltage output of the full bridge to axial forces and moments in large-scale testing. In order to get an accurate calibration coefficient, measured section dimensions such as those in Table 4.1 and Table 4.2 were used to calculate these coefficients. A summary of the calibration factor and excitation voltage used for each full bridge is presented in Table 5.1.

5.2.3 **Load cells and load pins**

Figure 5.9 shows the locations of load cells and load pins for the DBF. To measure the base reaction of the DBF a pair of load pins produced by Strainsert are provided at each column base where they were inserted into a clevis. Each load pin was calibrated to measure ± 450 kips of shear force and has a diameter of 3-1/2 inch and a length of 10 inch. Figure 5.10 shows the configuration of the two pins in the clevis. In order to find the total reaction force at either of the two clevises it is necessary to sum the

measurements of the two pins at that clevis. The load pins located at the south end of the DBF were oriented to measure vertical force while the load pins at the north end of the DBF were oriented to measure lateral force.

The lateral force carried by the ground links was measured by a load cell at both sides of the test structure. The locations of these load cells are indicated in Figure 4.1. These load cells were manufactured by Houston Scientific and have a range of ±600 kips. They are 12 inch long with a diameter of 6 inch, and coupled with a threaded rod on either side. They were held in place by a pair of tapered collars, which prestressed the load cell and prevented slip in the threaded rod. Further details of the ground link configuration can be found in Dong (2013).

Load cells are also be provided for each damper. These differ depending on the type of damper.

5.2.4 **Displacement transducers**

A combination of LVDTs, temposonics, and linear potentiometers are used to measure displacements and relative displacements of the two frames and their fixtures.

5.2.4.1 DBF

Figure 5.11 shows the initial placement of displacement transducers used in the DBF. One-quarter inch stroke LVDTs are used to measure any horizontal axial deformation of the ground links. In the initial configuration three instruments were used on each ground link, one measuring the deflection of the spreader beam that transfers the ground link force to the braces that carry it into the laboratory strong floor and two on either side of

the ground link load cell, measuring the load cell axial deformation. It was later determined that a better configuration was to use two instruments and to measure the lateral movement of the column flanges at the center of the ground link. This configuration appears in Figure 5.12.

During MR damper testing, linear potentiometers were used to measure damper displacement, (i.e. the stroke of the damper), because they are less susceptible to the interference caused by the damper's magnetic field. For testing using other damper types, LVDTs will be used to measure damper displacement because linear potentiometers have more noise due to any variation in supply current. To measure damper displacement an instrument with ±3 inch of stroke was used. During initial testing LVDTs were installed to measure axial deformation of the rigid links. These instruments were installed on either side of the rigid link tube as shown in Figure 5.13.

The displacement of each floor of the DBF and MRF relative to the bracing frame was measured by a displacement transducer mounted at the middle of each bay. This transducer was mounted to the top flange of the beam as shown in Figure 5.14. The decision to mount the instrument on the top flange was to mimic the node location in previously produced computer models. During initial characterization of the structure short range LVDTs were used to measure the first and second floor displacement as these provided more accurate reading over the smaller displacements that the frame was subjected to. Once a damper was installed, the frame was subjected to larger lateral displacements, so longer range linear potentiometers and temposonics were used instead. Linear potentiometers were used in locations near where an MR damper was installed to

prevent any possible electronic interference. The decision to used temposonics instead of LVDTs was due to the availably of more long range temposonics.

Axial deformation and rotation of the T-connection were determined using four-½ inch range LVDTs (± ½ inch) arranged in the configuration shown in Figure 5.15. The average of the four sensors was used to measure the deformation across the T-connection. Rotation reported in radians was determined using the following formula:

$$\theta = \frac{\Delta_{top} - \Delta_{btm}}{d_{LVDT}} \tag{5-3}$$

where,

θ = rotation across T-connection (radians)

Δ_{top}= average deformation of top flange LVDTs

Δ_{btm}= average deformation of bottom flange LVDTs

d_{LVDT}= distance between LVDTs

5.2.4.2 MRF

Figure 5.16 shows the locations of displacement transducers on the MRF. To measure horizontal floor displacements, linear temposonics are mounted at mid bay. These will measure the floor displacement relative to the bracing frame. This configuration is the same as that shown in Figure 5.14. The third floor uses a 44 inch (± 22 inch), while the other two floors use 30 inch (± 15 inch) temposonics to allow testing to over 6% story

drift. The ground floor will have a 1-inch range LVDT (± 1 inch) mounted in a similar manner to that shown in Figure 5.14.

At the RBS sections a set of 4 LVDTs are used to measure rotation as well as axial deformation in the RBS. The instruments will be mounted on the inside of the flanges, two LVDTs on the top flange on either side of the web and two LVDTs on the bottom flange on either side of the web, as shown in Figure 5.17. This configuration is similar to that used to measure the axial deformation of the T-connections in the DBF. Equation (5-3) will be used to determine the rotation in radians. Sizing of these instruments is based on expected plastic rotation of up to 3% radians within the RBS. Accounting for the depth the shallower third floor beams requires a ½ inch range LVDTs (± ½ inch), while the other stories with deeper W14 and W18 beams require 1 inch range LVDTs (± 1 inch).

The deformation of the MRF south ground link will be measured with two-¼ inch range LVDTs (± ¼ inch) mounted on each side of the column, which will measure lateral displacement at the ground link column interface relative to the ground. This configuration is the same as on the DBF north ground link.

Two ¼ inch range LVDTs (± ¼ inch) will be fixed to either side of each column base plate to measure column uplift. This uplift is important to know because it could indicate slop in the load pins supporting the column.

5.2.4.3 Other displacements and deformations

The deformation of the bay link will be measured in a similar manner, with two - ¼ inch range LVDTs (± ¼ inch) mounted to the column on either side of the link, but instead of using a fixed reference point on the ground, the LVDT will measure relative displacement between the MRF and DBF inner columns. Figure 5.5 shows the placement of the bay link displacement transducers.

5.2.5 **Strain gauges**

Figure 5.18 shows the single strain gauge locations for the DBF. Strain gauges were placed in areas that were deemed critical and likely to yield during testing. To determine which locations were most likely to yield, structural analysis were conducted. Areas where strain gauges were located include the first and third story gusset plates connecting the beams to the braces, the column flanges at the bottom of the structure, and the first story braces. It was determined that the second story braces and gussets were unlikely to yield before the other stories so these did not receive gauges. All strain gauges on the DBF were 350-ohm strain gauges with a range of ± 3 percent.

Figure 5.19 shows the location of strain gauges for the MRF. Two different types of strain gauges were installed on the MRF. The first kind are rosette strain gauges. These gauges were installed in the panel zones and measure strain vertically, horizontally and 45° diagonally. A rosette was installed on both sides of each floor's panel zone. Additionally strain gauges were installed within the RBS section to measure deformation. Two gauges were installed on the outside of each flange and two gauges were installed on each side of the web of the beam, for a total of 8 strain gauges per RBS.

Figure 5.22Figure 5.20 through Figure 5.21 show the layout of these strain gauges at the first, second and third floors, respectively. All MRF strain gauges are of a 120 ohm resistance.

5.2.6 **Accelerometers**

Figure 5.23 shows the locations of 7 accelerometers used to measure frame accelerations of the DBF. These accelerations were needed as feedback signals for various MR damper control laws. The accelerometers located on the columns were attached to the outer flange of the north column in line with each floor. The three accelerometers located on the braces were attached to the lower brace gusset as shown in Figure 5.23 and measured horizontal brace accelerations. One accelerometer was located at midbay on the ground floor beam. All accelerometers were single axis accelerometers manufactured by Kistler which were capable of measuring ± 3g's and measured accelerations in the North-South direction as indicated in Figure 5.23.

5.3 Determination of Internal Force from Instrumentation

One objective of the instrumentation of the two frames was to measure internal member forces, frictional forces and reactions during a test. Whenever it was practical, the force was directly measured via load cells or full bridges. The following describes how member forces are obtained that are not directly measured.

5.3.1 **Column and brace shears**

Axial forces and moments in the columns and braces were directly measured. Using the moment measured from two full bridges on a single member and the free body diagram

shown in Figure 5.24 it was possible to determine the member shear force, V, from statics where:

$$V = \frac{M_2 - M_1}{d} \tag{5-4}$$

where,

V= Shear in column

M_1= Moment output of lower full bridge

M_2= Moment output of upper full bridge

d= distance between full bridges

5.3.2 **Beam internal forces**

The internal forces in the beams of the DBF can be determined using measured moments and axial forces from the column and brace full bridges. Considering the free body diagram shown in Figure 5.25 for the DBF, the shear V_B, axial force P_B and moment M_B in the beam can be obtained by statics using the following three equations:

$$V_B = F_{LC} - F_{UC} + cos\theta * F_{BR} - sin\theta * V_{BR} \tag{5-5}$$

$$F_B = -V_{LC} + V_{UC} - sin\theta * F_{BR} - cos\theta * V_{BR} \tag{5-6}$$

$$M_B = -V_{UC} * HUC - V_{LC} * HLC - V_B * L - V_{BR} * LBR - M_{UC} + M_{LC} + M_{BR} \tag{5-7}$$

where the column (V_{LC}, V_{UC}) and brace (V_{BR}) shears were determined using Equation (5-4). To determine the forces in the MRF beams, the brace terms in the above equations are set to zero. A free body of this configuration is shown in Figure 5.26.

5.3.3 **Story shear**

There are several instances where story shear will be a useful quantity to know during testing, including assessing friction in the test setup. In order to determine story shear a horizontal cut through the structure at a floor is made and the story shear is obtained from statics.

5.3.4 **Friction on test structure**

The free body diagram in Figure 5.27 shows static lateral forces applied to the DBF where the MRF is not connected to the loading beams. In order to assess the amount of 3rd story friction in the due to friction the free body diagram in Figure 5.28 was used in which the frame has been cut through the third story. A story shear could be derived by summing the horizontal components of the brace axial and shear force and adding those to the column shear force. Then by summing lateral forces the magnitude of the 3rd story friction force could be determined. To find the 2nd story friction force the free body in Figure 5.29 was used in a similar manner, only this time the now known 3rd story friction force is considered. Once the 2nd story friction force is solved for the 1st story friction force is found using the free body diagram in Figure 5.30.

Figure 5.31 shows the lateral forces applied to the MRF from the loading beams. Friction will be determined following the procedure specified for determining friction force in the DBF, by where the friction force will be found in each floor by comparing the measured

applied load to the measured story shear. To determine the friction in the 3rd story the free body diagram in Figure 5.32 will be used. By setting the sum of these forces equal to zero the friction force is solved for. In a similar manner the free body in Figure 5.33 will be used to assess the friction force in the second story and the free body in Figure 5.34 to assess the friction force in the first floor.

5.4 Calibration of the Bay Link Full Bridge

The full bridge on the bay link was calibrated in order to determine the relationship between bridge output voltage and axial force in the link. Calibration was done using a 2670 kN Sactec universal test machine. The link was subjected to 75kips of compressive force. The voltage change and deformation during the test was recorded. This calibration was repeated twice.

An excitation voltage of 6V used to measure voltage change in the full bridge on the bay link. Voltages were manually read using a volt meter and recorded every 7.5kips. The relationship between voltage change and axial force was then used to establish the calibration constant. A plot of this relationship appears in Figure 5.35. This calibration constant is included in Table 5.1.

Table 5.1 – Full bridge inputs

Name	Type	Location	X Factor	Input Voltage (V)	X Factor Units
FB1	Moment	DBF First Story Column	82818	10	kip-in/volt
FB2	Axial	DBF First Story Column	41853	10	kip/volt
FB3	Moment	DBF First Story Column	82818	10	kip-in /volt
FB4	Moment	DBF Second Story Column	82818	10	kip-in/volt
FB5	Axial	DBF Second Story Column	41853	10	kip/volt
FB6	Moment	DBF Second Story Column	82818	10	kip-in/volt
FB7	Moment	DBF Third Story Column	82818	10	kip-in/volt
FB8	Axial	DBF Third Story Column	41853	10	kip/volt
FB9	Moment	DBF Third Story Column	82818	10	kip-in/volt
FB10	Moment	DBF First Story Column	82818	10	kip-in/volt
FB11	Axial	DBF First Story Column	41853	10	kip/volt
FB12	Moment	DBF First Story Column	82818	10	kip-in/volt
FB13	Moment	DBF Second Story Column	82818	10	kip-in/volt
FB14	Axial	DBF Second Story Column	41853	10	kip/volt
FB15	Moment	DBF Second Story Column	82818	10	kip-in/volt
FB16	Moment	DBF Third Story Column	82818	10	kip-in/volt
FB17	Axial	DBF Third Story Column	41853	10	kip/volt
FB18	Moment	DBF Third Story Column	82818	10	kip-in/volt
FB19	Axial	DBF First Story Brace	19057	10	kip/volt
FB20	Moment	DBF First Story Brace	23173	10	kip-in/volt
FB21	Moment	DBF First Story Brace	23173	10	kip-in/volt
FB22	Moment	DBF First Story Brace	23173	10	kip-in/volt
FB23	Moment	DBF First Story Brace	23173	10	kip-in/volt
FB24	Axial	DBF First Story Brace	19057	10	kip/volt
FB25	Axial	DBF Second Story Brace	19057	10	kip/volt
FB26	Moment	DBF Second Story Brace	23173	10	kip-in/volt

Name	Type	Location	X Factor	Input Voltage (V)	X Factor Units
FB27	Moment	DBF Second Story Brace	23173	10	kip-in/volt
FB28	Moment	DBF Second Story Brace	23173	10	kip-in/volt
FB29	Moment	DBF Second Story Brace	23173	10	kip-in/volt
FB30	Axial	DBF Second Story Brace	19057	10	kip/volt
FB31	Axial	DBF Third Story Brace	19057	10	kip/volt
FB32	Moment	DBF Third Story Brace	23173	10	kip-in/volt
FB33	Moment	DBF Third Story Brace	23173	10	kip-in/volt
FB34	Moment	DBF Third Story Brace	23173	10	kip-in/volt
FB35	Moment	DBF Third Story Brace	23173	10	kip-in/volt
FB36	Axial	DBF Third Story Brace	19057	10	kip/volt
FB37	Axial	DBF Ground Floor Column	41853	10	kip/volt
FB38	Moment	MRF First Story Column	132635	6	kip-in/volt
FB39	Moment	MRF First Story Column	132635	6	kip-in/volt
FB40	Moment	MRF First Story Column	68585	6	kip/volt
FB41	Moment	MRF First Story Column	132635	6	kip-in/volt
FB42	Moment	MRF Second Story Column	132635	6	kip-in/volt
FB43	Axial	MRF Second Story Column	68585	6	kip/volt
FB44	Moment	MRF Second Story Column	132635	6	kip-in/volt
FB45	Moment	MRF Third Story Column	132635	6	kip-in/volt
FB46	Axial	MRF Third Story Column	68585	6	kip/volt
FB47	Moment	MRF Third Story Column	132635	6	kip-in/volt
FB48	Moment	MRF First Story Column	132635	6	kip-in/volt
FB49	Axial	MRF First Story Column	68585	6	kip/volt
FB50	Moment	MRF First Story Column	132635	6	kip-in/volt
FB51	Axial	MRF Second Story Column	132635	6	kip/volt
FB52	Moment	MRF Second Story Column	68585	6	kip-in/volt
FB53	Moment	MRF Second Story Column	132635	6	kip-in/volt

Name	Type	Location	X Factor	Input Voltage (V)	X Factor Units
FB55	Axial	MRF Third Story Column	132635	6	kip/volt
FB56	Moment	MRF Third Story Column	68585	6	kip-in/volt
FB57	Axial	MRF Ground Story Column	132635	6	kip/volt
FB58	Axial	MRF Ground Story Column	68585	6	kip/volt
FB59	Axial	First Story Loading Beam	68585	6	kip/volt
FB60	Axial	First Story Loading Beam	59236	6	kip/volt
FB61	Axial	Second Story Loading Beam	59236	6	kip/volt
FB62	Axial	Second Story Loading Beam	59236	6	kip/volt
FB63	Axial	Third Story Loading Beam	59236	6	kip/volt
FB64	Axial	Third Story Loading Beam	59236	6	kip/volt
FB65	Axial	Bay Link	17161	6	kip/volt

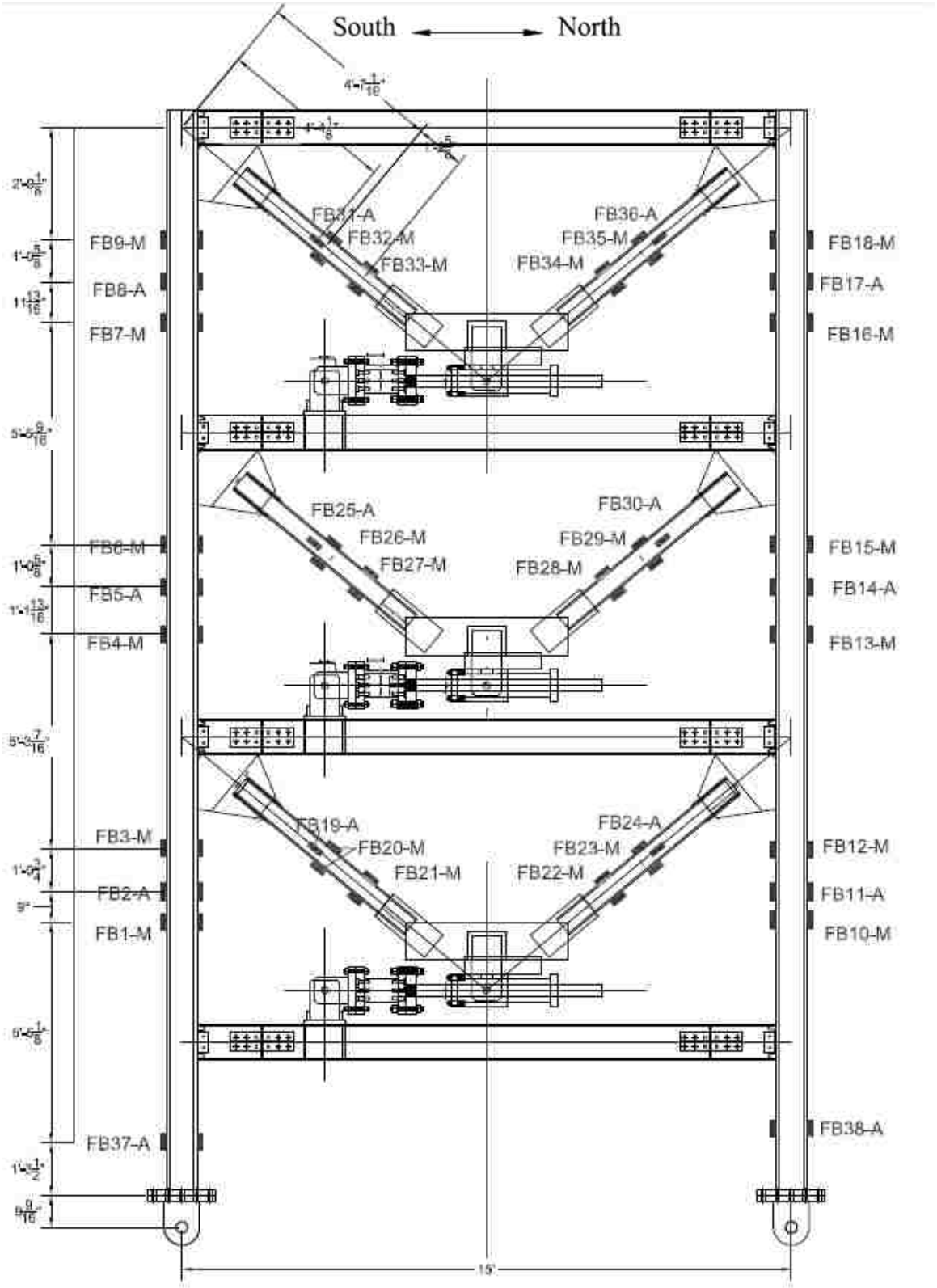

Figure 5.1 – DBF Full Bridge Locations

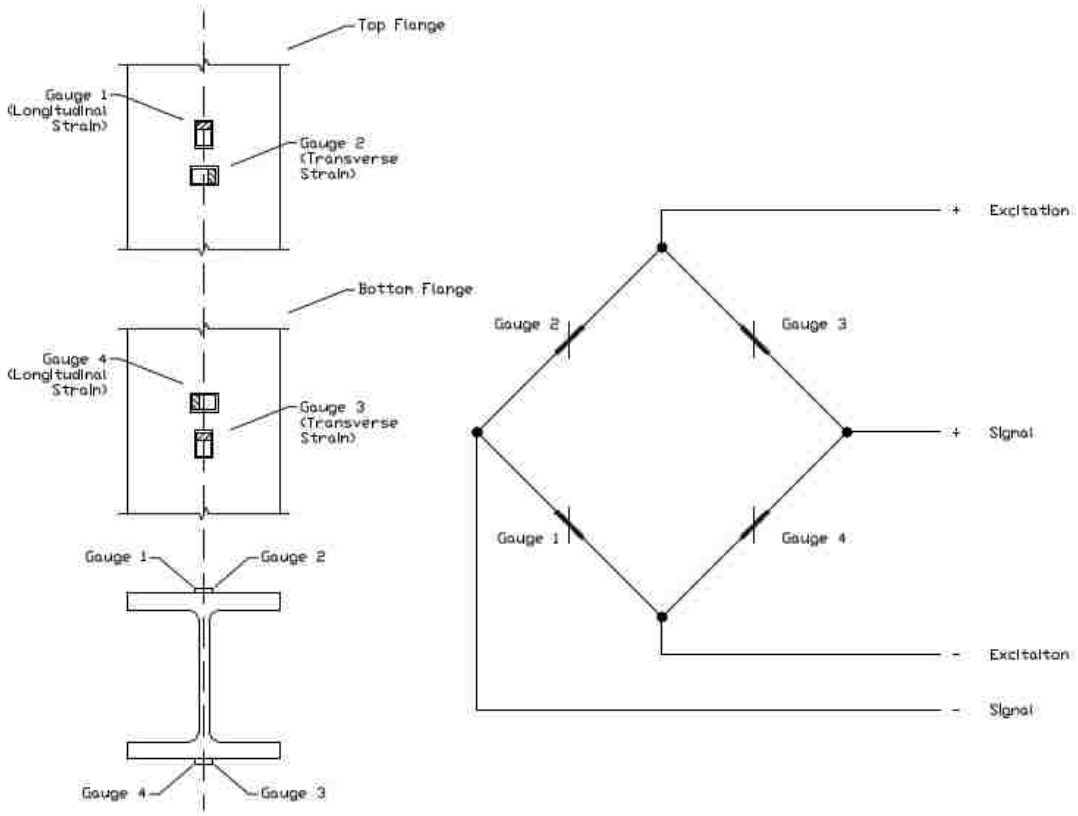

Figure 5.2 – Axial Force Full Bridge Geometry and Wiring Schematic

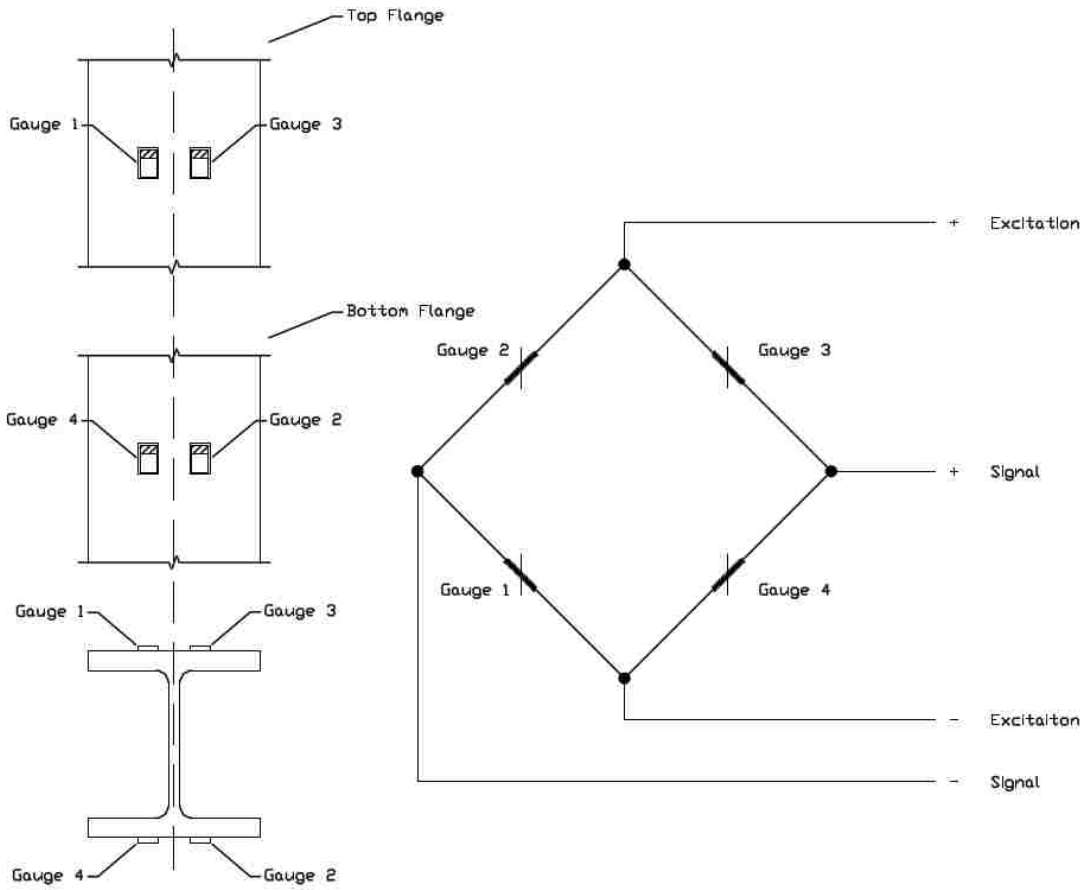

Figure 5.3 – Bending Moment Full Bridge Geometry and Wiring Schematic

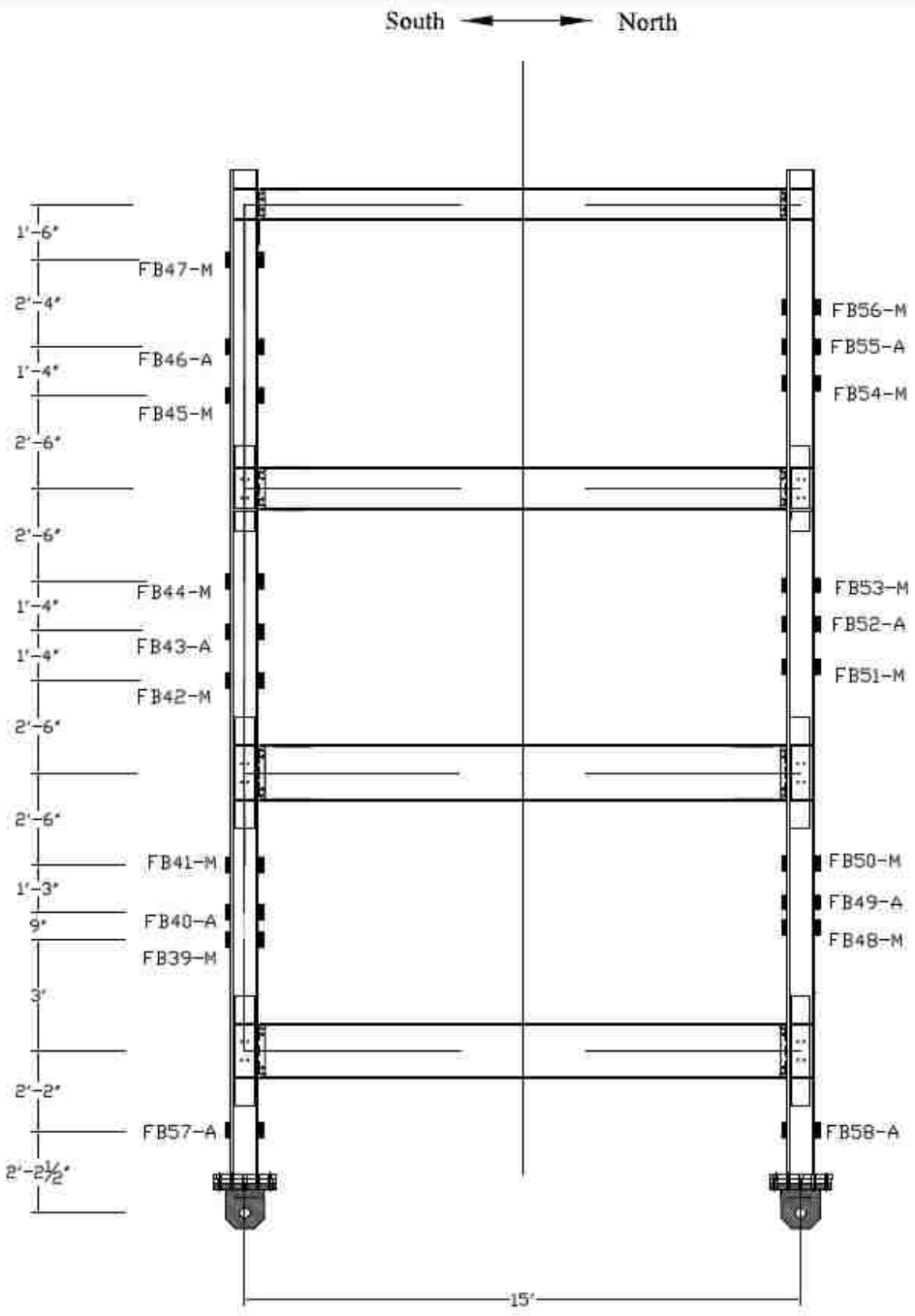

Figure 5.4 – MRF Column Full Bridge Locations

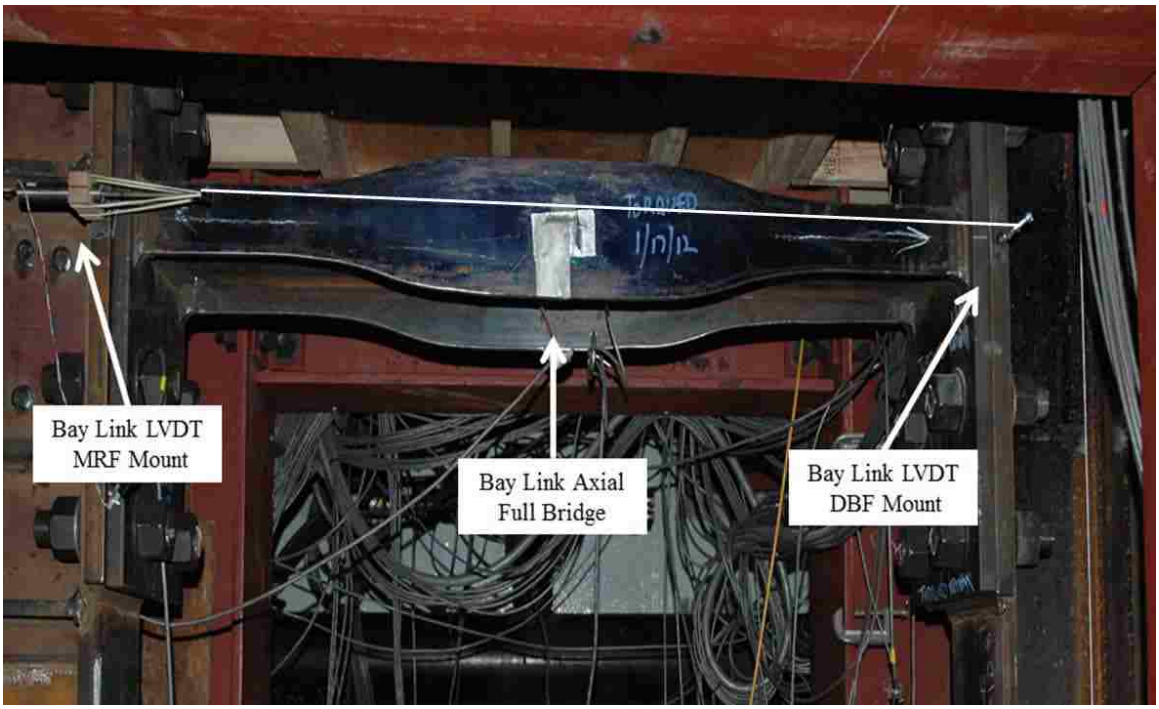

Figure 5.5 – Bay Link Instrumentation

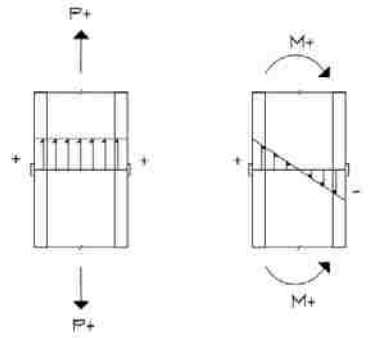

Figure 5.6 – MRF and DBF Column Axial Force and Moment Sign Convention

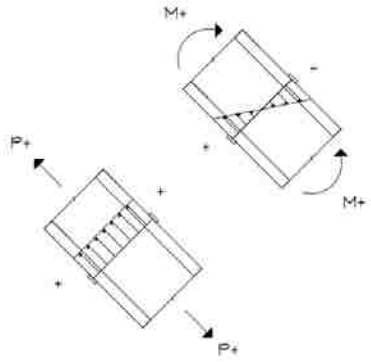

Figure 5.7 – DBF South Brace Axial Force and Moment Sign Convention

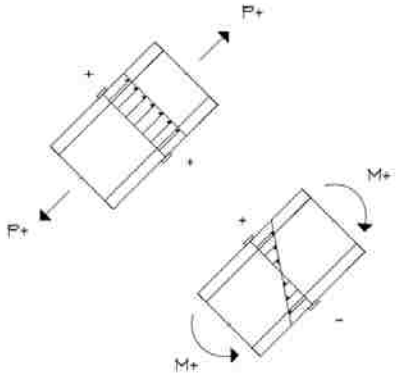

Figure 5.8 – DBF North Brace Axial Force and Moment Sign Convention

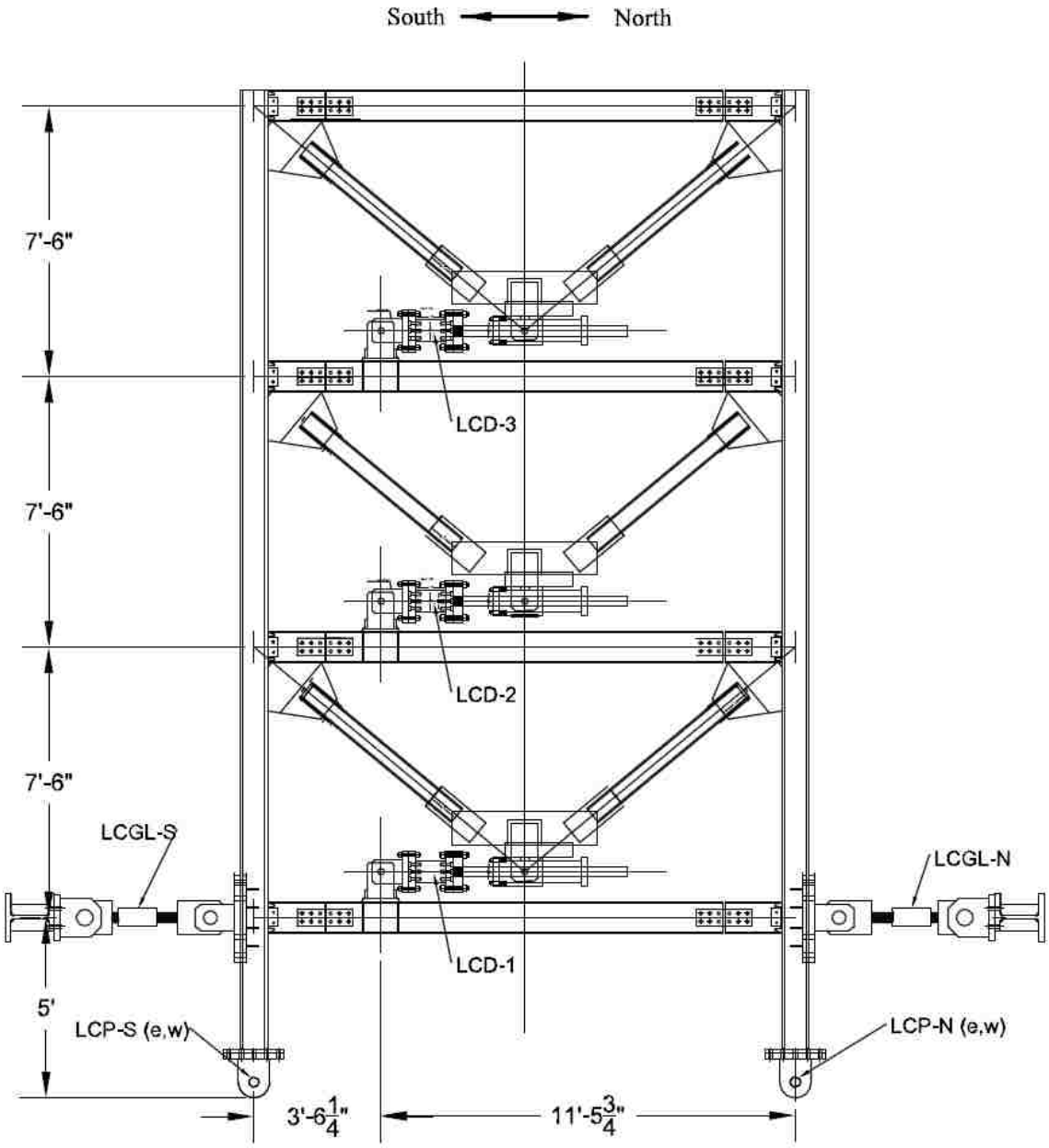

Alias	Instrument	No. of Channels
LCP-x	Load Pin Load Cell	4
LCGL-x	Ground Link Load Cell	2
LCD-x	Damper Load Cell	3

Figure 5.9 – DBF Load Cell Locations

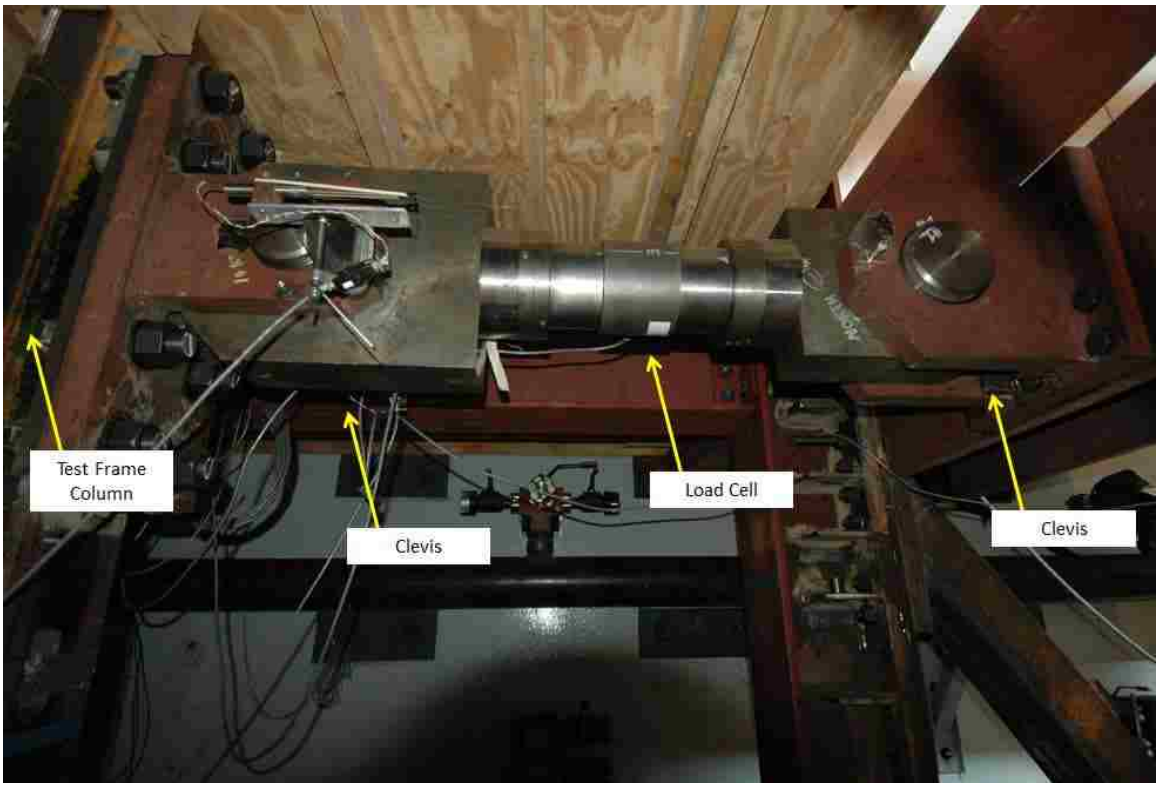

Figure 5.10 – Ground Link Load Cell

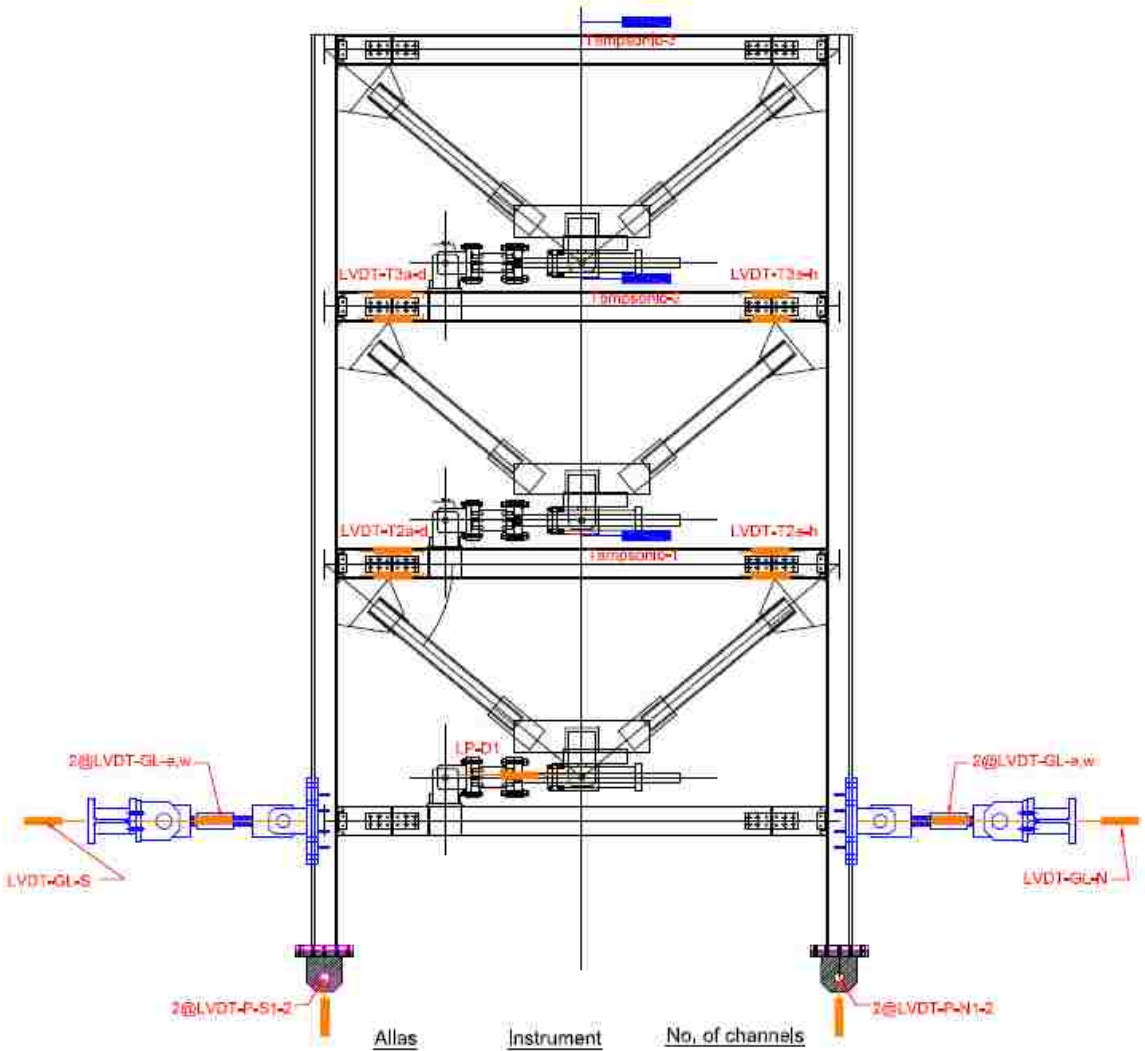

Alias	Instrument	No. of channels
LP-xx	Linear Potentiometer (damper & floor)	2
LVDT-xxx	0,5"~1" LVDT for TEE	16
LVDT-GL-xx	0,25" LVDT for ground-link	6
LVDT-P-xx	0,25" LVDT for column-base	4
Temposonic-xx	Temposonics	3

Figure 5.11 – Location of DBF Displacement Transducers

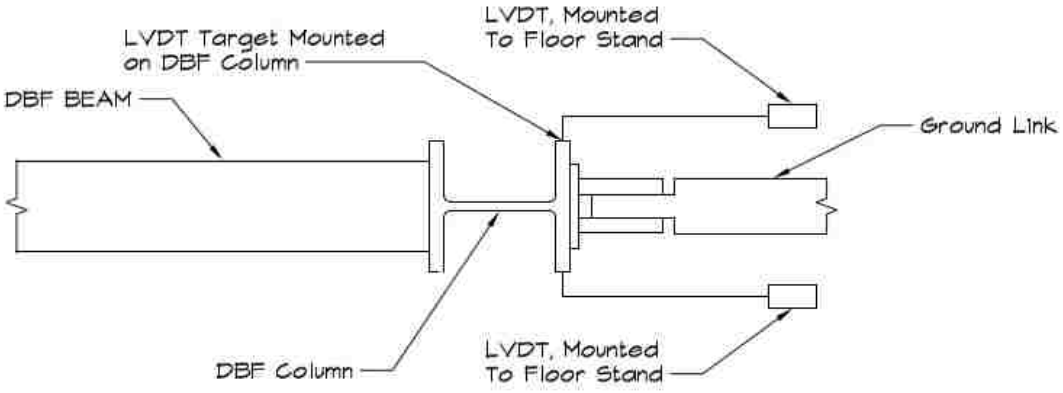

Figure 5.12 – Ground Link Displacement Transducer Plan

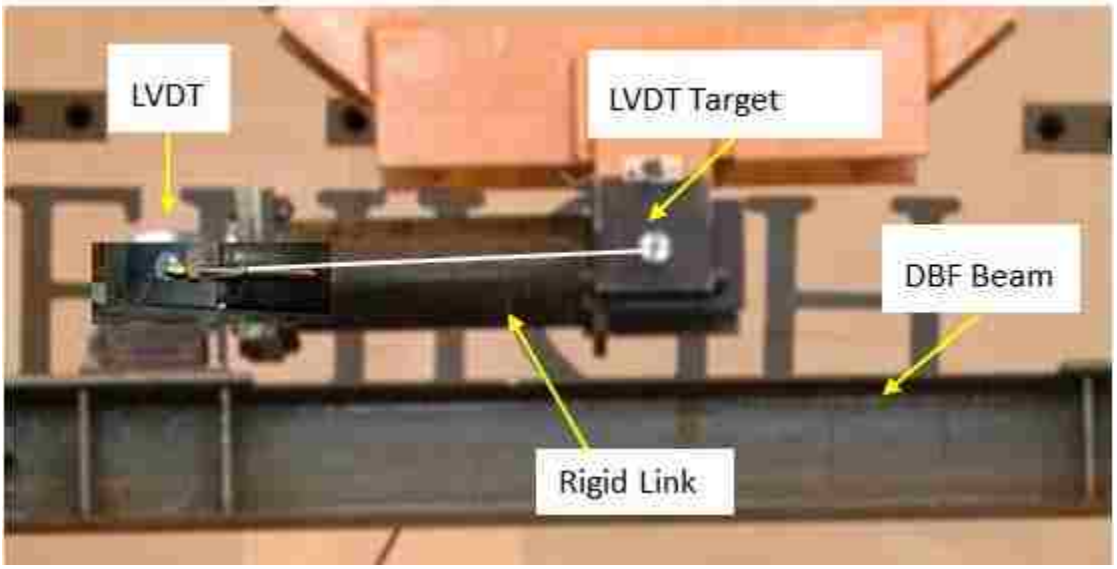

Figure 5.13 – Rigid Link Displacement Transducer

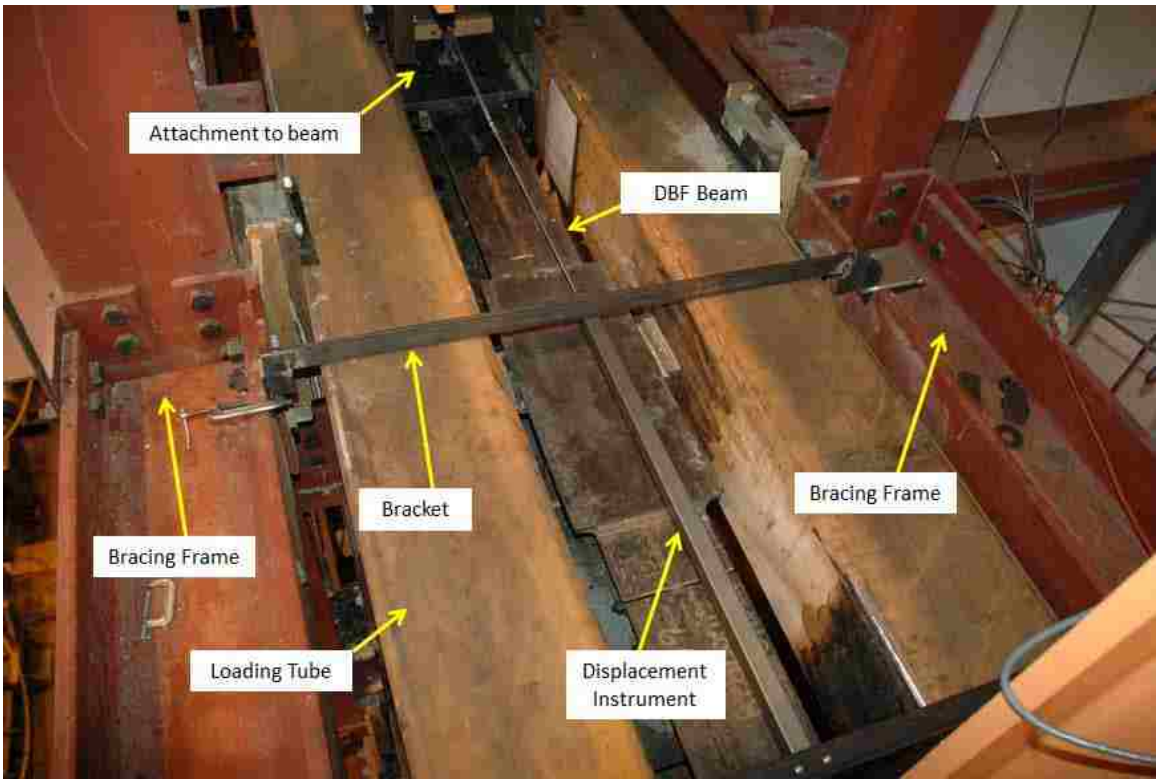

Figure 5.14 – DBF Floor Displacement Transducer

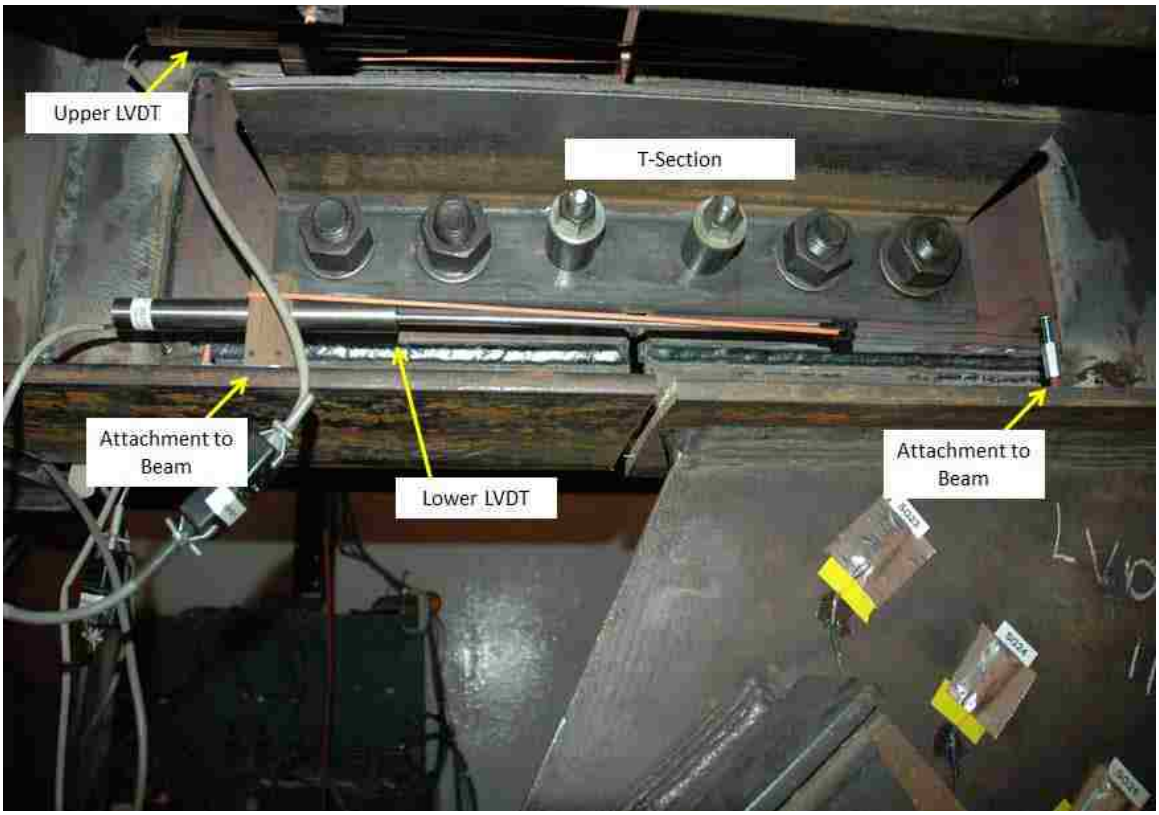

Figure 5.15 – DBF T-Connection LVDT Placement

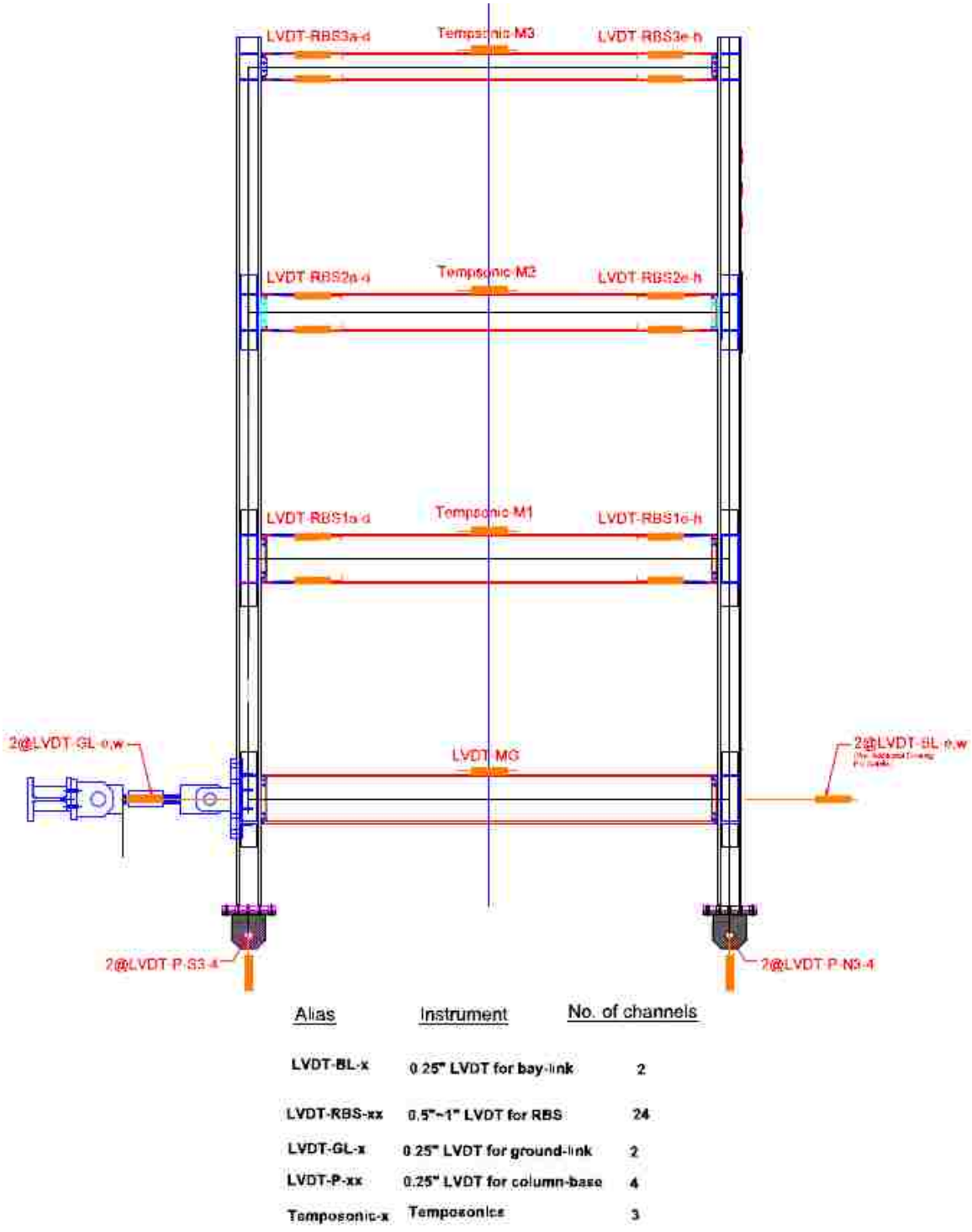

Alias	Instrument	No. of channels
LVDT-BL-x	0.25" LVDT for bay-link	2
LVDT-RBS-xx	0.5"~1" LVDT for RBS	24
LVDT-GL-x	0.25" LVDT for ground-link	2
LVDT-P-xx	0.25" LVDT for column-base	4
Temposonic-x	Temposonics	3

Figure 5.16 – MRF Displacement Transducer Locations

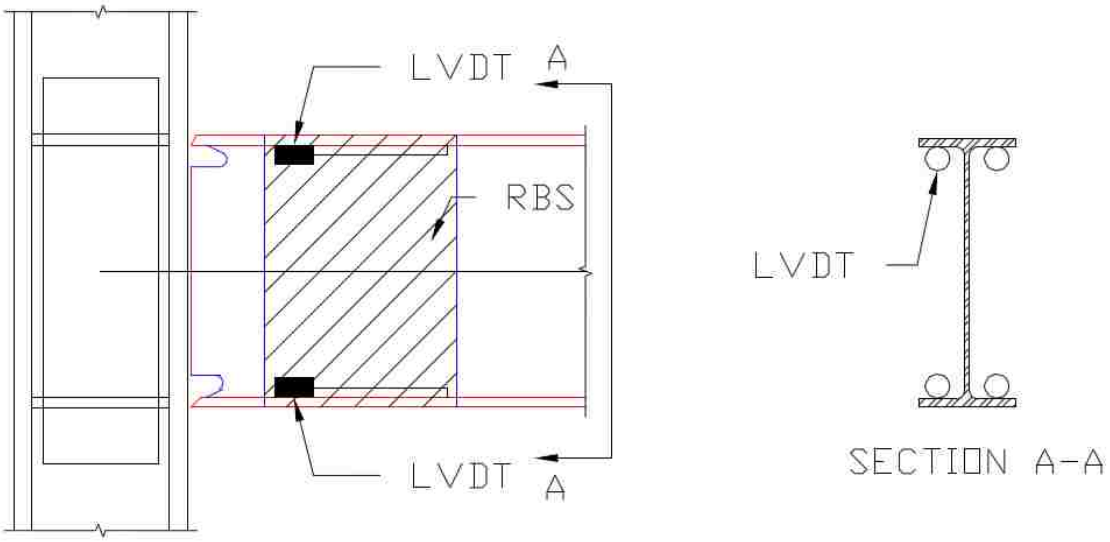

Figure 5.17 – RBS LVDT Placement

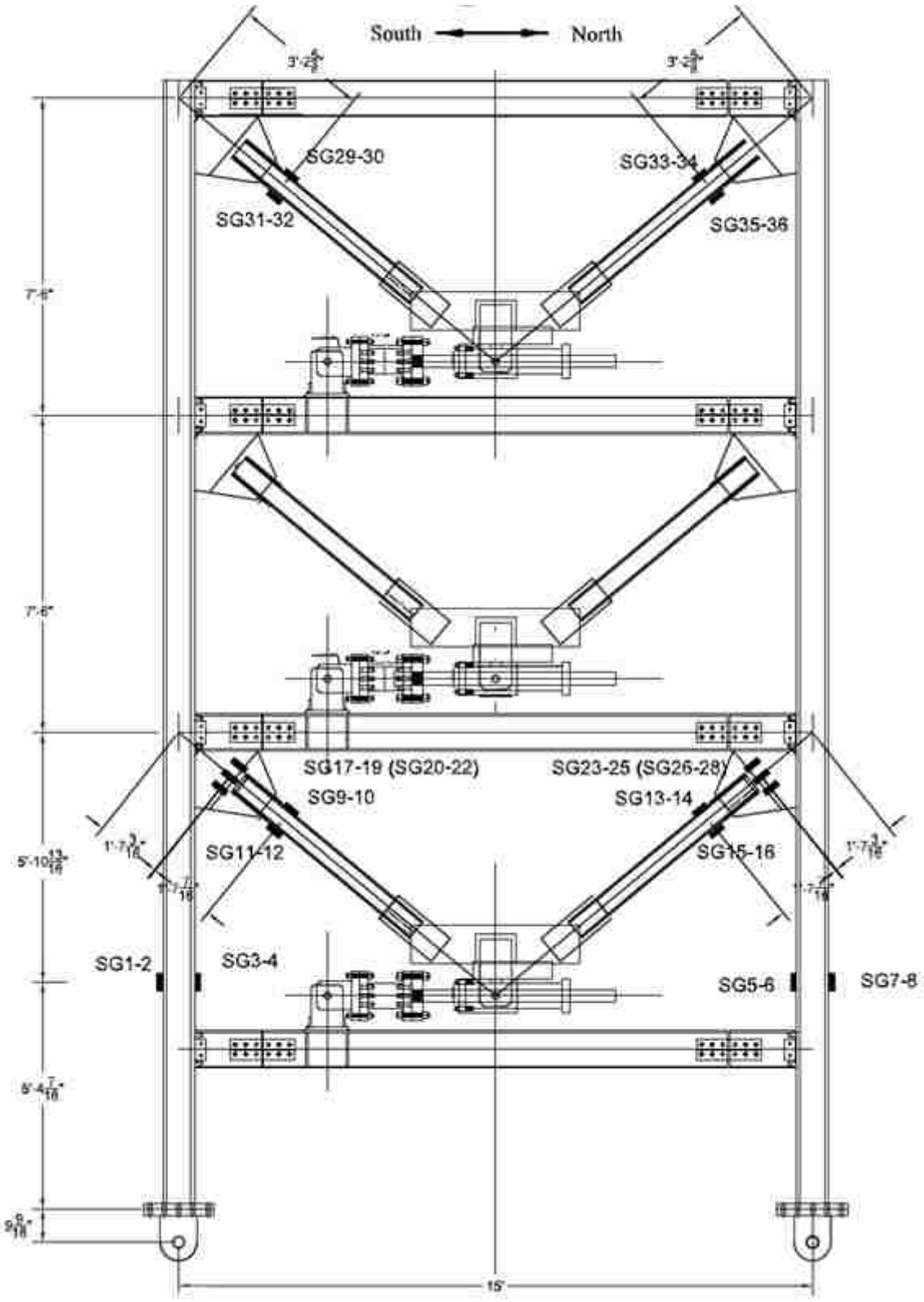

Figure 5.18 – DBF Strain Gauge Locations

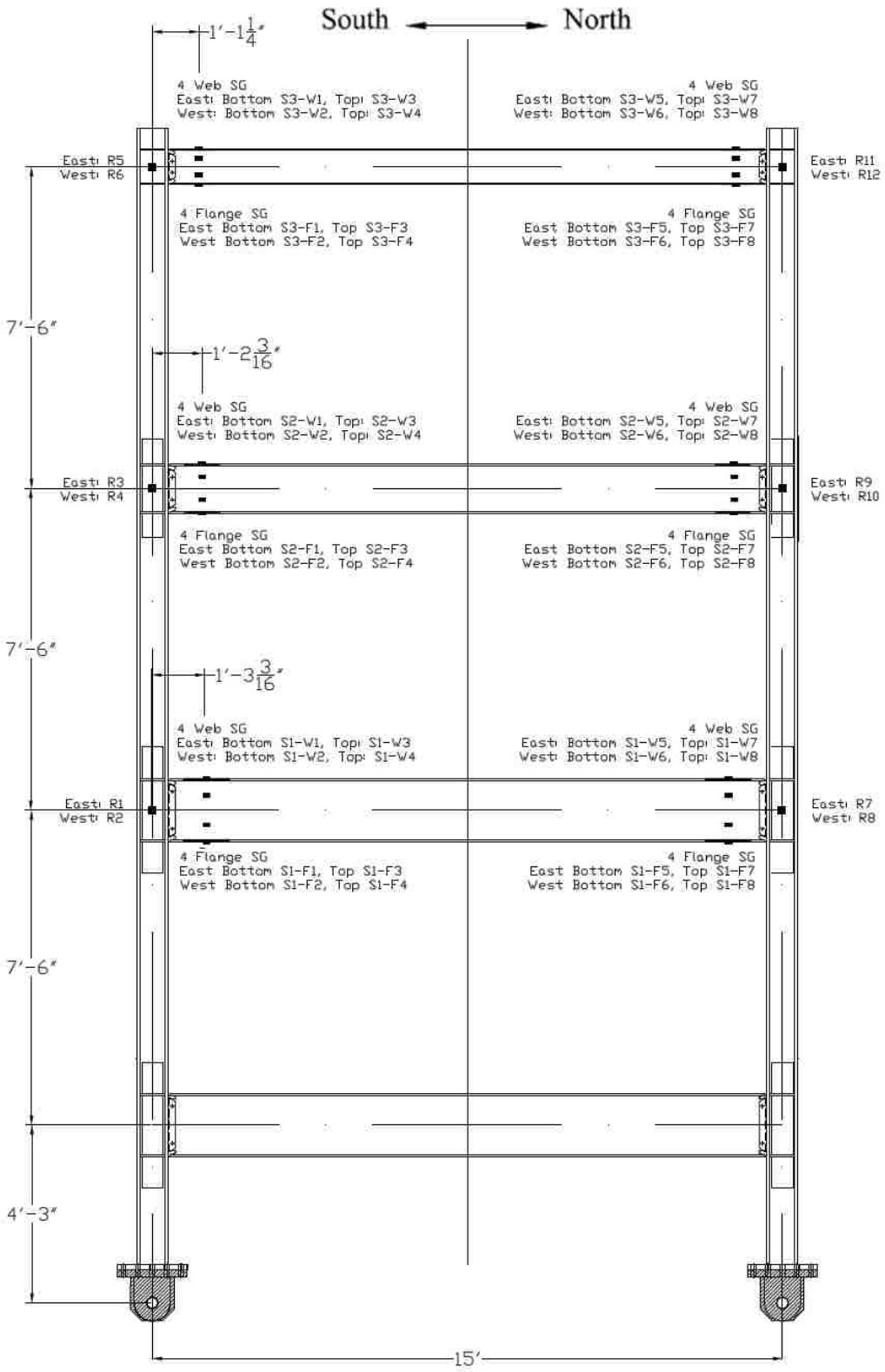

Figure 5.19 – MRF Strain Gauge Locations

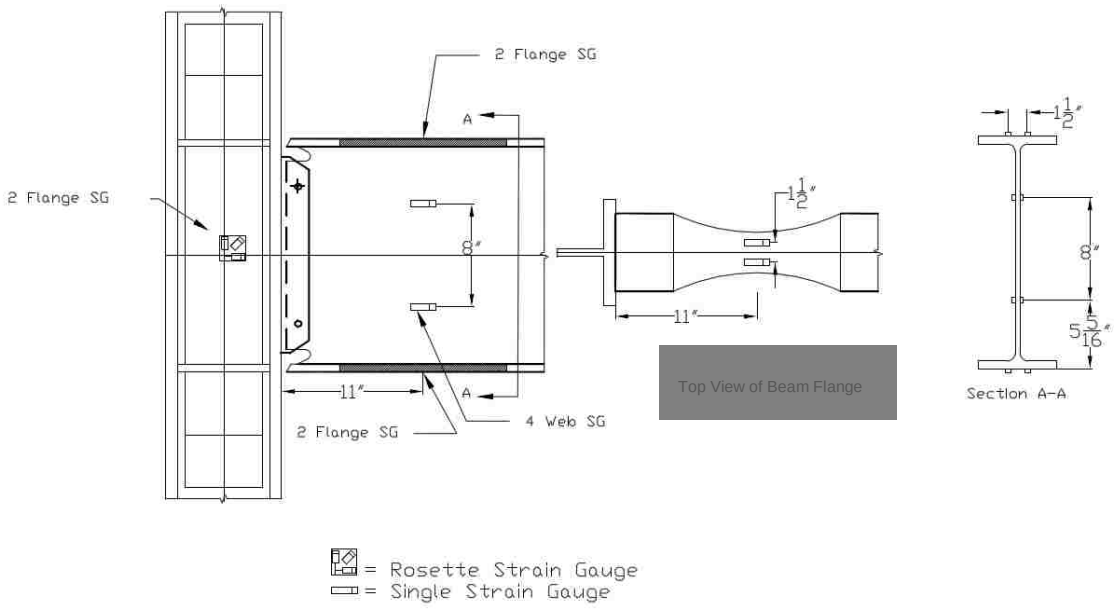

Figure 5.20 – MRF 1st Floor Strain Gauge Locations

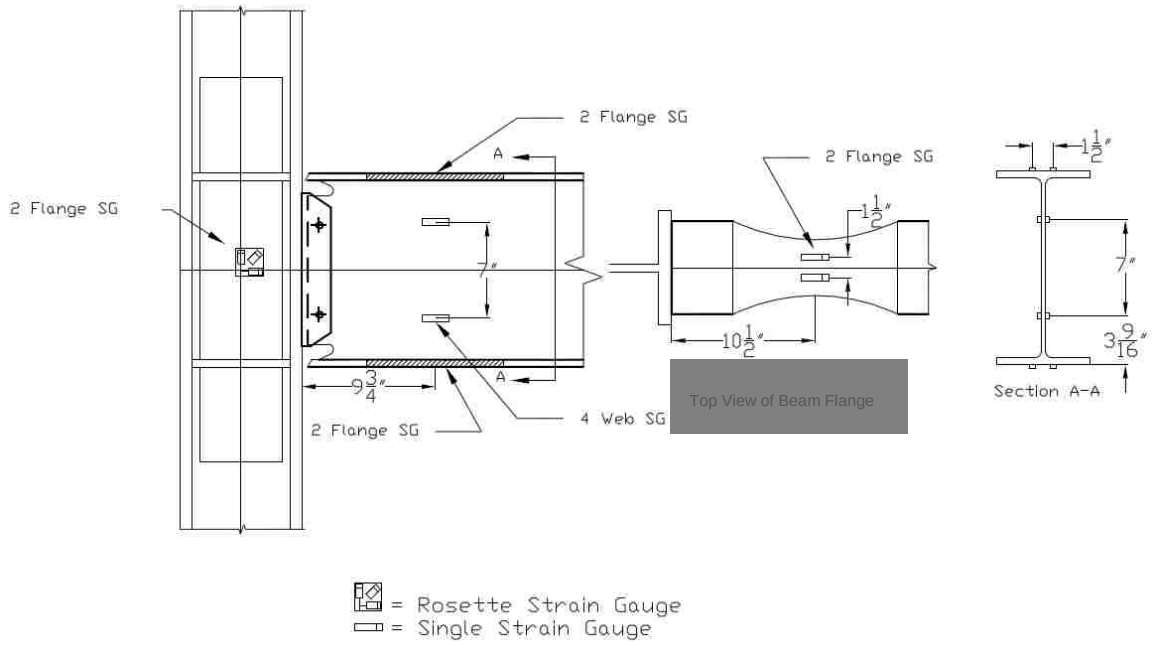

Figure 5.21 – MRF 2nd Floor Strain Gauge Locations

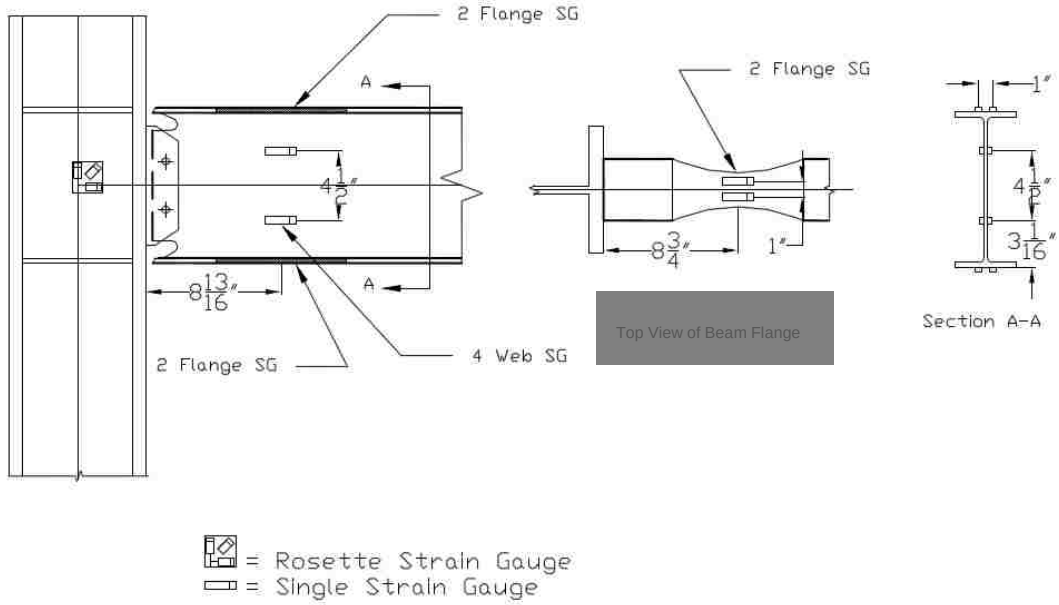

Figure 5.22 – MRF 3rd Floor Strain Gauge Locations

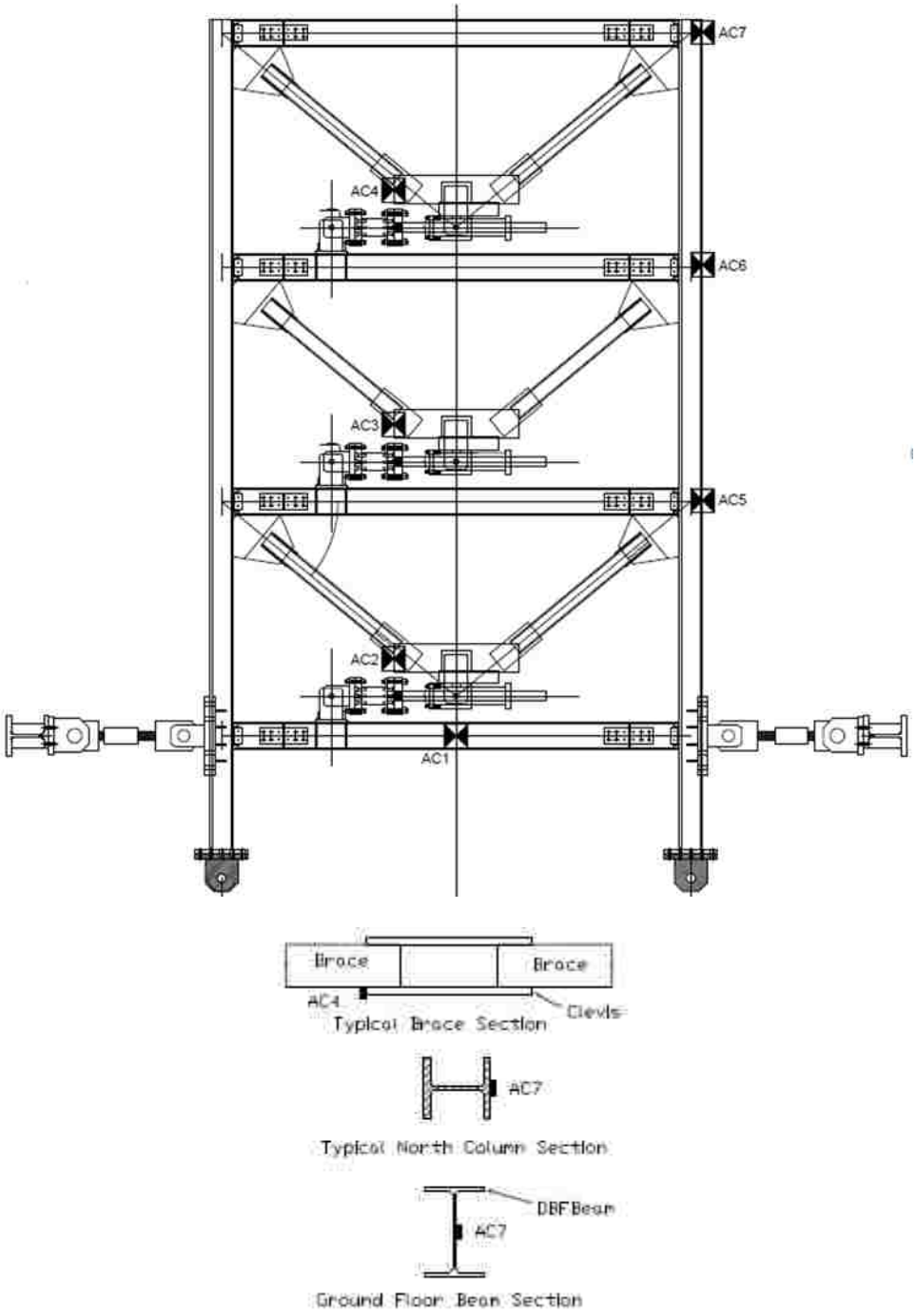

Figure 5.23 – DBF Accelerometer Locations

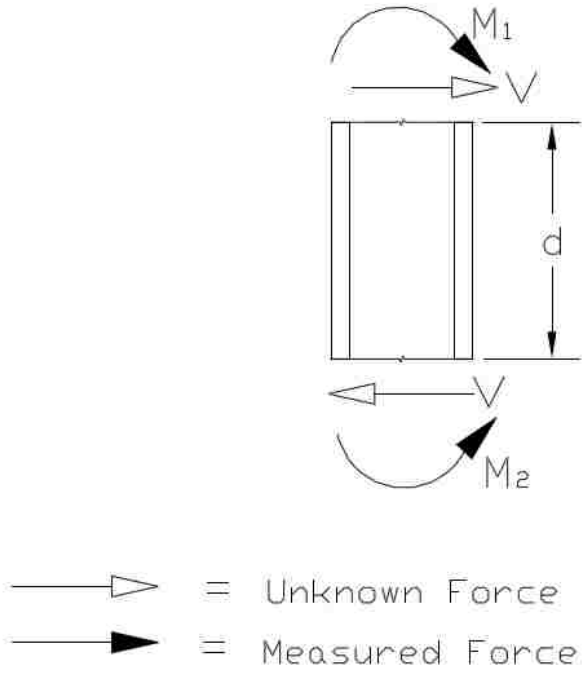

Figure 5.24 – Free Body Diagram Used to Solve Column and Brace Moments (Forces Shown Acting Positive Sense)

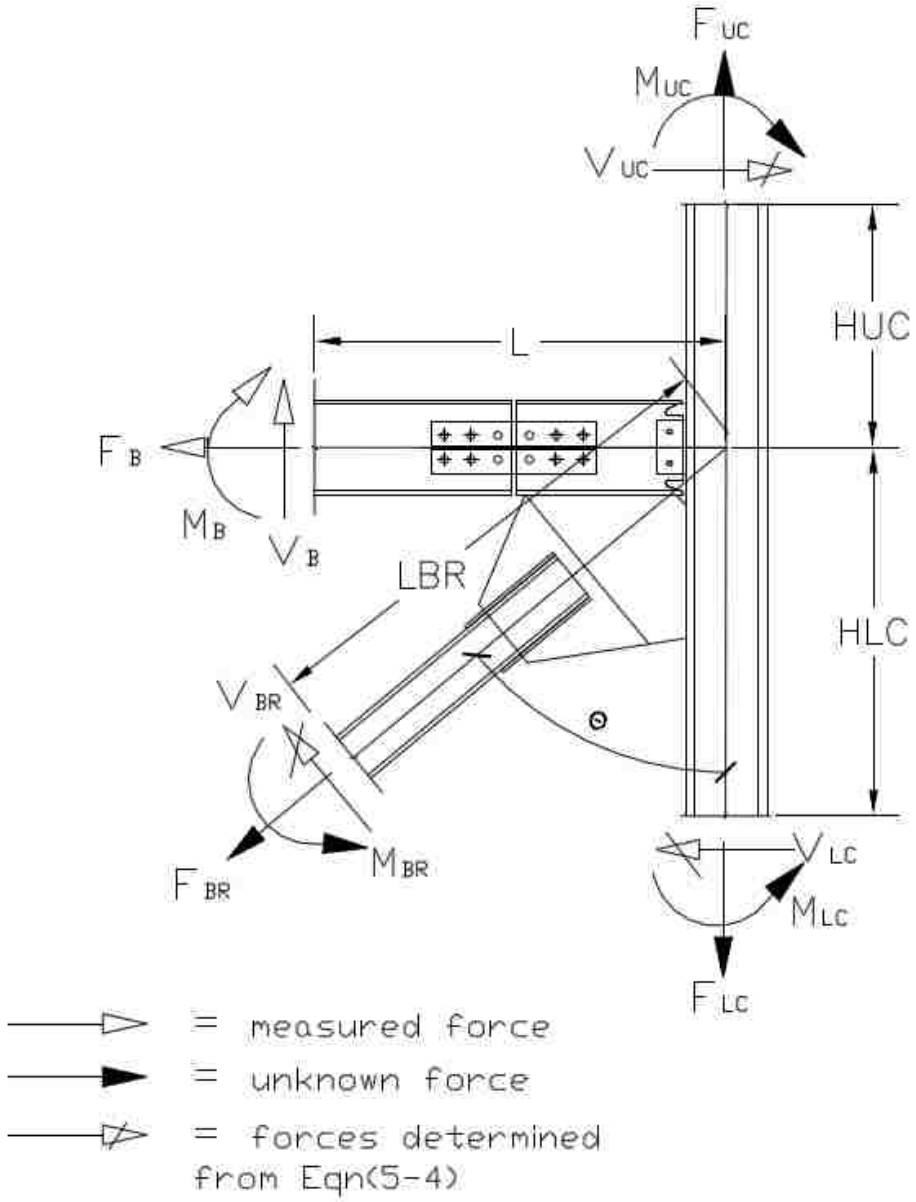

Figure 5.25 – Typical Free Body Diagram Used to Calculate DBF Beam Forces, and Diagonal Brace and Column Shear Forces (Forces Shown Acting Positive Sense)

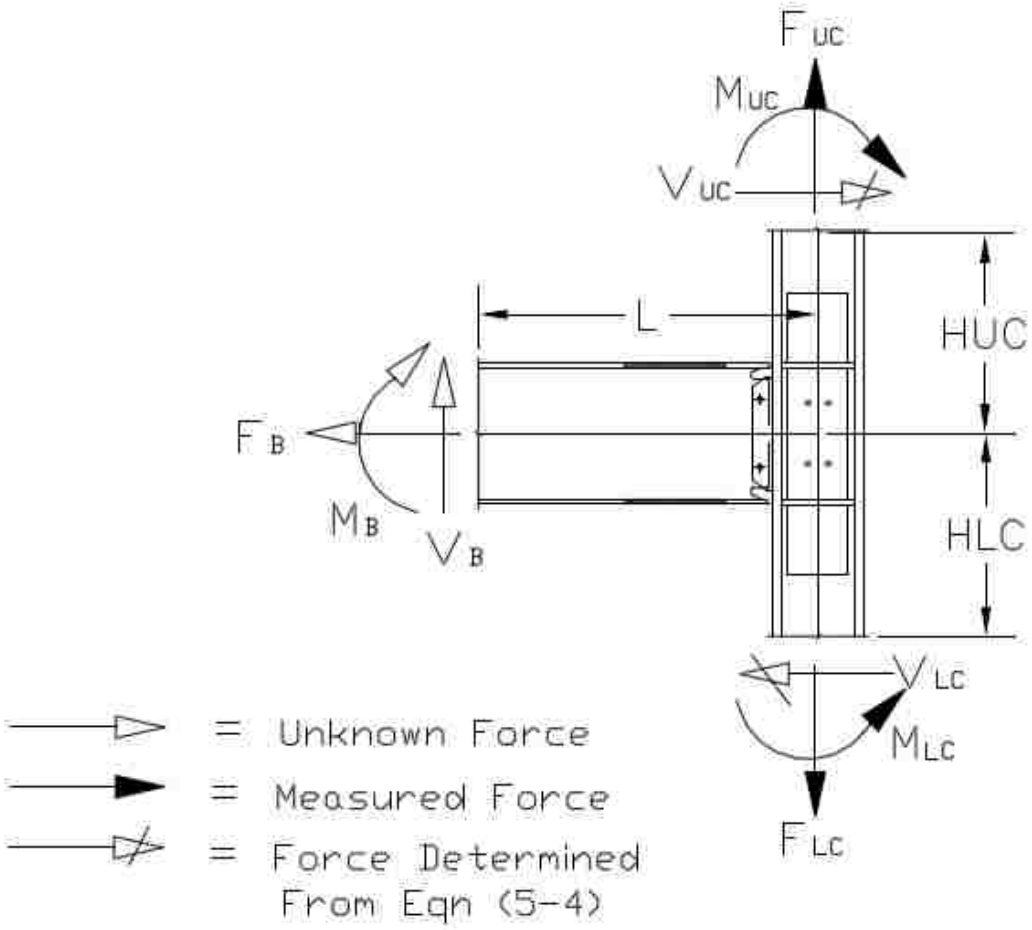

Figure 5.26 – Typical Free Body Diagram Used to Calculate MRF Beam Forces and Column Shear Forces (Forces Shown Acting Positive Sense)

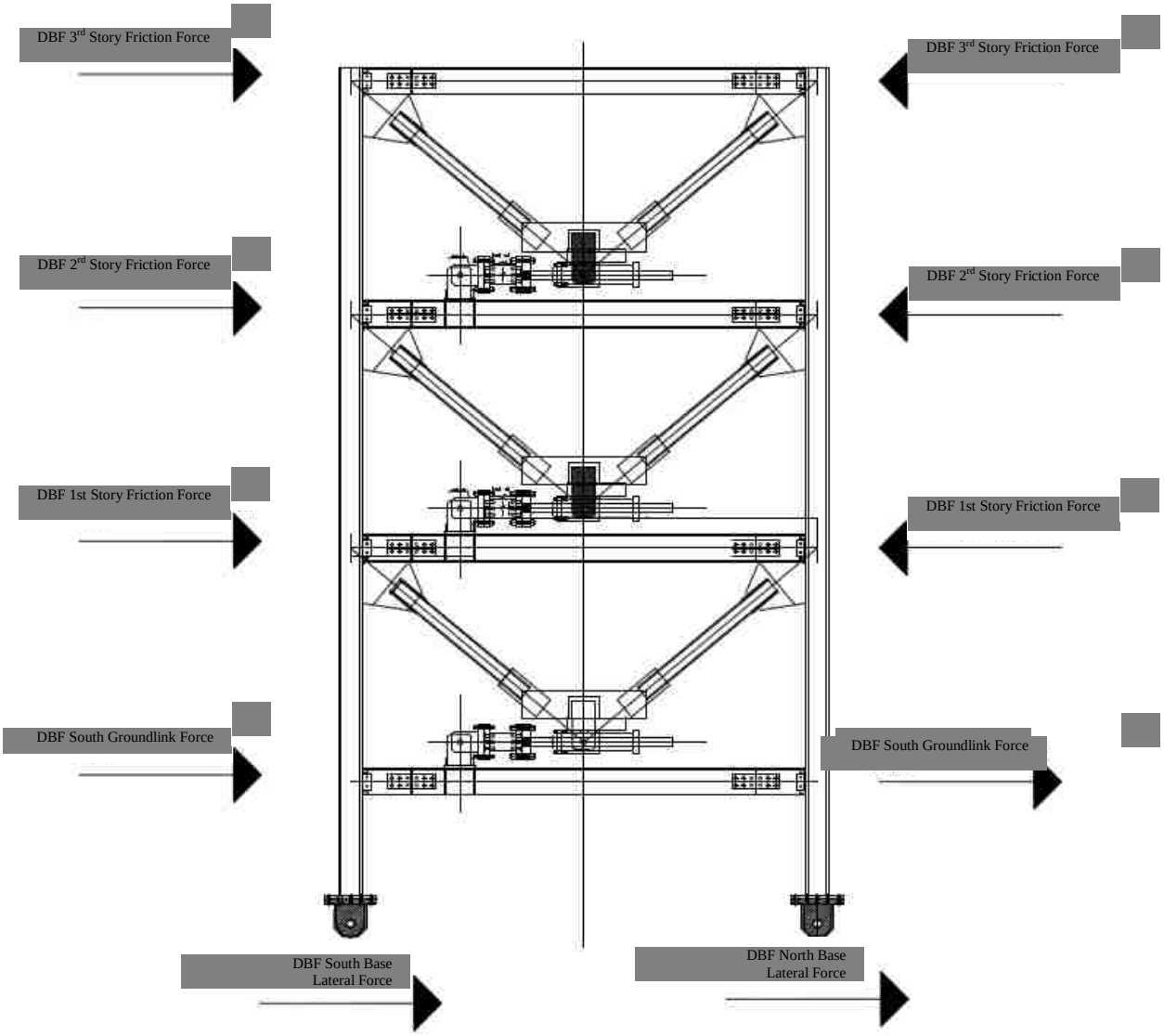

Figure 5.27 – DBF External Lateral Force Diagram

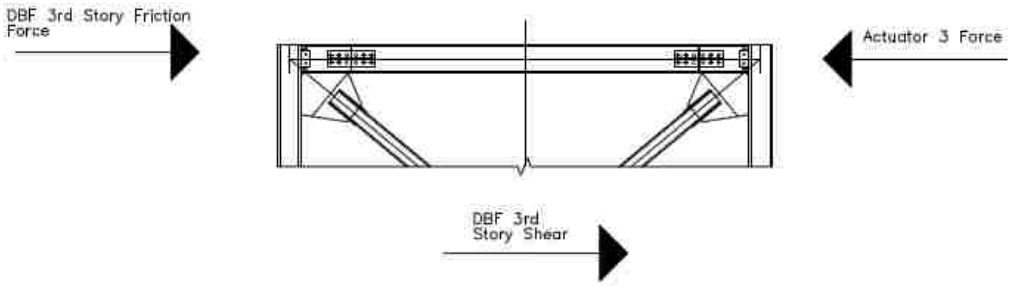

Figure 5.28 - 3rd Story DBF Freebody Diagram

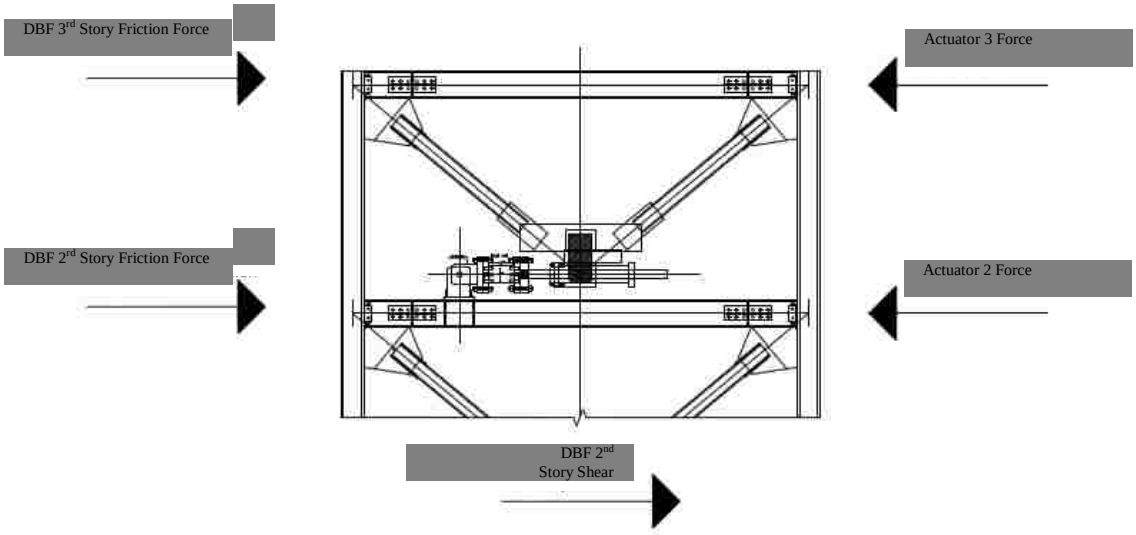

Figure 5.29 – 2nd Story DBF Freebody Diagram

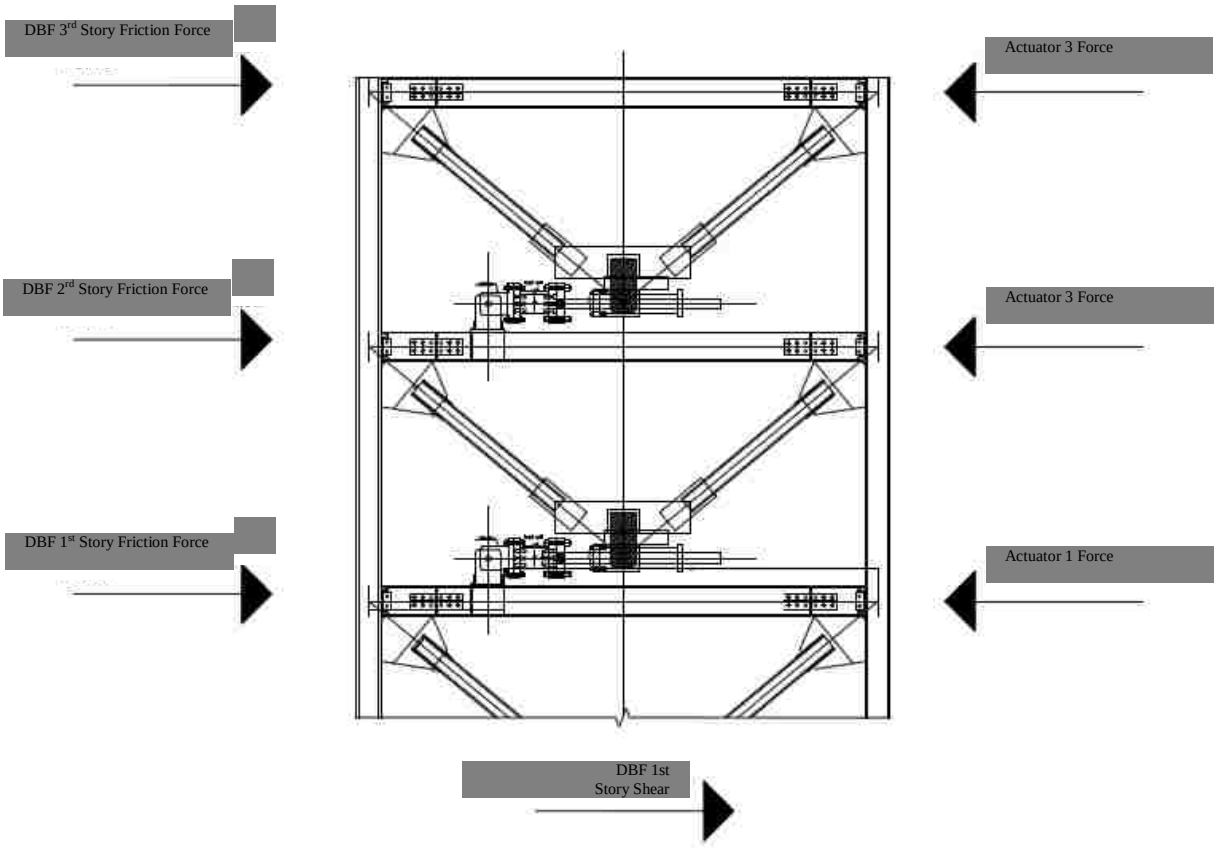

Figure 5.30 – 1st Story DBF Freebody Diagram

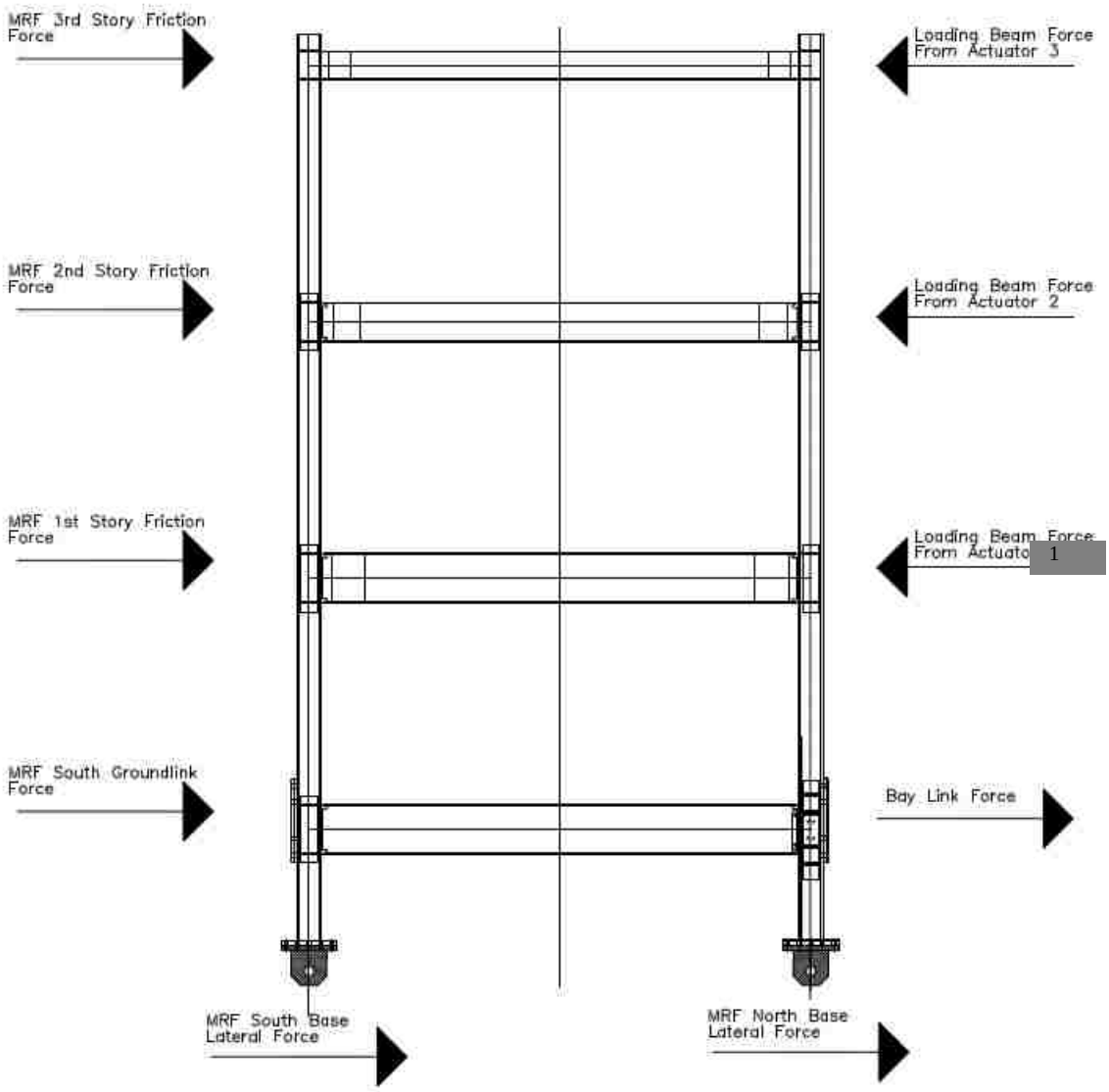

Figure 5.31 – MRF External Lateral Forces

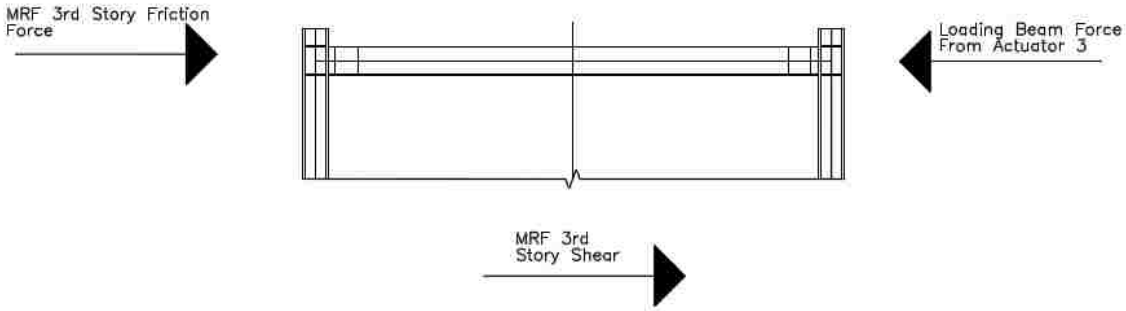

Figure 5.32 - Free Body Diagram Used to Determine 3rd Story MRF Friction

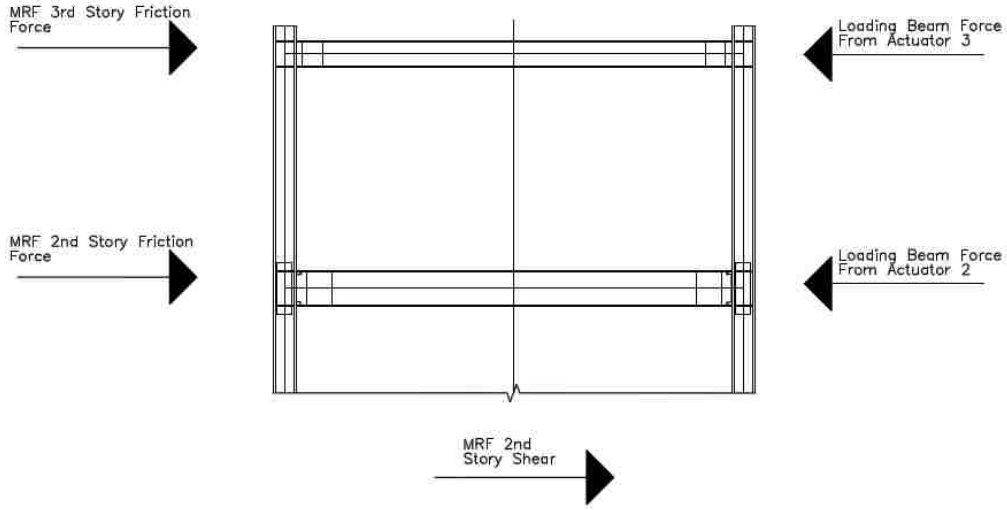

Figure 5.33 – Free Body Diagram Used to Determine 2nd Story MRF Friction

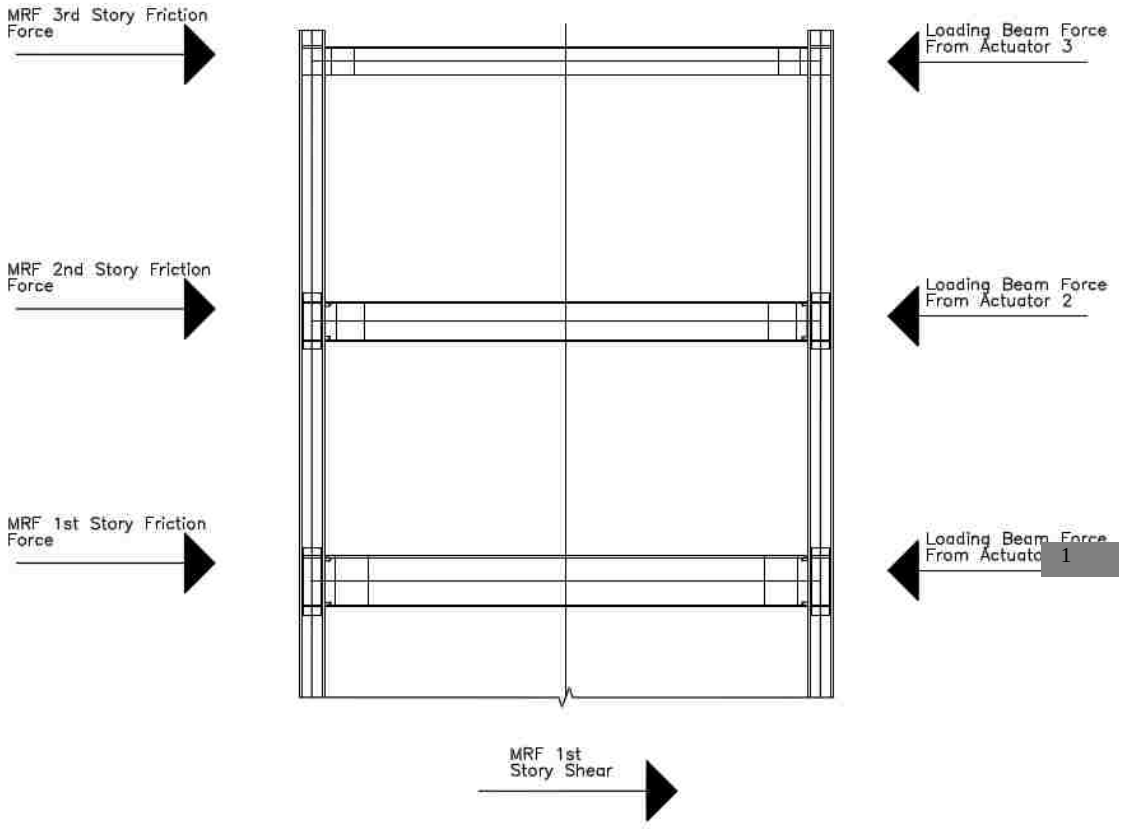

Figure 5.34 – Free Body Diagram Used to Determine 1st Story MRF Friction

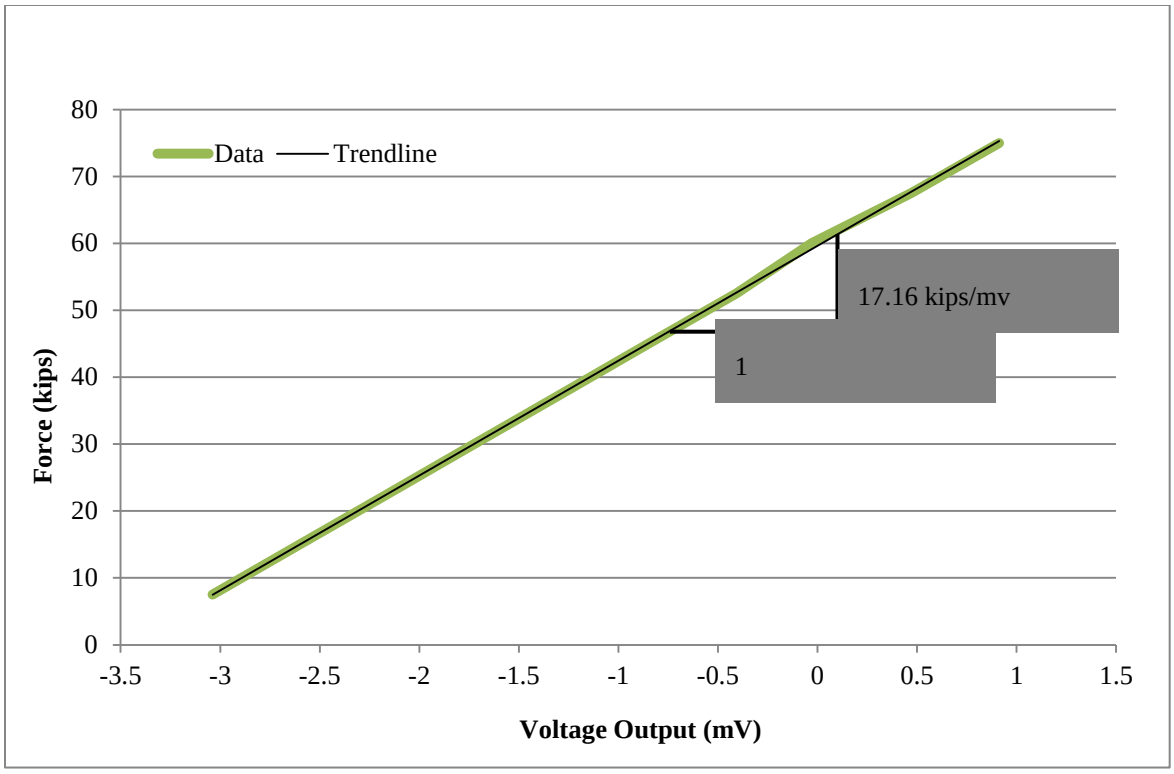

Figure 5.35 - Bay Link Calibration Force vs Voltage Output

Chapter 6.
Damped Brace Frame Characterization Testing

6.1 General

In order to conduct hybrid testing using the DBF, the initial elastic lateral stiffness of the frame needs to be known. The types of DBF characterization tests conducted, their purpose and results are discussed in this chapter. Also discussed are modifications made to both the test fixtures and the DBF as a result of this testing.

6.2 Testing Methodologies

In order to assess various characteristics of the DBF several different types of characterization tests were conducted. These included quasi-static tests (commonly referred to as static test), slow predefined sinusoidal displacement tests, and sinusoidal tests at rates of up to 1 Hz. In total, 84 characterization tests were conducted. Much of the testing was repeated with different instrument configurations to assess different frame components. Testing was also conducted both before and after adjustments were made to test fixtures and the DBF.

6.2.1 Quasi-static testing

Quasi-static tests were performed to measure the stiffness of the DBF and to evaluate the behavior of individual frame components. The DBF flexibility matrix was derived from data obtained from the quasi-static tests involving three actuators (discussed later). During quasi-static testing each floor was loaded individually with a known force, while

the other two floors were allowed to displace with no force being applied. This testing was used with the frame in several different configurations. The first being an individual actuator attached to the frame at a single floor and the rigid links attached, the second being three actuators attached to the frame and the rigid links attached, and the third being three actuators attached, one MR damper in the frame, and the rigid links detached at the remaining floors.

A model of the frame, constructed by Dong (2013), was used to determine the level of force required to produce first yielding in the frame. Roughly half of the force needed to provide first yield was the used in static testing. This was deemed sufficiently high enough to allow an accurate measurement of the stiffness to be made while remaining low enough to not damage (yield) the frame. Forces were calculated for two different frame arrangements, the first with the rigid links attached and the second without the rigid links attached. Table 6.1shows the forces that were applied to the frame for both rigid link configurations.

Quasi-static tests were conducted several times during frame characterization, including quasi-static tests that loaded the frame at the third floor. Loading at the third floor engaged the T-section connections at all floors in the DBF whereas loading at another floor only engaged some of the T-section connections. Table 6.2 shows all quasi-static tests completed as of the writing of this thesis.

Data from quasi-static tests were sampled at 128 Hz in order to decrease the size of data files associated with these tests. Due to the relatively low velocity during testing this produced sufficiently dense data plots.

6.2.2 **Sinusoidal tests**

During sinusoidal tests each floor was displaced under displacement control by a predefined displacement history. In order to determine appropriate displacement amplitudes for the testing a displacement pattern of the first mode shape floor displacements were taken and scaled to a level that would not produce yielding in the DBF. The scaled amplitudes for frame configurations can be found in Table 6.3. A haversine function was used to provide two ramp-up cycles and two ramp-down cycles. A plot of the three story displacements for a test without the rigid links is shown in Figure 6.1. Sinusoidal testing was limited to frequencies of no more than 1Hz in order to avoid inertial effects.

Sinusoidal tests are important because that they subjected the DBF to dynamic loading. Since the frame would be tested dynamically it was felt that this would allow any issues in fixtures that only occurred when the frame was loaded dynamically to be observed. Data from sinusoidal tests were sampled at 1024 Hz in order to capture as much detail as possible.

6.3 Friction Force Assessment

It is important to assess the amount of external friction in the test setup because it could impact that amount of force that was being transferred to the test specimen and the results of the test. The most likely source of friction is between the loading beams and the external bracing frame. This bracing is shown in Figure 4.4 and Figure 4.5. If it was determined if friction is an issue the plates bracing the loading beams would be adjusted

outward as described in Section 4.4.2. The method for analyzing the amount of friction developed on the test setup is discussed in Section 5.3.4.

Figure 6.2 through Figure 6.4 show the results of a friction force analysis for a sinusoidal test. The maximum friction force developed in the test setup was 2% of the applied actuator loads. It was concluded from this test and others like it that the amount of friction force was negligible and the Teflon® plates do not have to be adjusted. The level of friction however will be checked periodically to determine if anything changed.

6.4 DBF Stiffness Matrix

The three by three stiffness matrix associated with the lateral degree of freedom at each floor of the DBF was experimentally acquired. These degrees of freedom are shown in Figure 6.5. The stiffness matrix is valuable for a variety of reasons including evaluation of the accuracy and calibration of finite element models of the DBF; design of MR damper control laws and actuator control algorithms, and for use in real time hybrid simulation. Another use for the stiffness matrix is to help determine if the frame is damaged during testing. By comparing stiffness matrices of the frame before and after a test it would be possible to determine whether the frame stiffness had changed. If it had changed it would be an indication that the frame sustained some sort of damage and further investigation of the frame would be needed to understand what specific damage occurred.

6.4.1 **Development of stiffness matrix**

To develop the stiffness matrix first the flexibility matrix was found from the measured response. As established by structural theory, flexibility coefficients are the displacement

at degree of freedom i due to a unit force applied at degree of freedom j (Hibbler, 2011). By systematically applying a known actuator force at a single degree of freedom of the DBF at a time it is possible to determine the full 3x3 flexibly matrix, where the flexibility coefficients are obtained using the following formula:

$$f_{ij} = \frac{\Delta_{max} - \Delta_{min}}{F_{max} - F_{min}} \tag{6-1}$$

where,

f_{ij} = flexibility coefficient (e.g. displacement at DOF i due to a unit force at DOF j)

Δ_{max}= maximum displacement at DOF i

Δ_{min}= minimum displacement at DOF i

F_{max}= force at DOF j associated with maximum displacement

F_{min}= force at DOF j associated with minimum displacement

Due to hysteresis a slope was found for both the loading and unloading curve and an average of the two slopes was taken. This procedure was done for the coefficient established from Figure 6.6, and the resulting flexibility is plotted in addition to the data. Using a set of three tests (loading one floor at a time), nine flexibility coefficients are determined. They were then placed in a 3x3 matrix. An example of a flexibility matrix for the October 3, 2011 set of static tests (See Table 6.2) is shown in Table 6.5. Once this flexibility matrix was produced it is inverted to find the DBF stiffness matrix, and is

given in Table 6.6. Table 6.7 shows the DBF stiffness matrix where the off diagonal terms are averaged to make it symmetric.

6.5 Evaluation and Modification of Frame Components

One of primary goals of characterization of the DBF frame was to update finite element models of the frame which would be used to plan future testing and for parametric studies after the completion of the laboratory phase of testing. With this goal in mind it is important to understand the force deformation behavior of many of the frame components that are unique to this structure and could not initially be accurately modeled. This included the T-sections, the rigid links and the ground links. After initial testing nonlinearities were observed in the T-sections and the ground links, so these components were modified.

6.5.1 T-section connection modifications

The original goal of the T-section beam connection, as discussed in Section 3.4 and shown in Figure 3.14 was to allow for a pinned connection that would limit the moment developed within the gusset plate region. In order to avoid slipping in the T-section connection a set of tapered pins were used in addition to bolts. However during initial testing it became clear that this connection was not functioning as originally intended and that slip was occurring. This slip caused significant nonlinearities in the floor displacement response.

In order to correct the nonlinearity, the bolts of one side of the T-connection were removed and that side of the connection was welded with a single vertical fillet weld, which was sized to carry the moment developed in the connection. Figure 6.7 shows this

modification. Figure 6.8 shows the results of a static test of the third floor before and after this modification was made. It is clearly evident that this modification improved the linearity in the response.

The axial force deformation and moment rotation behavior of the modified T-section connections from each floor are shown in Figure 6.9 through Figure 6.14. The ground floor T-section connection response was not measured and was assumed to be similar to the other floors.

6.5.2 **Tightening of rigid link bolts**

Another source of nonlinearity in testing was the rigid links placed in the frame before the dampers were installed. These tubes, shown previously in Figure 4.46, are installed in place of dampers in the diagonal brace-to-beam connection. LVDTs were temporarily installed on these links to measure the force-deformation response of each link. It was determined that there was bolt slip occurring in the rigid links. The bolts used to attach the rigid links to the south end clevis were tightened and this reduced the slip. The change to overall floor displacement response due to this modification is show in Figure 6.15. However the rigid link response remained slightly nonlinear, and it was felt it was not possible to entirely remove this nonlinearity so it was simply included in future frame models. Figure 6.16 through Figure 6.18 show the axial force deformation behavior of each of the rigid links.

6.5.3 **Ground links**

Another component that was characterized was the true stiffness of the ground links. Figure 6.19 and Figure 6.20 shows the axial force-deformation behavior obtained for the south and north ground links, respectively.

6.5.4 **Bay link**

The bay link axial stiffness was determined during the calibration of the bay link full bridge as described in Section 5.4. Axial force-deformation data is plotted in Figure 6.21. The slope of the data was determined and used as the stiffness of the bay link. Data below 20 kips of compressive force was disregarded because it was assumed that this much force was required to properly seat the specimen in the test fixture. This stiffness was then used in all subsequent models that included both frames.

6.6 Application of Stiffness Matrix for Real-time Hybrid Simulation

Hybrid simulation results from two earthquakes were compared to numerical simulations using the stiffness matrix as a model of the stiffness of the DBF. These hybrid simulations and numerical simulations were conducted by Philips (2012) with one physical MR damper in the DBF, an analytical MRF and analytical lean-on-column. Information on the damper model used for the numerical simulations can be found in Philips and Spencer (2011). A comparison between the story displacements of the numerical simulations and the hybrid simulations involving the ground motions from the NS component of the Imperial Valley Irrigation District substation in El Centro, California recorded during the El Centro Earthquake of May 18th, 1940 are shown in

Figure 6.22 through Figure 6.24. Good agreement between the numerical and hybrid simulations results can be seen.

Table 6.1– Static Testing Applied Loads

Floor	Applied Load (kN)	
	With Rigid Links	Without Rigid Links
1st	220	225
2nd	180	125
3rd	180	90

Table 6.2 – Quasi-Static Test Matrix

Test #	Date	Frame Configuration	Floor Tested	Applied Load (Kn)
1	6/14/2011	Rigid Links, One Actuator 1st Floor	1st Floor	110
2	6/14/2011	Rigid Links, One Actuator 1st Floor	1st Floor	220
3	6/14/2011	Rigid Links, One Actuator 1st Floor	1st Floor	220
4	6/24/2011	Rigid Links, One Actuator 2nd Floor	2nd Floor	90
5	6/24/2011	Rigid Links, One Actuator 2nd Floor	2nd Floor	180
6	6/24/2011	Rigid Links, One Actuator 2nd Floor	2nd Floor	180
8	6/30/2011	Rigid Links, One Actuator 3rd Floor	3rd Floor	90
9	6/30/2011	Rigid Links, One Actuator 3rd Floor	3rd Floor	90
10	6/30/2011	Rigid Links, One Actuator 3rd Floor	3rd Floor	180
11	6/30/2011	Rigid Links, One Actuator 3rd Floor	3rd Floor	180
12	8/8/2011	Rigid Links, Three Actuators	3rd Floor	180
13	8/8/2011	Rigid Links, Three Actuators	3rd Floor	180
14	8/8/2011	Rigid Links, Three Actuators	3rd Floor	180
15	8/8/2011	Rigid Links, Three Actuators	3rd Floor	65
16	8/9/2011	Rigid Links, Three Actuators	3rd Floor	180
17	8/9/2011	Rigid Links, Three Actuators	3rd Floor	180
19	8/10/2011	Rigid Links, Three Actuators	1st Floor	220
20	8/10/2011	Rigid Links, Three Actuators	2nd Floor	180
21	8/10/2011	Rigid Links, Three Actuators	3rd Floor	180
23	8/10/2011	Rigid Links, Three Actuators	3rd Floor	180
24	8/10/2011	Rigid Links, Three Actuators	3rd Floor	180
25	8/22/2011	Rigid Links, Three Actuators	3rd Floor	180
26	8/22/2011	Rigid Links, Three Actuators	3rd Floor	180
27	8/23/2011	Rigid Links, Three Actuators	3rd Floor	180
28	8/24/2011	Rigid Links, Three Actuators	3rd Floor	180
29	9/21/2011	Rigid Links, Three Actuators	3rd Floor	180
30	9/26/2011	Rigid Links, Three Actuators	3rd Floor	180
31	10/3/2011	Rigid Links, Three Actuators	1st Floor	220
32	10/3/2011	Rigid Links, Three Actuators	2nd Floor	180
33	10/3/2011	Rigid Links, Three Actuators	3rd Floor	180
34	10/24/2011	Rigid Links, Three Actuators	3rd Floor	180
35	2/21/2012	No Rigid Links, 1st Floor MR Damper, Three Actuators	3rd Floor	90
36	2/22/2012	No Rigid Links, 1st Floor MR Damper, Three Actuators	3rd Floor	90
37	2/22/2012	No Rigid Links, 1st Floor MR Damper, Three Actuators	3rd Floor	90

Test #	Date	Frame Configuration	Floor Tested	Applied Load (Kn)
39	2/27/2012	No Rigid Links, 1st Floor MR Damper, Three Actuators	2nd Floor	125
41	2/27/2012	No Rigid Links, 1st Floor MR Damper, Three Actuators	3rd Floor	90
42	2/27/2012	No Rigid Links, 1st Floor MR Damper, Three Actuators	3rd Floor	90
44	2/28/2012	No Rigid Links, 1st Floor MR Damper, Three Actuators	1st Floor	225
45	3/3/2012	No Rigid Links, 1st Floor MR Damper, Three Actuators	1st Floor	225
46	3/3/2012	No Rigid Links, 1st Floor MR Damper, Three Actuators	2nd Floor	125
47	3/3/2012	No Rigid Links, 1st Floor MR Damper, Three Actuators	3rd Floor	90

Table 6.3 – Sinusoidal Tests Applied Displacements

Floor	Predefined Sine Wave Amplitude (mm)	
	With Rigid Links	Without Rigid Links
1st	8	50
2nd	5	27
3rd	2.5	9

Table 6.4 – Sinusoidal Test Matrix

Test #	Date	Frame Configuration	Frequency (Hz)
1	10/3/2011	Rigid Links	1
2	10/3/2011	Rigid Links	1
3	10/3/2011	Rigid Links	0.01
4	10/11/2011	Rigid Links	0.1
5	10/3/2011	Rigid Links	0.5
6	10/24/2011	Rigid Links	1
7	10/24/2011	Rigid Links	1
8	10/24/2011	Rigid Links	1
9	10/24/2011	Rigid Links	1
10	11/15/2011	Rigid Links	1
11	11/15/2011	Rigid Links	1
12	2/7/2012	1st Floor MR Damper	0.1
13	2/7/2012	1st Floor MR Damper	0.03
14	2/7/2012	1st Floor MR Damper	0.02
15	2/7/2012	1st Floor MR Damper	0.02
16	2/8/2012	1st Floor MR Damper	0.0167
17	2/16/2012	1st Floor MR Damper	0.0167
18	2/17/2012	1st Floor MR Damper	1
19	2/17/2012	1st Floor MR Damper	1
20	2/17/2012	1st Floor MR Damper	1
21	2/21/2012	1st Floor MR Damper	0.0167
22	2/21/2012	1st Floor MR Damper	0.0167
23	2/23/2012	1st Floor MR Damper	0.0167
24	2/23/2012	1st Floor MR Damper	0.0167
25	2/2/2012	1st Floor MR Damper	0.0167
26	2/27/2012	1st Floor MR Damper	1
27	2/27/2012	1st Floor MR Damper	0.0167
28	2/27/2012	1st Floor MR Damper	0.5
29	2/29/2012	1st Floor MR Damper	1
30	3/2/2012	1st Floor MR Damper	1
31	3/2/2012	1st Floor MR Damper	1
32	3/6/2012	1st Floor MR Damper	1
33	3/7/2012	1st Floor MR Damper	1
34	3/9/2012	1st Floor MR Damper	1
35	3/9/2012	1st Floor MR Damper	1
36	3/29/2012	1st Floor MR Damper	1
37	3/29/2012	1st Floor MR Damper	1

Table 6.5 – Flexibility Matrix of DBF from Tests 31, 32 and 33 (see Table 6.2)

	DOF 1	DOF 2	DOF 3
DOF 1	0.00226 in/kip	0.00238 in/kip	0.00250 in/kip
DOF 2	0.02440 in/kip	0.00478 in/kip	0.00506 in/kip
DOF 3	0.00253 in/kip	0.00511 in/kip	0.00822 in/kip

Table 6.6 – Stiffness Matrix of DBF from Tests 31, 32 and 33 (see Table 6.2)

	DOF 1	DOF 2	DOF 3
DOF 1	953.11 kip/in	-478.75 kip/in	4.90 kip/in
DOF 2	-515.31 kip/in	871.05 kip/in	-379.60 kip/in
DOF 3	26.81 kip/in	-394.40 kip/in	356.41 kip/in

Table 6.7 – Off-Diagonal Averaged Stiffness Matrix of DBF from Tests 31, 32 and 33 (see Table 6.2)

	DOF 1	DOF 2	DOF 3
DOF 1	953.11 kip/in	-497.03 kip/in	15.85 kip/in
DOF 2	-497.03 kip/in	871.05 kip/in	-386.98 kip/in
DOF 3	15.85 kip/in	-386.98 kip/in	356.41 kip/in

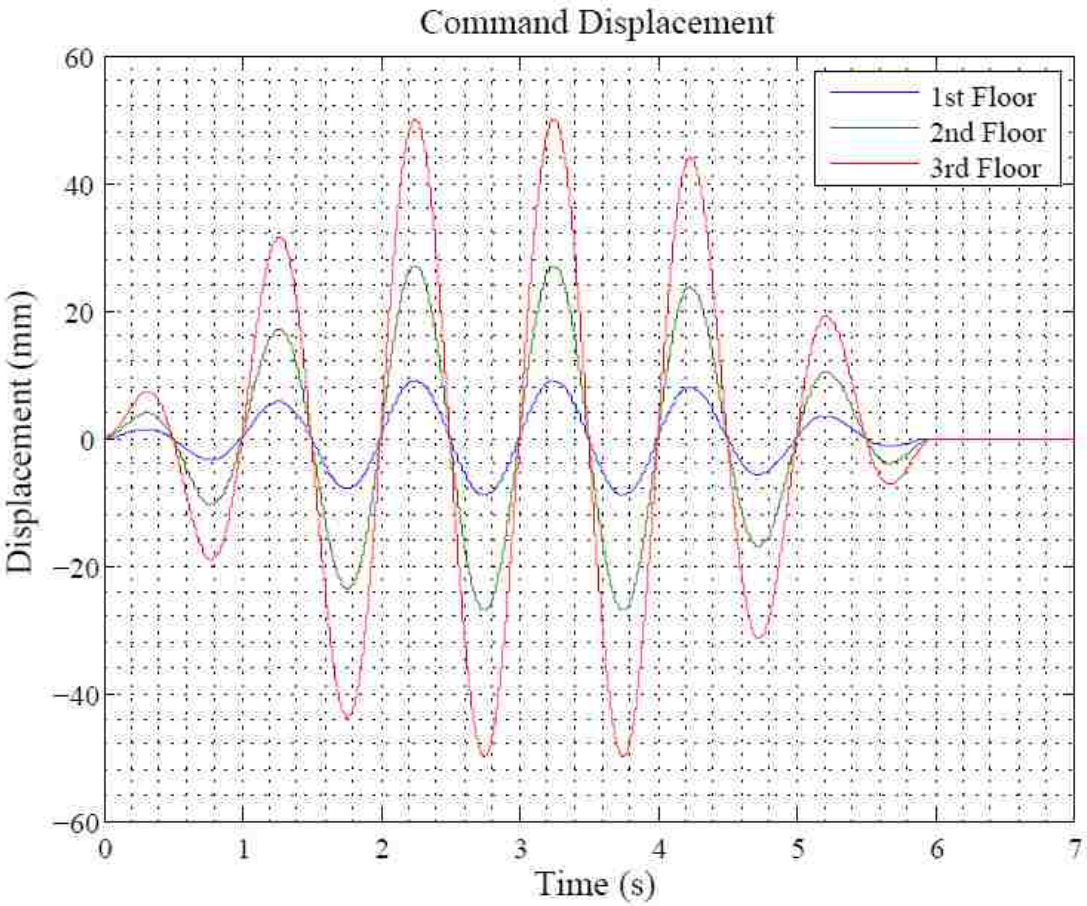

Figure 6.1 - DBF 1Hz Sinusoidal Test Displacements

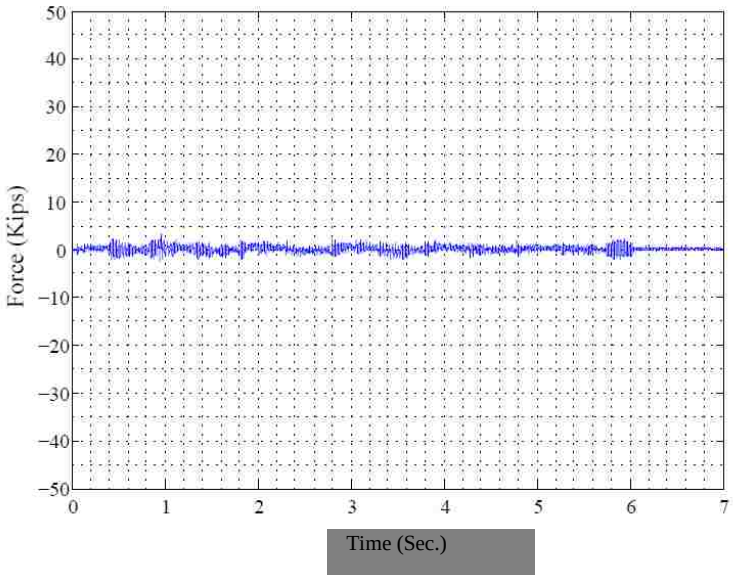

Figure 6.2 - Example 1st Story Friction Force Analysis Sinusoidal Test #11

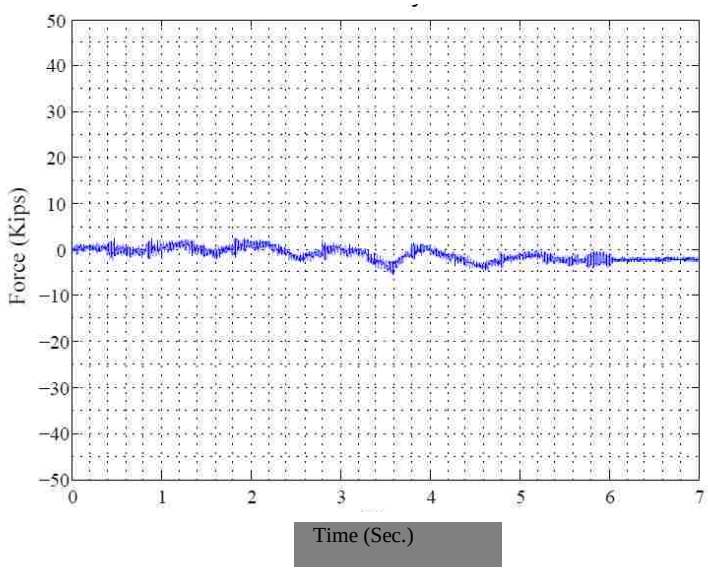

Figure 6.3 - Example 2nd Story Friction Force Analysis Sinusoidal Test #11

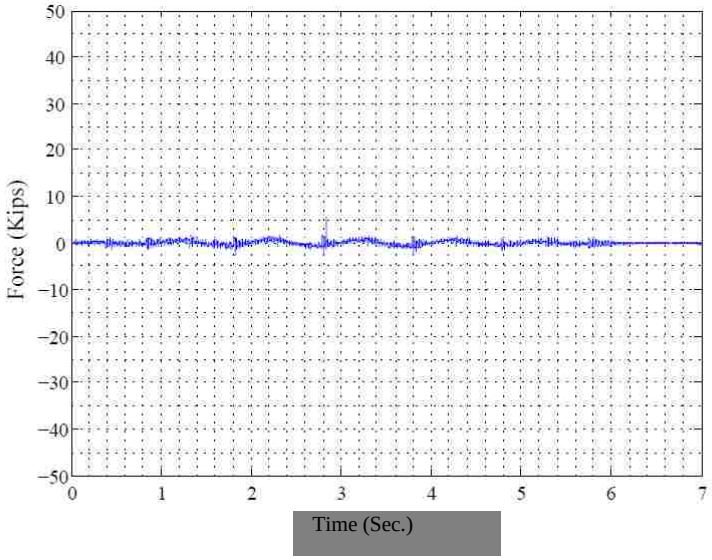

Figure 6.4 - Example 3rd Story Friction Force Analysis Sinusoidal Test #11

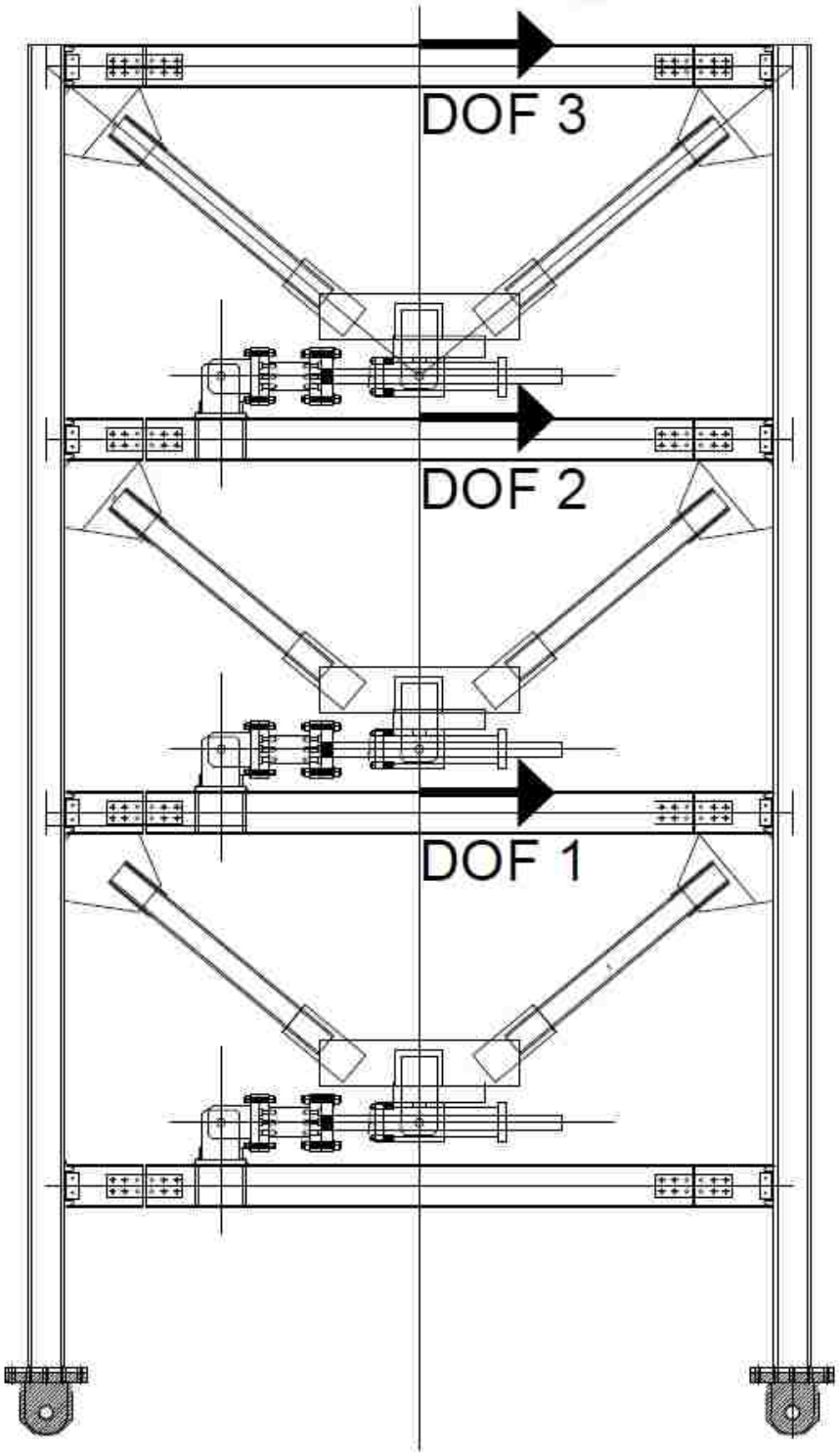

Figure 6.5 - DBF Stiffness Matrix Degrees of Freedom

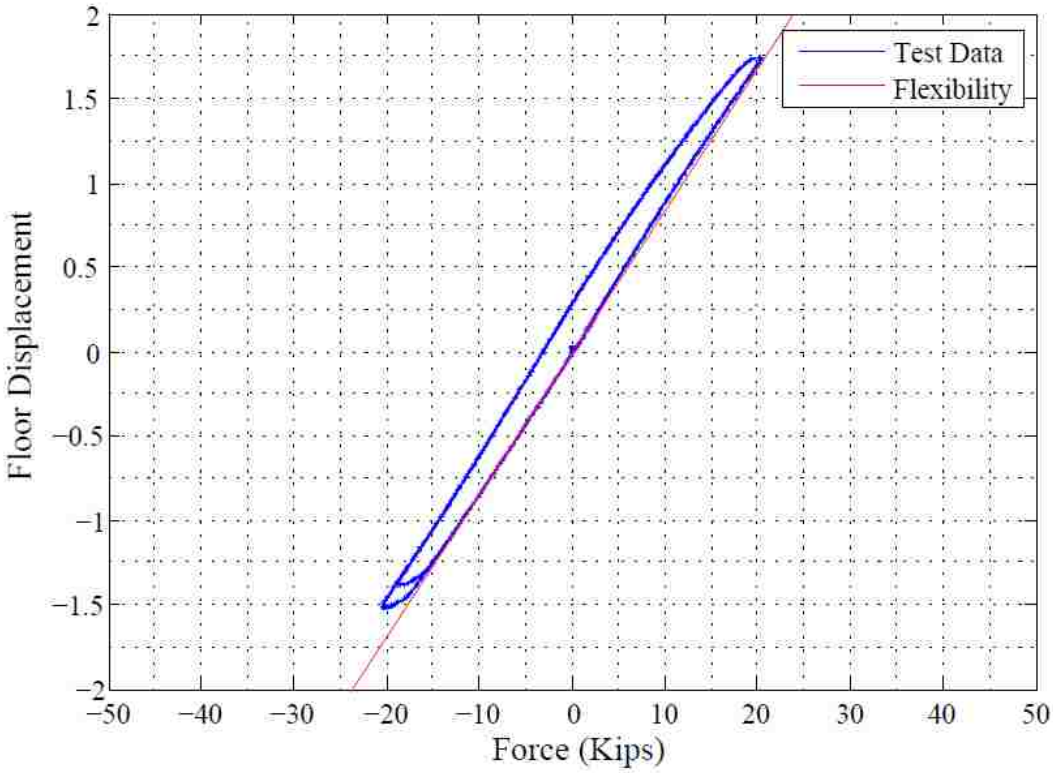

Figure 6.6 - Typical Force-Displacement Graph Used in Determining Flexibility Coefficients

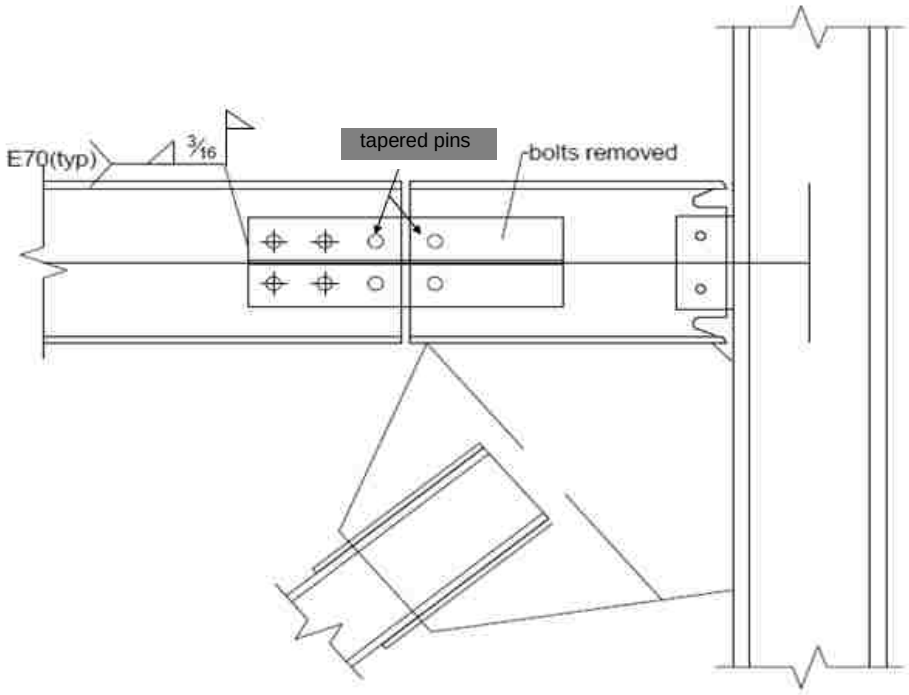

Figure 6.7 - T-Connection Modifications

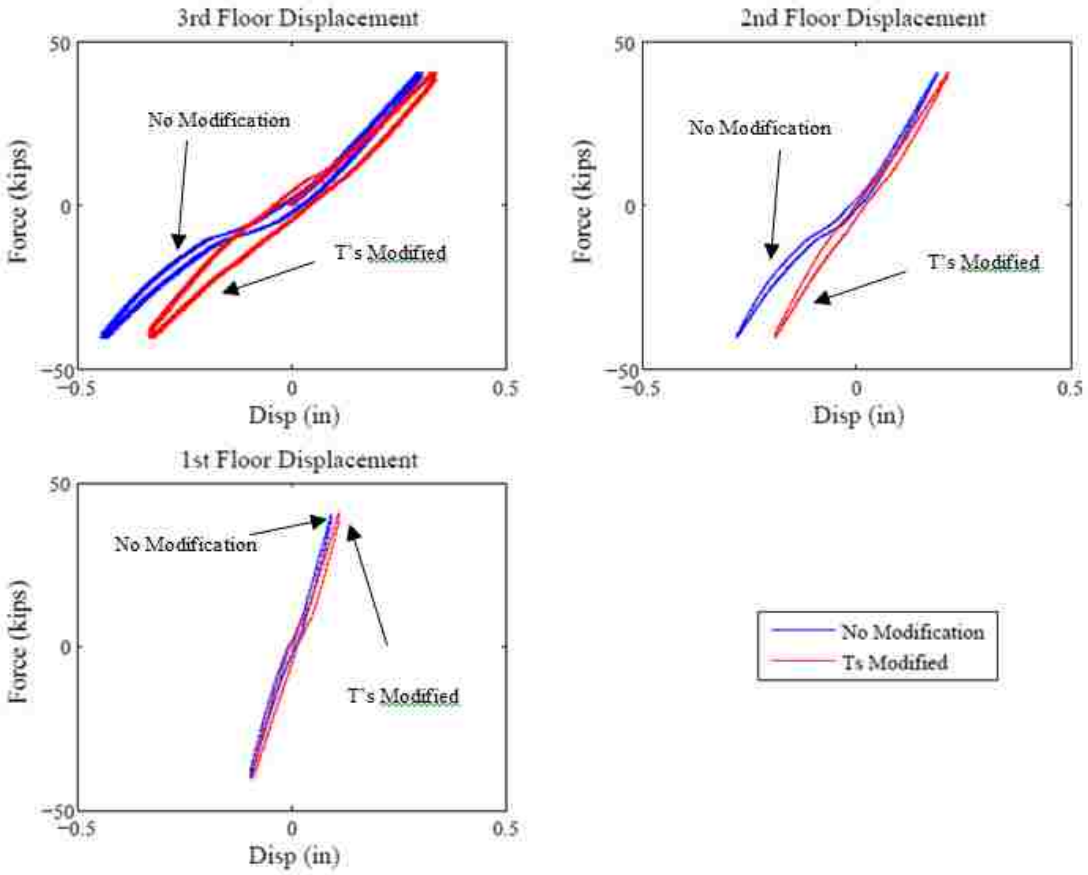

Figure 6.8 - Static Test Results Loading at 3rd Floor Before and After T- Connection Modification

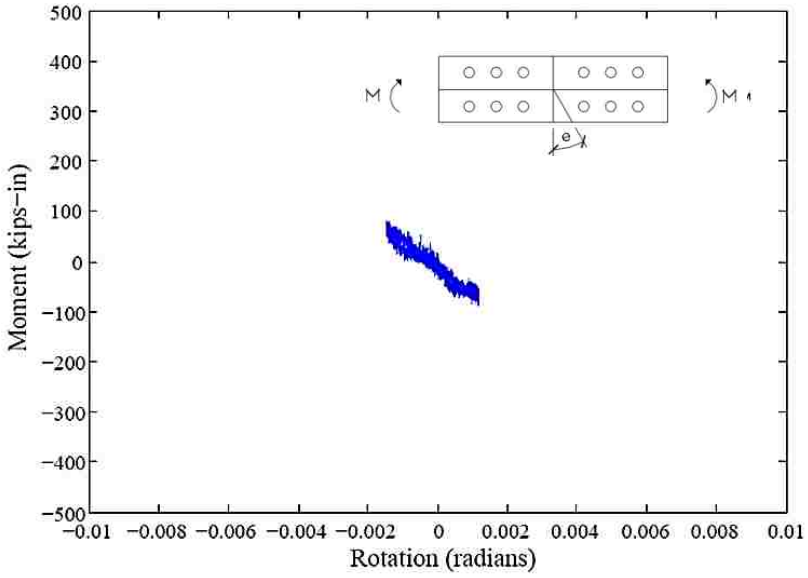

Figure 6.9 – 1st floor T-Connection Moment Rotation Behavior

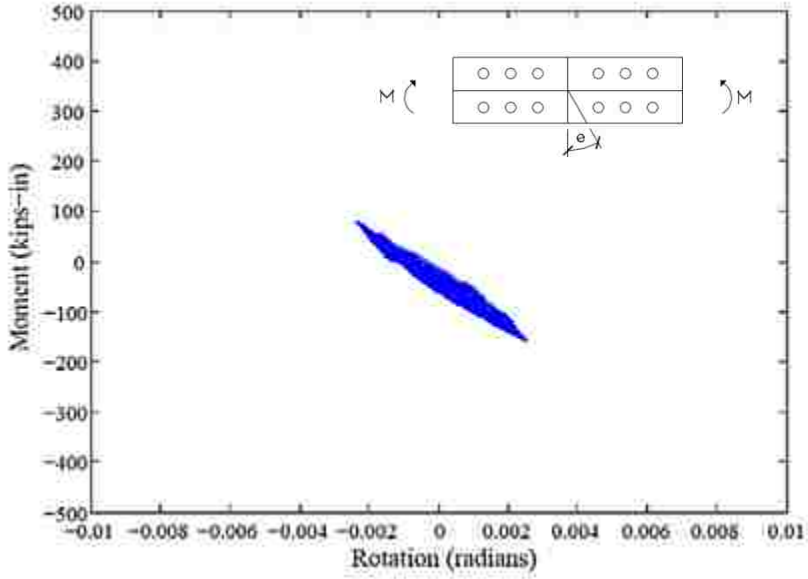

Figure 6.10 – 2nd floor T-Connection Moment Rotation Behavior

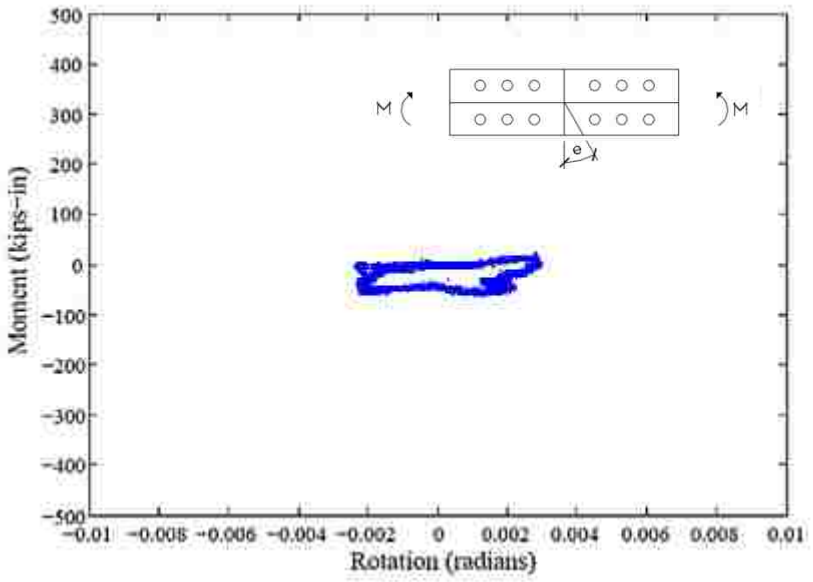

Figure 6.11 – 3rd floor T-Connection Moment Rotation Behavior

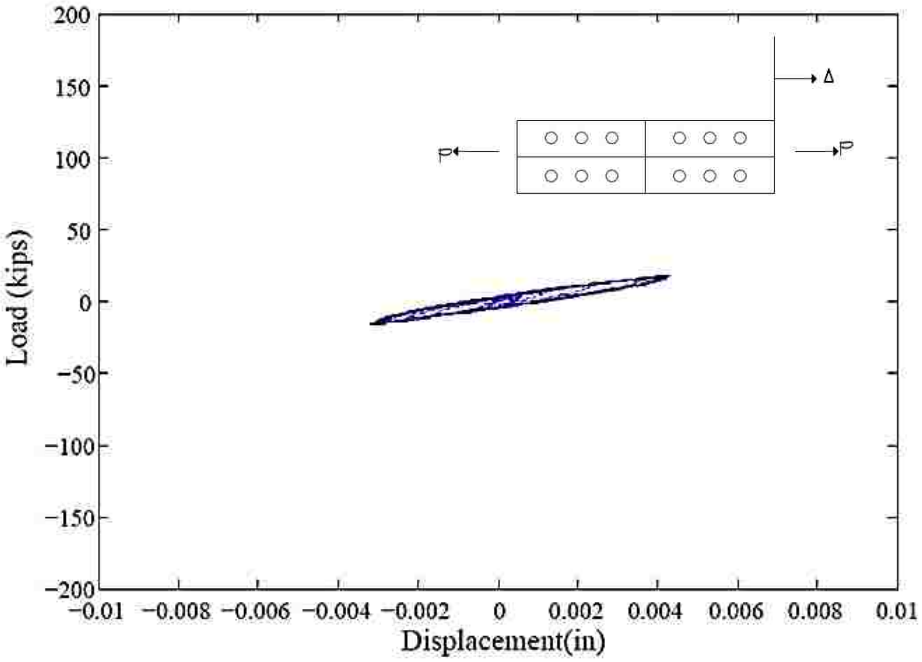

Figure 6.12 – 1st Floor T-Connection Axial Force vs Deformation

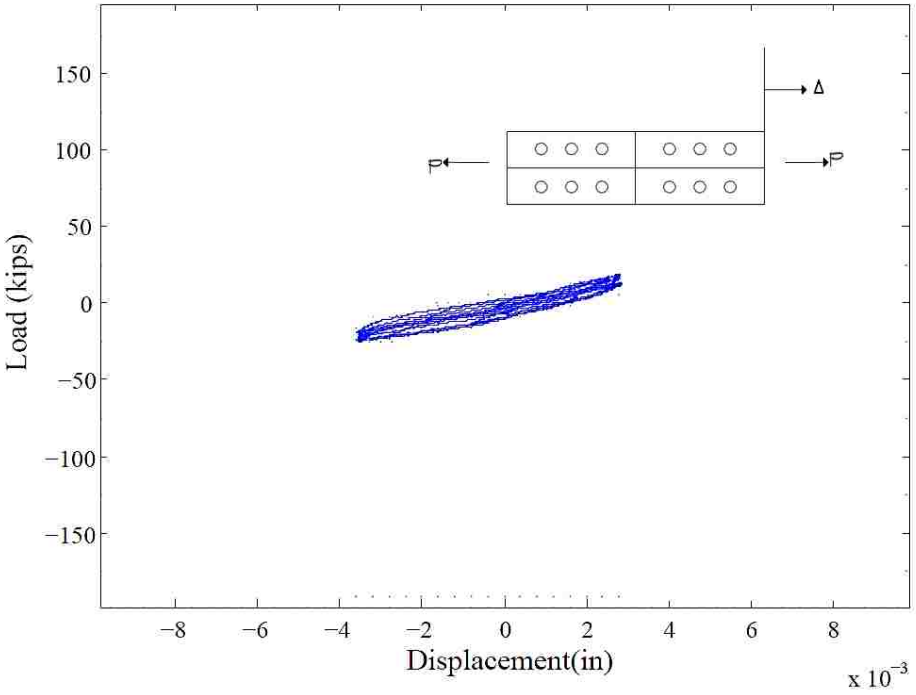

Figure 6.13 – 2nd Floor T-Connection Axial Force vs Deformation

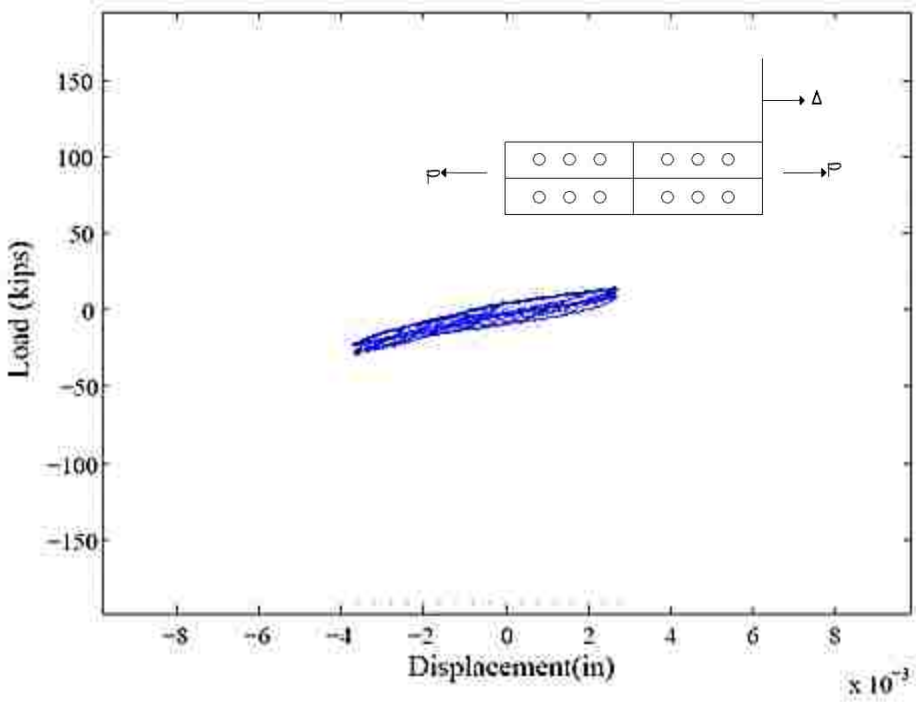

Figure 6.14 – 3rd Floor T-Connection Axial Force vs Deformation

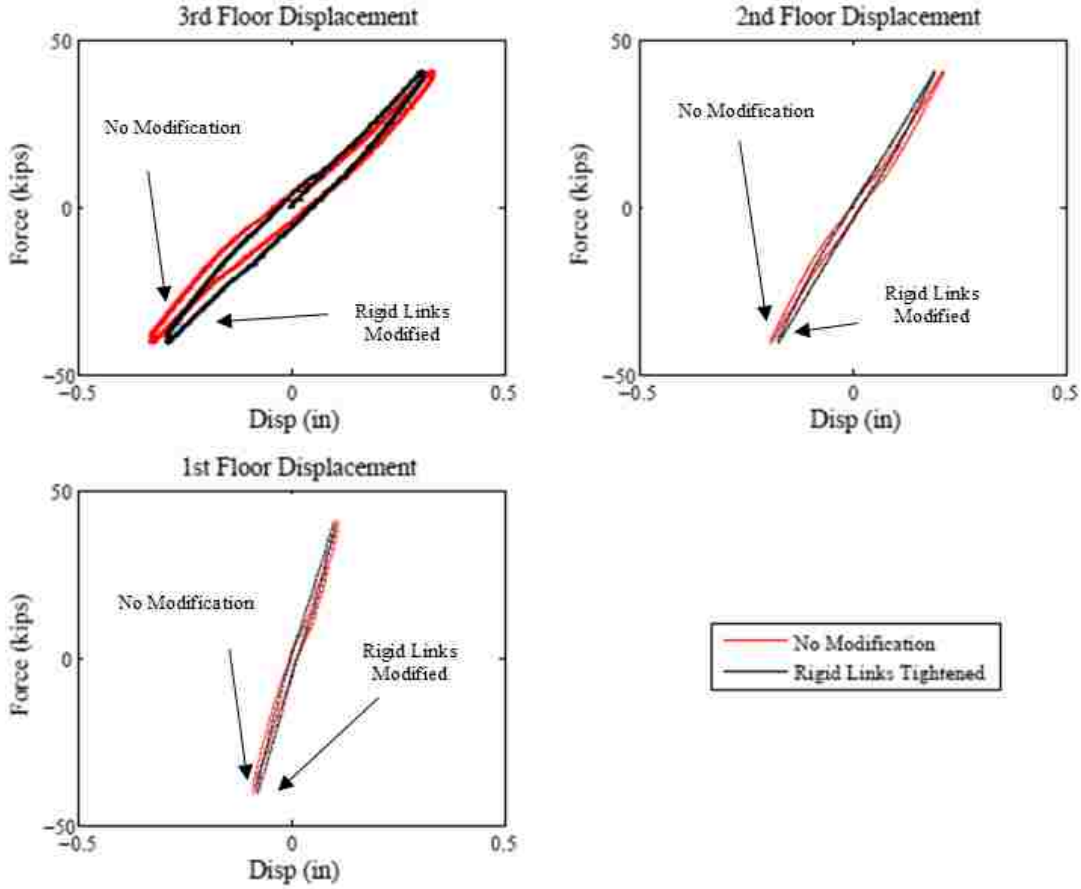

Figure 6.15 - Static Test Results Loading at 3rd Floor Before and After Tightening Rigid Links

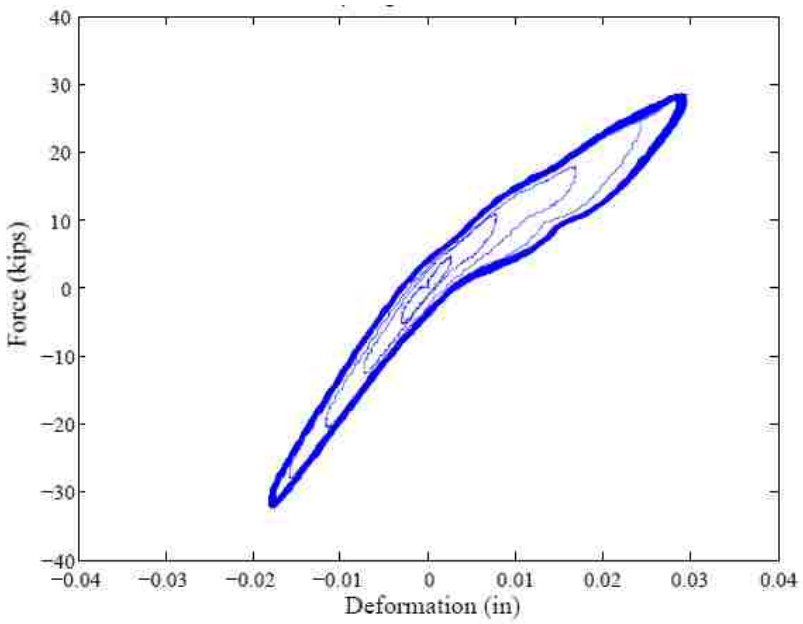

Figure 6.16 - 1st Story Rigid Link Axial Force-Deformation Behavior

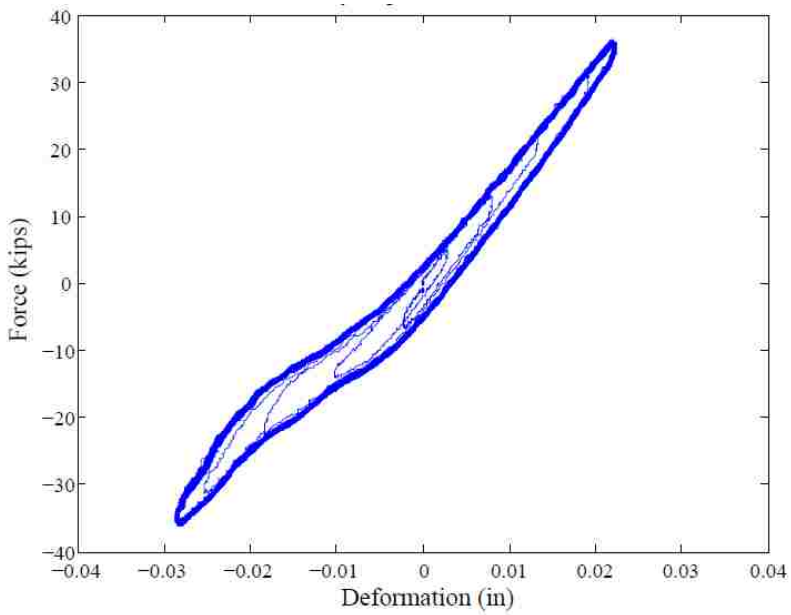

Figure 6.17 - 2nd Story Rigid Link Axial Force-Deformation Behavior

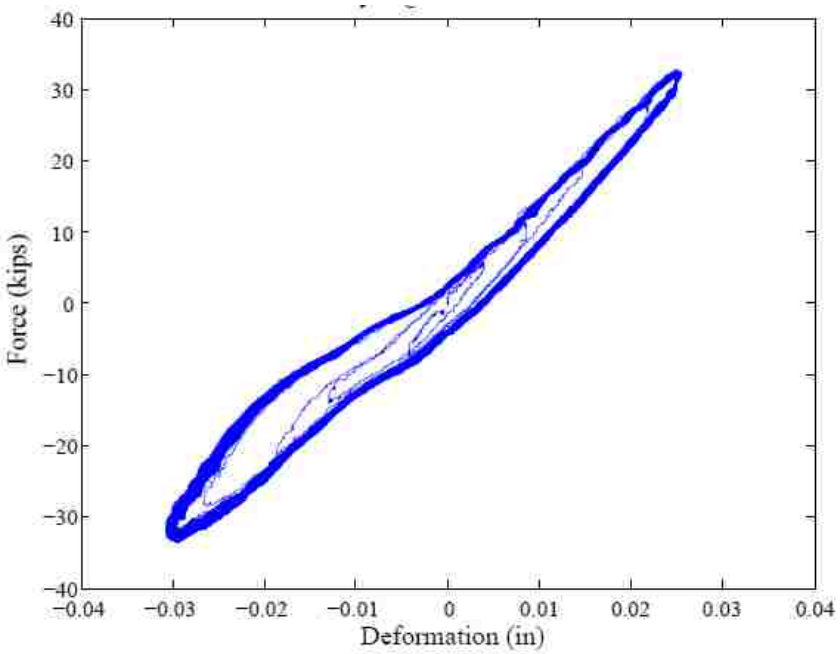

Figure 6.18 - 3rd Story Rigid Link Axial Force-Deformation Behavior

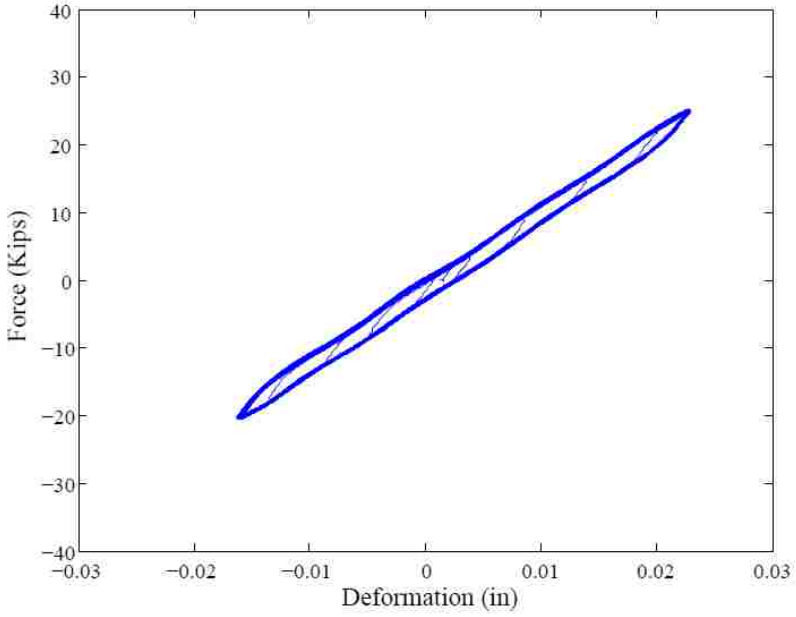

Figure 6.19 - South Ground Link Axial Force-Deformation Behavior

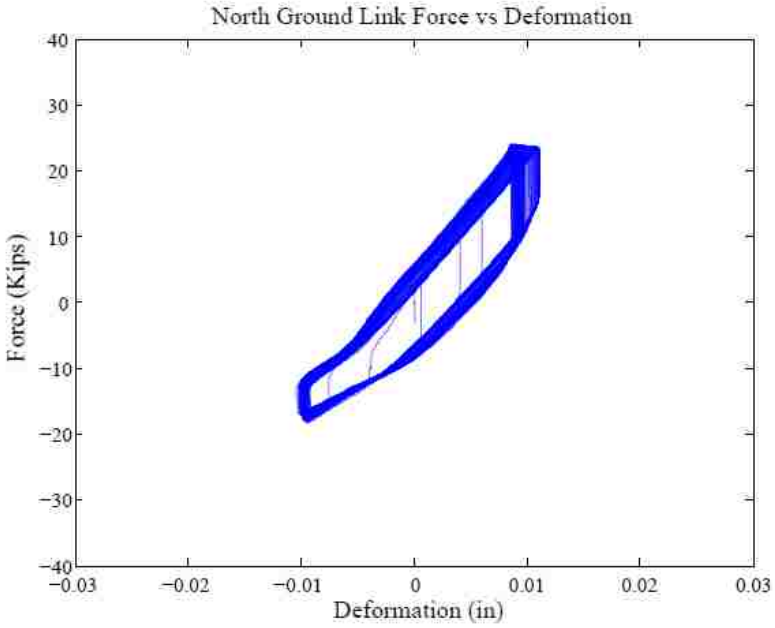

Figure 6.20 - North Ground Link Axial Force-Deformation Behavior

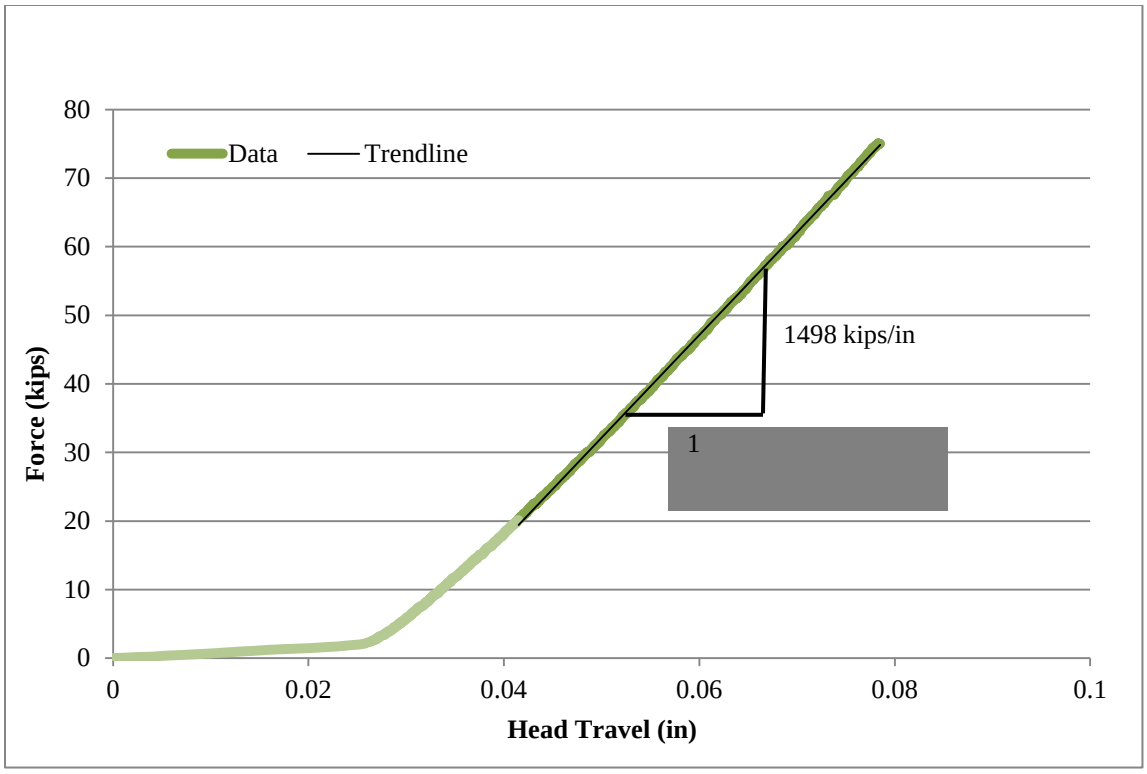

Figure 6.21– Bay Link Calibration Force-Head Travel Response

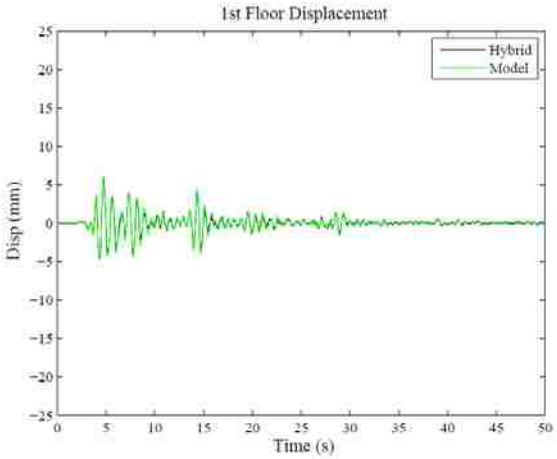

Figure 6.22 - Comparison of 1st Story Displacements for NS Component of the El Centro Ground Motion

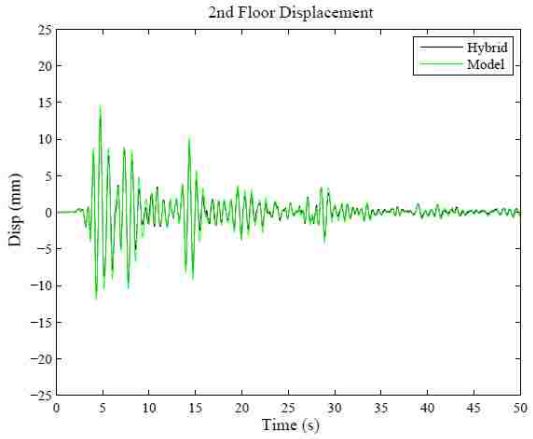

Figure 6.23 - Comparison of 2nd Story Displacements for NS Component of the El Centro Ground Motion

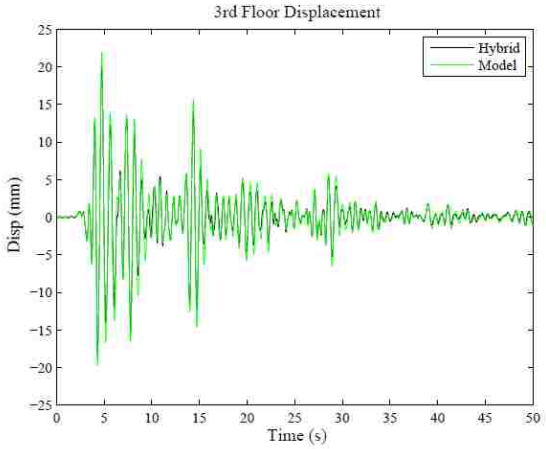

Figure 6.24 - Comparison of 3rd Story Displacements for NS Component of the El Centro Ground Motion

Chapter 7.
Summary, Conclusions and Recommendations

7.1 Summary

Chapter 1 provides a brief introduction and outlines the objectives of the research performed in this thesis. Chapter 2 discusses background information on the use of supplemental damping devices to improve structural response and the types of dampers used in this study. Dampers included are elastomeric dampers, viscous fluid dampers and magneto rheological (MR) dampers. The use of a simplified design procedure for designing structures with dampers is included. Finally, Chapter 2 concludes by discussing the development of a prototype structure designED using the simplified design procedure.

Chapter 3 presents the design of the test structure. It begins by discussing the scaling of the protype structure and selection of structural members by Dong (2012). It then covers the development of details for the MRF test structure to avoid column damage during testing. The design of continuity plates, doubler plates and welds is presented.

Chapter 4 describes the fabrication of the MRF test structure and the experimental test setup of the DBF and MRF. An external bracing frame designed by Herrera (2005) is used to provide out of plane bracing for both frames. Loading systems for each frame as well as fixtures reacting the forces are described in this chapter.

Chapter 5 describes the instrumentation plan for the test structure. Sensors including LVDTs, linear potentiometers, temposonics, accelerometers, simple strain gauges, full

bridges and load cells used to measure deformations and internal forces are described. The derivation of calibration factors to determine axial force and moment from full bridges is presented. Statics is provided for the calculation of internal forces not found from direct measurement. A method for determining external friction force is also presented. This chapter concludes with the calibration of the bay link fixture.

Chapter 6 describes the characterization of the DBF and development of the stiffness matrix. An assessment of external friction in the test setup was performed and showed that there is very little friction present in the test setup for the DBF. The assessment of force-deformation behavior of various components of the test structure and fixtures is conducted. This data will be used in future research to update finite element models of the structural system. The development of a procedure for developing a stiffness matrix based on the results of static test data and the use of a flexibility approach is shown. This matrix is then used as the basis for numerical simulations and is compared to hybrid simulation results.

7.2 Conclusions

The following conclusions were drawn from the work reported in this thesis:

1. Large-scale MRF and DBF test structures could be fabricated and erected in laboratory.
2. T-connections needed modifying to reduce nonlinearities.
3. Rigid links could be successfully used in place of dampers to gather initial characterization data for the calibration of numerical models of the DBF.

4. The use of load cells, full bridge load cells and displacement transducers allowed global and local force-deformation responses to be obtained.
5. Friction force in test setup could be analyzed through the use of full bridge load cells and frictional forces were determined to be low.
6. Development of a static stiffness matrix for use in hybrid simulations showed that large scale steel test structure can have its stiffness accurately assessed through static testing and the use of a flexibility approach.

7.3 Recommendations

The following recommendations are made for future work.

1. Perform characterization testing of the MRF to determine its elastic stiffness by either detaching the DBF at its load attachment point to the loading beams or by making use of the full bridges in the loading beams to determine the applied forces in the MRF.
2. Preform coupon tests on drops of DBF and MRF structural members to determine material properties. The most critical sections to test of the MRF are the beams and columns as well as the DBF structural T sections.
3. Develop and improve the OpenSEES models of the test structure to improve correlation between the model and the test structure.
4. Validate the simplified design procedure (SDP) by comparing the response of the structure from the SDP with results of nonlinear time history analysis and by showing the performance objectives of the SDP are met.

5. Comparisons should be made between the results from numerical and hybrid simulations using the two possible testing configurations of the test structure with dampers, (i.e., between hybrid testing using physical dampers, a physical test structure and analytical mass; hybrid simulation using physical dampers, analytic substructure of the test structure and analytical mass) to the determine the cost-benefit relationship for each testing configuration and the necessity for future frame tests in this area.
6. During testing the frame stiffness should be reassessed periodically to monitor changes due to yielding of frame components.
7. An evaluation of the friction in the test setup when the MRF is attached to the loading beams.

References

ASCE (2005), "Minimum Design Loads for Buildings and Other Structures," ASCE Standard 7-05, American Society of Civil Engineers (ASCE), Reston, VA.

AISC (2005a), *Steel Construction Manual, 13th edition*, American Institute of Steel Construction (AISC), Chicago, IL.

AISC (2005b), *Seismic Provisions for Structural Steel Buildings*, American Institute of Steel Construction (AISC), Chicago, IL.

AWS (2005). "Structural Welding Code – Steel," AWS D1.1/D1.1M:2005, AWS, Miami, Florida

AWS (2010). "Structural Welding Code – Steel," AWS D1.1/D1.1M:2010, AWS, Miami, Florida

Chen, S.J., Yeh, C.H., and Chu, J.M. (1996), "Ductile Steel Beam-to-Column Connections for Seismic Resistance," *Journal of Structural Engineering*, Vol. 122, No. 11, 1292-1299.

Cheng, J.J.R., Grondin, G.Y., and Yam, M.C.H. (2000), "Design and Behavior of Gusset Plate Connections," *Fourth International Workshop on Connections in Steel Structures*, Roanoke, VA, pp. 307-317.

Dong, B. (2013), "'Performance-based Design for Cost-effective Seismic Hazard Hazard Mitigation in Buildings Using Passive Damper Devices", PhD Dissertation, Civil and Environmental Engineering Department, Lehigh University, Bethlehem, PA

El-Sheikh, M.T., Pessiki, S., Sause, R., and Lu, L.-W. (2000), "Moment-Rotation Behavior of Unbonded Post-Tensioned Precast Concrete Beam-Column Connections," *ACI Structural Journal*, Vol. 97, No. 1, pp. 122-131.

Engelhardt, M.D., and Sobol, T.A. (1998). "Reinforcing of Steel Moment Connections with Cover Plates: Benefits and Limitations," *Engineering Structures*, Vol. 20, No. 4-6, pp. 510-520.

FEMA (2000), "Recommended Seismic Design Criteria for New Steel Moment-Frame Buildings", Report FEMA 350, Federal Emergency Management Agency (FEMA), Washington, D.C.

FEMA (2003), "NEHRP Recommended Provisions and Commentary for Seismic Regulations for New Buildings and Other Structures", Report FEMA 350, Federal Emergency Management Agency (FEMA), Washington, D.C.

Fahnestock, L. (2006), "Analytical and Large-Scale Experimental Studies of Earthquake-Resistant Buckling-Restrained Braced Frame Systems," Ph.D. Dissertation, Civil and Environmental Engineering Department, Lehigh University, Bethlehem, PA.

Garlock, M., Ricles, J.M., Sause, R., Zhao, C., and Lu, L.-W. (2000), "Seismic Behavior of Post-Tensioned Steel Frames," *Proceedings of 3rd International Specialty Conference on Behavior of Steel Structures in Seismic Areas – STESSA 2000*, Montreal, pp. 593-599.

Garlock, M.M., Ricles, J.M., and Sause, R. (2005), "Experimental Studies on Full Scale Post-Tensioned Steel Connections," *Journal of Structural Engineering*, Vol. 131, No. 3, pp. 438-448.

Gonner, N. (2009), "Design and Experimental Setup for Self-Centering Steel Concentrically Braced Frame Test Structure," M.S. Thesis, Civil and Environmental Engineering Department, Lehigh University, Bethlehem, PA.

Herrera, R. (2005), "Seismic Behavior of Concrete-Filled Tube Column-Wide Flange Beam Frames," Ph.D. Dissertation, Civil and Environmental Engineering Department, Lehigh University, Bethlehem, PA.

Lee, K.-S., Ricles, J., and Sause, R. (2009). "Performance-Based Seismic Design of Steel MRFs with Elastomeric Dampers." Journal of Structural Engineering, Vol. 135, No. 5, 489–498.

Lee, K.-S., Fan, C.-P., Sause, R., and Ricles, J. (2005). "Simplified design procedure for frame buildings with viscoelastic and elastomeric structural dampers." Earthquake Eng. Struct. Dyn., 34, 1271–1284.

Lewis, B. (2004), "Experimental Test Program for Evaluating the Seismic Behavior of Moment-Resisting Frame with Concrete-Filled Tubular Columns," M.S. Thesis, Civil and Environmental Engineering Department, Lehigh University, Bethlehem, PA.

Mahvashmohammadi, A. (2013), "Performance-Based Design for Cost-Effective Seismic Hazard Mitigation in New Buildings Using Supplemental Elastomeric Dampers.", PhD Dissertation, Civil and Environmental Engineering Department, Lehigh University, Bethlehem, PA

Phillips, B.M. (2012). "Model-Based Feedforward-Feedback Control for Real-Time Hybrid Simulation of Large-Scale Structures." PhD Dissertation, University of Illinois at Urbana-Champaign, Urbana, Illinois.

Phillips, B.M. and Spencer B.F. Jr. (2011). "Model-based Feedfoward-Feedback Tracking Control for Real-Time Hybrid Simulation." Newmark Structural Engineering Laboratory Report Series, University of Illinois, Urbana, IL, No. 28.

RTMD (2012), "Real-Time Multi-Directional Earthquake Simulation Facility User's Guide," RTMD site at ATLSS Research Center, Lehigh University, Bethlehem, PA, http://www.nees.lehigh.edu/index.php?page=rtmd-user-s-manual.

Ricles, J.M., Xiaofeng, Z., Lu, L, Fisher, J. (2004), "Development of Seismic Guidelines for Deep-Column Steel Moment Connections", ATLSS Report No. 04-13, Civil and Environmental Engineering Department, Lehigh University, Bethlehem, PA.

SAP2000, Computers and Structures, Inc.

Soong, T.T. and Spencer Jr., B.F. (2002) "Supplemental energy dissipation: state-of-the art and state-of-the-practice" *Engineering Structures*, 24, pp.243-259.

Yang, G. (2001) "Large-scale magneto-rheological fluid damper for vibration mitigation: modeling, testing and control." *Ph.D. Dissertation*, Dept of Civil Eng. and Geological Sciences, University of Notre Dame, Notre Dame, Indiana.

Youssef, N., Bonowitz, D., and Gross, J. (1995). "A Survey of Steel Moment Resisting Frame Buildings Affected by the 1994 Northridge Earthquake," *Report No. NISTIR 5625*, National Institute of Standards and Technology, Gaithersburg, MD.

Appendix

MRF Weld Inspection Report

WELDER TRAINING AND TESTING INSTITUTE

WWW.WTTI.COM

1144 N. GRAHAM ST. · ALLENTOWN, PA 18109 · TEL 610-820-9551 · FAX 610-820-0271

Certificate of Inspection - Ultrasonic Report

Customer:	Atlss Labs	***P.O. No.:***	
Description:	MRF Frame	***Job No.:***	542138
Drawing No.:		***Drawing Revision:***	

Test Data

	☑ *Straight Beam*	☑ *Shear Wave*
	Reference Test Standard	*Reference Test Standard*
Type / S/N:	05-6660	05-6660
Sweep Dist.:	1"	3" - 7"
Alloy:	steel	steel
Sensitivity Ref.:	58db	58db
	Transducer	***Transducer***
Make / S/N:	LI1137	KB704619
Beam Angle:	0	70
Frequency:	2.25 MHZ	2.25 MHZ
Size / Shape:	Round	Rectangular
Surface Condition:	As Welded	As Welded

Instrument

Mfg. / Model:	KB USN58L
S/N:	0134KX
Couplant:	Preforma Gel
Method:	Pulse Echo/Contact
Ref. Level dB:	58db
Scan dB:	77db
Screen Range:	10"
Code / Spec:	AWS D1.1
Acceptance Criteria:	Art 6 Part F
Procedure ID / Rev.:	

Notes and Sketches: Calibrated instrument in accordance with AWS D1.1 -2010 Article 6 Part F with IIW block for distance, B.I.P. , probe L and sensitivity on 10" FSW range from .060 SDH at 70% FSH at 58dB RL

Inspected the top and bottom CJP flange welds on 6 moment connections. One relevant indication found. The weld was repaired, re-inspected, and accepted.

Inspector: Daniel Sladovnik Level II U.T.

Date of Examination: 9/27/2011

VITA

Ryan James Ahn, the son of Timothy and Sandra Ahn was born on July 10, 1987 in Dover, Delaware. In May 2010 Ryan earned a Bachelor of Science in Civil Engineering from the Pennsylvania State University at University Park, Pennsylvania. Ryan began his graduate studies in the Department of Civil and Environmental Engineering in Bethlehem Pennsylvania in August of 2010. He will receive a Master of Science in Structural Engineering in 2012n